Source-Receiver Interaction for Structure-Borne Sound Sources on Floor Assemblies with Floating Toppings

Mohamed Abou Hamed

Thesis submitted to the Faculty of Engineering
in partial fulfillment of requirements for the degree of

Master of Applied Science

in Mechanical Engineering

University of Ottawa
Ottawa, Ontario

Abstract

Neighbor noise has repeatedly been proven to have a detrimental effect on multi-unit residential buildings (MURBs) residents' physical and mental health. Impact noises have been shown to cause the most indoor noise annoyance amongst residents. Moreover, lightweight assemblies are known for their general poor sound insulation and are becoming increasingly popular as an alternative to concrete and steel structures in North America and Europe. Floating toppings have been used to control impact noise, but the effect of the source-receiver interaction is often neglected when they are modelled by engineers in the industry. More research needs to be done to determine the actual influence of the source-receiver interaction on floor assemblies with floating toppings. Studying the source-receiver interaction is fundamental to tackling the issue of structure-borne noise in MURBs because it has been shown to influence the first of five factors of impact sound transmission: the power injected. The power injected into a floor due to an impact source has been shown to depend on the mechanical mobility match (or the source-receiver interaction) between the impact source and the impacted floor. However, many questions remain around the significance of the source-receiver interaction. This project investigates the significance of the source-receiver interaction for structure-borne sound sources on floor assemblies with floating toppings, and how much it varies from one source-floor combination to another.

Table of Contents

List of Figures

Acknowledgements

I would firstly like to sincerely extend my gratitude to my supervisor Dr. Markus Mueller-Trapet and co-supervisor Dr. Natalie Baddour who have been of utmost support throughout the completion of this thesis. I would also like to thank the acoustics team at the National Research Council Canada from whom I felt warmly welcomed during my work at their establishment and who facilitated some of the laboratory work that was involved. Finally, I am grateful for my family and friends, who provided a lot of the mental support that was crucial to the fulfilment of this project, especially during the trying times of the COVID19 pandemic.

1 Introduction

The Introduction begins with a section about the motivation of this project, which highlights the importance of studying the "Source-Receiver Interaction for Structure-Borne Sound Sources on Floor Assemblies with Floating Toppings". The second section of the Introduction concisely lists the specific objectives of this project, followed by the third section, which presents the contributions this thesis has contributed to the literature.

1.1 Motivation

Neighbor noise has repeatedly been proven to have a negative impact on individuals' quality of life and well-being, having both adverse mental and physical health effects on residents of multi-unit residential buildings (MURBs) [1,2]. For example, one study finds that there is a strong correlation between self-reported neighbour noise and a plethora of symptoms such as perceived stress, poor mental health, fatigue, sleeping problems and more. It was also revealed that respondents perceived neighbor noise as being more annoying than traffic noise, which has been addressed in the past a lot more than the issue of neighbor noise [1]. In another example, the majority of respondents from a recent study performed in Toronto on two student MURBs reported that the noise conditions had a negative impact on their ability to study and work from home. Due to impact noise specifically, around 30% of participants indicated having difficulty working and studying, as well as sleep disturbances [2]. Other research has highlighted the seriousness of the problems associated with neighbor noise annoyance [3,4,5]. Unfortunately, since the beginning of the COVID-19 pandemic, this problem has become more prevalent [6,7,8] due to lockdowns, teleworking, and tele-education, which ultimately caused more people to spend additional time at home.

Moreover, in North America and Europe, the construction industry is shifting towards construction of MURBs using wood-framed lightweight assemblies, such as those made out of cross-laminated timber (CLT) and joist floors using oriented strand board (OSB), instead of heavyweight assemblies, namely those made from concrete and masonry. However, although lightweight assemblies offer speedier and more affordable construction among other benefits, they are notorious for their general poor noise insulation, especially at low frequencies. Timber building residents are more disturbed by impact noises than those living in concrete buildings [9].

Nevertheless, especially due to their eco-friendly and sustainable qualities, it is likely that lightweight structures will continue to gain popularity in the future. For these reasons, lightweight assemblies are of particular concern when discussing neighbor noise.

When it comes to neighbor noise, there are different types of sources, and they can be grouped as either outdoor noise or indoor noise. Outdoor noise includes sources such as traffic, construction, and weather conditions, such as strong winds or storms. Indoor source examples include, but are not limited to, heating and cooling, water pipes, and occupants that reside in the same building. Furthermore, noise sources can be divided into airborne sources and impact sources. Examples of airborne sources could be a loud television or people shouting, while impact noises include individuals walking, children running and jumping, and objects being dropped onto the floor. Impact sources in particular are the cause of many complaints amongst residents in MURBs. For instance, Figure **1.1** shows the results of a case study, where the responses from 471 participants who live in MURBs across Canada showed that the most frequently reported indoor noise annoyance was from impact sources, which were reported to be even more annoying than outdoor noise [10].

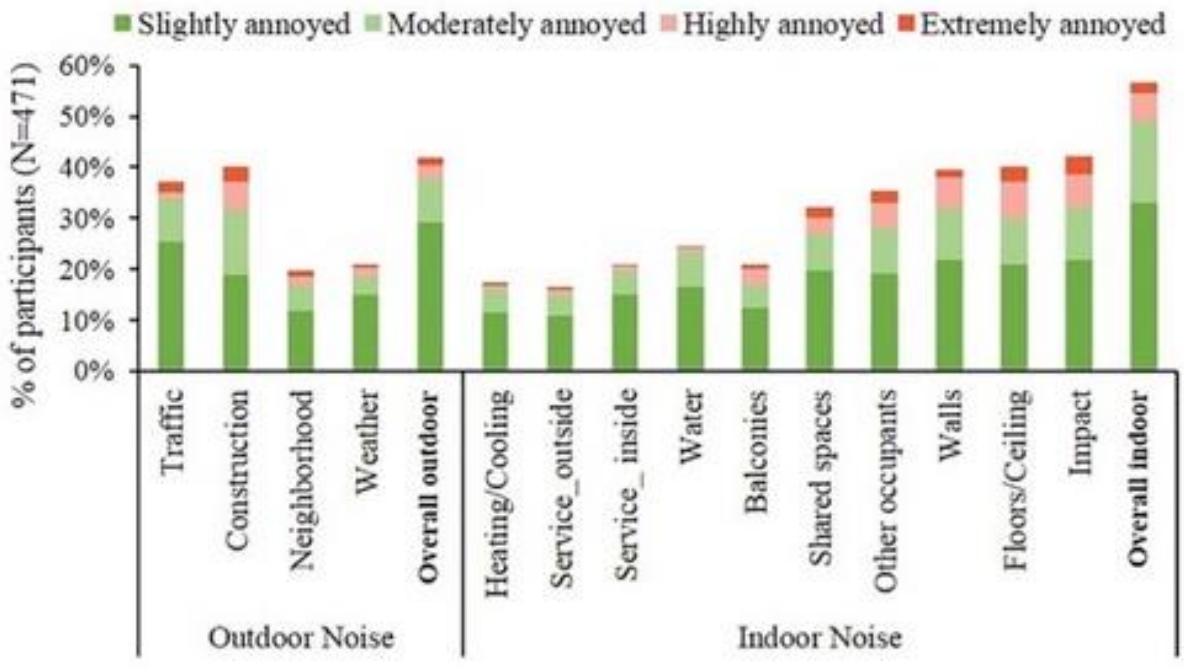

Figure 1.1 Annoyance levels with various noise sources [10].

Regarding impact sound, it is important to study the interaction between the source (the object which causes an impact) and the receiver (the structure which receives the impact). This interaction is called the source-receiver interaction. It has been shown that the sound power injected into a receiver structure, such as a floor, due to an impact source depends on the mechanical mobility match between the impact source and the receiver floor [11]. In other words, the interaction between the impact source and the receiver floor determines how much sound power is transmitted from the impact source unto the floor. When the mobility of the impact source and receiver floor are closer to each other, there is more power injected into the receiver floor. This means that the same impact source will behave differently when impacting one receiver floor to another and will inject a different amount of sound power into them. The sound power injected by the impact source into the receiver floor is the first of five factors in the five-factor method [12,13,14] which is used in determining how much sound is transmitted through a floor structure due to impact. In the end, the sound power that is transmitted through the floor and radiated into the receiver room is perceived by occupants in that room as noise [15]. It is therefore important to study the source-receiver interaction and determine how it changes for different source-receiver combinations. In terms of bare receiver floors, the source-received interaction has been shown to particularly matter for lightweight assemblies, whereas heavyweight assemblies are not affected as much by the source-receiver interaction [16].

The incorporation of floating toppings on bare base floors alters the way a floor assembly is affected by the source-receiver interaction. The technology of floating toppings is commonly used to minimize impact noise between units in MURBs. However, incorporating a floating topping will alter the mobility of the floor, and depending on the mobility of the source, this could increase the influence of the source-receiver interaction [11]. Furthermore, the standard modelling procedure for floating toppings [17] does not take into consideration the source-receiver interaction. For these reasons, it is important to assess the influence of the source-receiver interaction when floating toppings are involved.

1.2 Objectives

This thesis investigates the effect of floating toppings on the power injected into a floor at impact, since floating toppings are often used as a means of impact sound insulation and may affect the

influence of the source-receiver interaction. Furthermore, floor assemblies that include floating toppings are more complicated to model compared to bare floors and therefore, of certain interest.

The specific objectives of this thesis are

- to investigate the interaction between impact sources and floor receivers by quantifying how much the source-receiver interaction affects the sound power injected into real-life floors. This will be done by examining impact sources and floor receivers separately, as well as their combinations.
- to find the most appropriate measurement configuration using the most suitable equipment for both the sources and the receivers, as there are various challenges involving the measurements of their mobilities.

Ultimately, further understanding the source-receiver interaction will aid in controlling structure-borne noise due to impact sources, which is a known and serious aggravator to residents' general quality of life. In turn, this will contribute to an improved understanding of the first factor of impact noise transmission: the power injected into a floor.

1.3 Contributions

The contributions of this thesis in the field of impact sound transmission and the source-receiver interaction are measuring, plotting, and analyzing the following variables:

1) Mobility of standard impact sources, namely the tapping machine and the impact rubber ball, as well as a human walker's foot with and without shoes

2) Mobilities (transfer mobility between impact positions and other positions as well as overall mobility of the floors) of a typical 6-inch bare concrete floor and bare 5-ply CLT floor

3) Same mobilities mentioned in point 2, but with the incorporation of a laminate floating topping to the bare floors

4) Injected power, when considering the source-receiver interaction and when neglecting the source-receiver interaction, unto the four floor assemblies mentioned in points 2 and 3 when using with the four sources mentioned in point 1 as impact sources

5) Relative error between the powers injected for all 16 source-receiver combinations mentioned above, when considering and without considering the source-receiver interaction

The first three points provide good data to the literature for the mobility of the two most common standard impact sources and two of the most common real-life impactors in MURBs (a human walker, with and without shoes), as well as the overall floor mobility of a concrete and a CLT slab, with and without laminate. All measurements have been performed multiple times using various measurement setups, settings, and tools, in order to obtain robust data. The mobilities of the sources and receivers, alongside another variable named the blocked force of the sources, which was also obtained by measurement and analytical models, are used to compute the injected powers from the fourth point. The mobilities of the sources and receivers are also utilized in computing the final variable, the relative error, which helped provide insight on the importance of the source-receiver interaction for structure-borne sound sources on floor assemblies with floating toppings.

2 Literature Review

In one previous analytical study [16], it was found that for low frequencies (below 500Hz), due to the assemblies having much lower mobilities than those of the sources, the source-receiver interaction has little to no influence on the power injected by the source into the floor. Modifications made to specimens showed consistent variations with all different sources, implying that the source is behaving similarly when impacting all different receivers. This could mean that the only parameter affecting the injected power is the force generated by the source without the influence of the receiver (called the blocked force) and the influence of the source-receiver interaction is negligible. The current thesis expands on the study from reference 16 by testing different source-receiver combinations and incorporating floating toppings.

Standard impact sources are utilized in order to provide a reference for the testing of impact noise insulation of floor assemblies. The two most used standard impact sources are the tapping machine and the Japanese impact rubber ball, both defined in ISO10140-5 [18]. The tapping machine was first standardized in 1938 in Germany and then included in the American Society for Testing and Materials (ASTM) standard in the 1960s. The impact rubber ball is a standard heavy impact sound source which was introduced by Tachibana and included in the Japanese Industrial Standards (JIS) more recently in February 2000.

The tapping machine has been criticized due to the fact that it does not represent typical day-to-day noise produced by humans, such as adults walking or children jumping on the floor. The frequency characteristics of the sound produced by the tapping machine are different than those of real-life sources [19,20]. The impact sound pressure level (SPL) spectrum of the tapping machine is dissimilar to the one that is produced by humans walking barefooted or with soft-soled shoes. That is because while the spectrum of its blocked force may be similar to walkers wearing hard-heeled shoes on a heavy concrete floor, it is dissimilar to that of humans walking barefooted or children jumping. Additionally, the mechanical mobility of the tapping machine steel hammers does not match with the mobility of human feet, which also shapes the SPL spectrum. Moreover, the tapping machine has been shown to produce too little low frequency sound [21]. It is important to consider lower frequencies when it comes to impact sound insulation, especially because

lightweight assemblies are known to have poor low-frequency sound attenuation. It is at low frequencies where floor constructions often fail impact sound insulation standard tests [22, 23].

Nevertheless, the tapping machine is a standardized source used in the measurements of impact noise; its purpose is not to replicate typical human sources, but to provide a standard reference. However, it is not a source of constant impact since the received impact depends on the floor as well and its interaction with the tapping machine (the source-receiver interaction). In the cases of floating floors, it even depends on the interaction between the floating floor and the base floor. Figure **2.1** shows the impact sound improvement of a floating floor, which is the metric used to quantify the effectiveness of a floating floor to minimize impact sounds, using the tapping machine on a timber joist floor versus the impact sound improvement of the same floating floor using the same tapping machine but on concrete base floor [24]. It is seen that especially at frequencies above 500Hz, there are large deviations between the two.

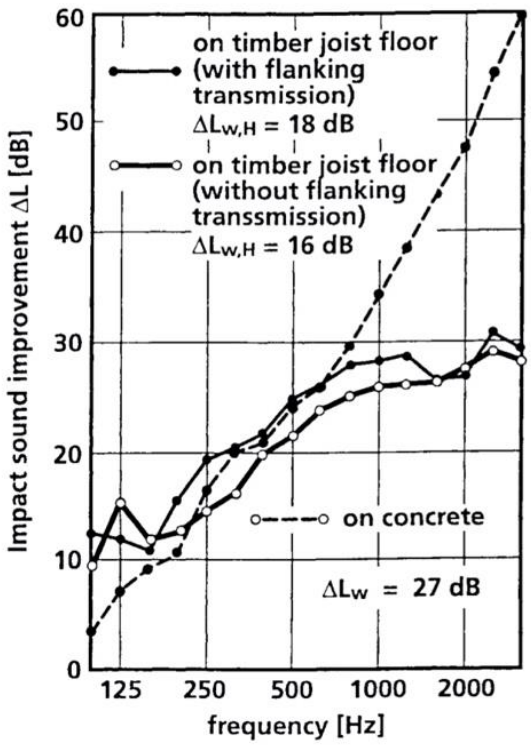

Figure 2.1 Impact sound improvement of a floating floor on a concrete and a timber joist base floor [24].

With the tapping machine, non-linearities can also be expected. For example, a soft floor covering's stiffness depends on the amplitude of the force of the impact. Other non-linearities could arise from the contact between the tapping machine hammers and the floor. As seen from Figure **2.2**, the nature of the contact area varies between the tapping machine hammer and different floors. Also, there is probably unevenness and deformations on the surface of the hammers or the floor. These non-linearities can be expected to cause variations in measurements [24].

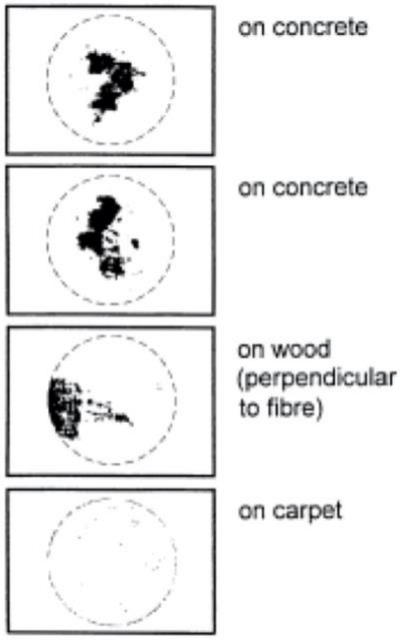

Figure 2.2 "Footprints" of a standard tapping machine on different floor surfaces [24].

Due to the unique results between the standard tapping machine and different test floors, it is impossible to predict human impact noise from the tapping machine. Converting from the standard tapping machine to human activity such as footsteps is also not possible, since measurements are dependent on the source-receiver interaction, the interaction between the floating floor and base floor, non-linearities, and more [24]. To address this problem, the tapping machine was modified so that the hammer mobility better matches that of human feet. This way, the tapping machine can act as a walker, or at least more similar to a walker, on floors of all types. It was modified simply by adding corks underneath the hammers, which is included in ISO 10140-5 [18]. The modification can be implemented to existing tapping machines. This way, the older tapping machine may be

kept [25]. Figure **2.3** shows the impact SPL frequency spectra produced on a concrete floor as well as a timber joist floor by two individuals walking with and without shoes (averaged), the tapping machine, and the modified tapping machine. It is seen that after the modification, the impact SPL spectrum looks more like that of a walker, especially at higher frequencies. However, there is a lack of sufficient data regarding the modified tapping machine.

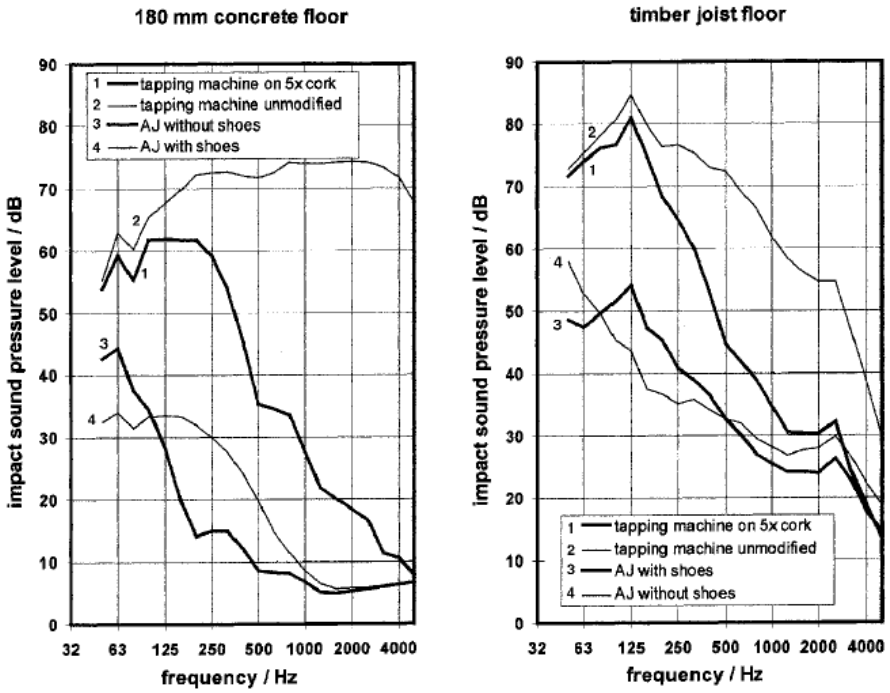

Figure 2.3 Impact SPL frequency spectra of two floors using the tapping machine and the modified tapping machine, and a walker with and without shoes [25].

The standard Japanese impact rubber ball was created to better reproduce human activity (such as adult walkers or children jumping) and replace the bang (or tire) machine, which was another standard impact source causing damage to wood-based floors [26]. In comparison with the impact rubber ball, the Japanese impact ball force spectra has a better correlation with those of barefoot walkers or children jumping due to its mobility better matching that of the common impactors. As shown in Figure **2.4**, among all impactors, the impedance (the inverse of mobility) and the resonant frequency of the impact ball are closest to those of a human bare foot. It can be seen from Figure **2.5** that its impact SPL spectrum also best correlates with that of children jumping and

running. Moreover, the impact rubber ball is known for its ease of handling and operation, lack of required maintenance, as well as its lower cost compared to the tapping machine [27, 28].

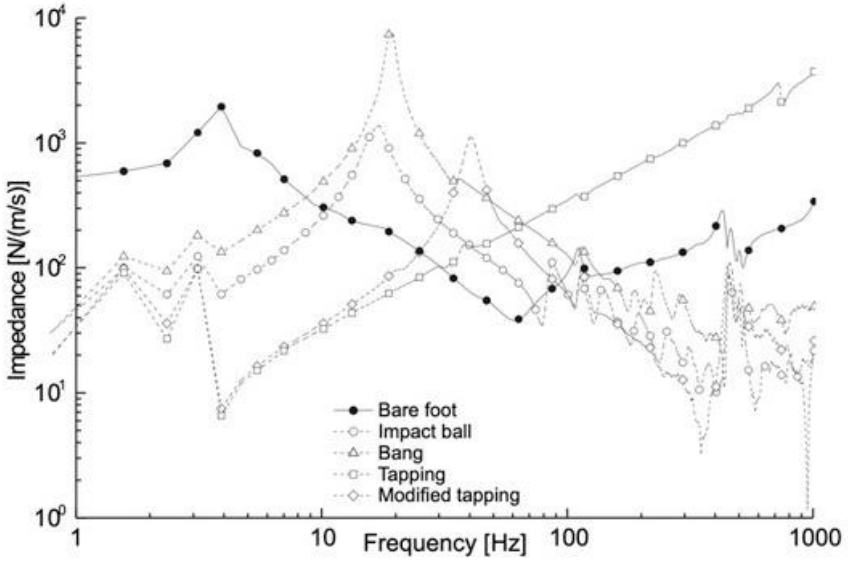

Figure 2.4 Impedance of various impact sources [28].

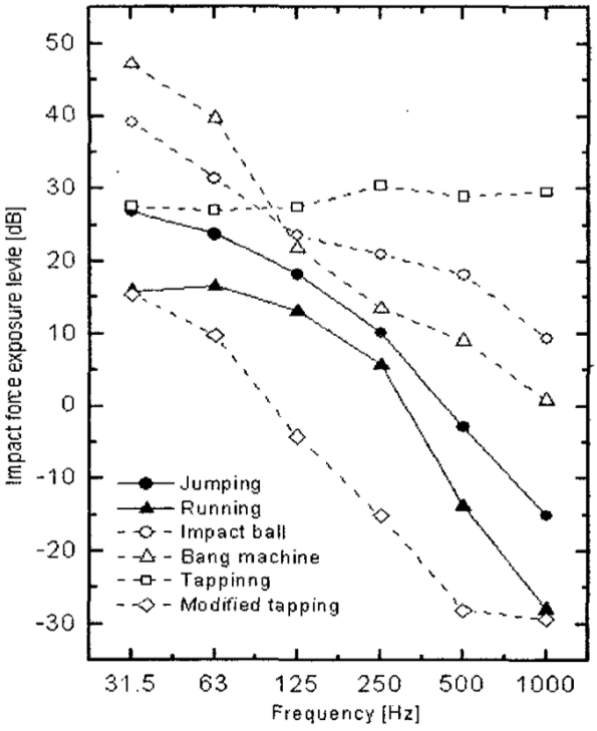

Figure 2.5 Impact force exposure level for different sources [29].

Although there are multiple benefits related to the use of the rubber ball as a standard impact source, there are no reliable prediction models for impact sound insulation of floor assemblies using the impact rubber ball. Prediction models for sound transmission in buildings such as ISO 15712-2 [30] use statistical energy analysis (SEA), which works for stationary or quasi-stationary impact sources like the ISO tapping machine but not for the impact rubber ball, which produces transient (impact) sounds. Moreover, while the impact rubber ball is most effective at producing low frequency impact noise, it does not produce enough high-frequency sound and is ineffective at exciting structures at high frequencies [27]. Therefore, due to the abovementioned reasons as well as the tapping machine's long history and large amounts of available data, the tapping machine has never been abandoned [31].

In a study conducted by Roozen and his peers [32], a new measurement procedure, which assessed the airborne sound insulation of partitions from mobility vibration measurements, was suggested. He proposed a method that provides an estimate for the radiated sound power that only depends on the properties of the partition while neglecting the source altogether. In his method, he found that his approach is consistent with the standardized ISO10140-2:2010 measurement approach, which is based on the diffuse field assumption. While there were significant discrepancies at frequencies below the Schroeder frequency (100Hz-200Hz) due to the breakdown of the diffuse field assumption, the findings suggest that for airborne sources, the effects of the source-receiver interaction are insignificant (for frequencies above the Schroeder frequencies).

As for structure-borne sound insulation, in an approximate method for obtaining source quantities for the calculation of structure-borne sound transmission into lightweight buildings, Mayr & Gibbs [33] studied the effect of the blocked force condition approximation (also known as the force-source condition), where the mechanical mobility of the receiver is considered to be much lower than that of the source. The blocked force condition assumption is often made by engineers when dealing with impact sound transmission. If the blocked force condition holds, the source-receiver interaction is neglected. As shown in Figure **2.6**, making the blocked force condition assumption causes a substantial overestimation of the power injected into the structure. However, while the Mayr and Gibbs study addressed structure-borne sound power, it was only conducted on a centrifugal fan unit rigidly attached to a timber joist floor, which is considered a mechanical

installation in a lightweight building and does not specifically address impact sources or other receivers.

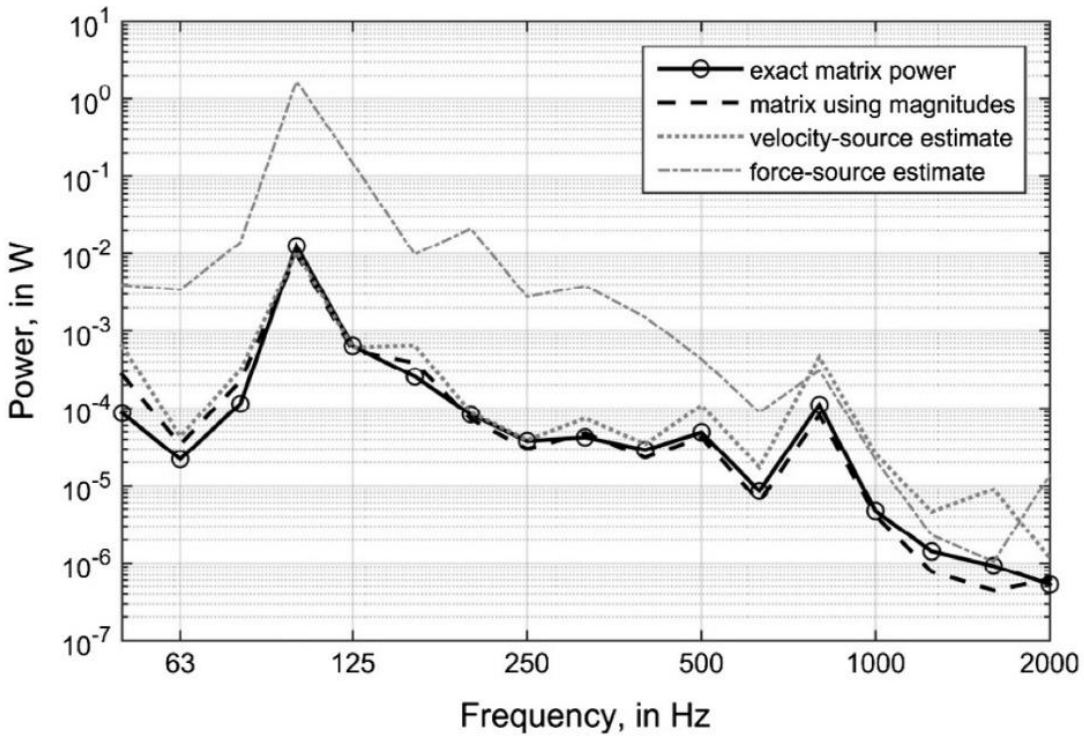

Figure 2.6 Power injected by fan on timber joist floor, employing the force-source estimate [25].

So, what about impact sources? Figure **2.7** references the analytical study mentioned in the first paragraph of this section [16] and shows the difference in normalized (by the force of the source) power injected (due only to mobility matching) between the impact ball and the tapping machine for a frequency range from below 63Hz to over 4000Hz. It is seen that due to mobility matching only, they both inject equal amounts of power into the concrete floors throughout the whole range of frequencies as a consequence of the concrete having a much lower mobility than the sources, and therefore, the blocked condition approximation holds. As for the two lightweight OSB floors of different thicknesses, the power injected into them by the tapping machine and the impact rubber ball is also about the same amount (with the thicker one having slightly less power injected) but only until about 500Hz. For higher frequencies, the tapping machine injects more power than the

impact ball. This implies that below 500Hz, mobility matching did not have an influence regarding impact sound transmission. However, only analytical models were considered. In addition, assemblies that included floating floors were also not considered, which might add a resonance below 500Hz to the system and ultimately affect the power injected due to mobility matching. Moreover, when adding a floating floor, it is expected that the receiver mobility increases, and therefore, the blocked force condition approximation may no longer hold since the receiver mobility now better matches the source mobility. In conclusion, more research is required in the investigation of the source-receiver interaction for impact sources and its effects on the power injected.

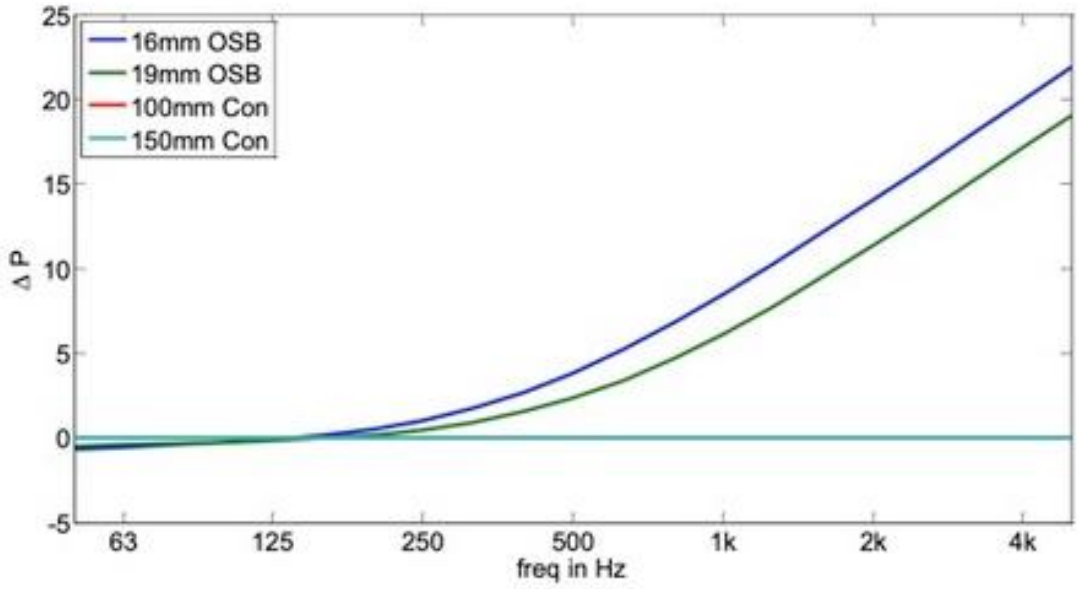

Figure 2.7 Difference in power injected between Hammer and Ball. Positive value means Hammer injects more power into floor due to mobility matching than Ball. Red curve is hidden under light blue curve [31].

In another study, conducted by Warnock [31], it was shown that the mean difference between the impact sound pressure levels produced by the standard tapping machine and those produced by a walker for different floor toppings vary. As shown in Figure **2.8**, the spectra vary mostly above 500Hz but they begin to vary at around 125Hz for carpeted floors. This would mean that the

blocked force condition approximation does not apply in this case while the source-receiver interaction matters, since the difference between the two impact sources' (namely the tapping machine and the walker) impact SPL spectra is not constant and varies from one receiver floor topping to another. Ultimately, this suggests that studying the source-receiver interaction when floor coverings are involved is also important.

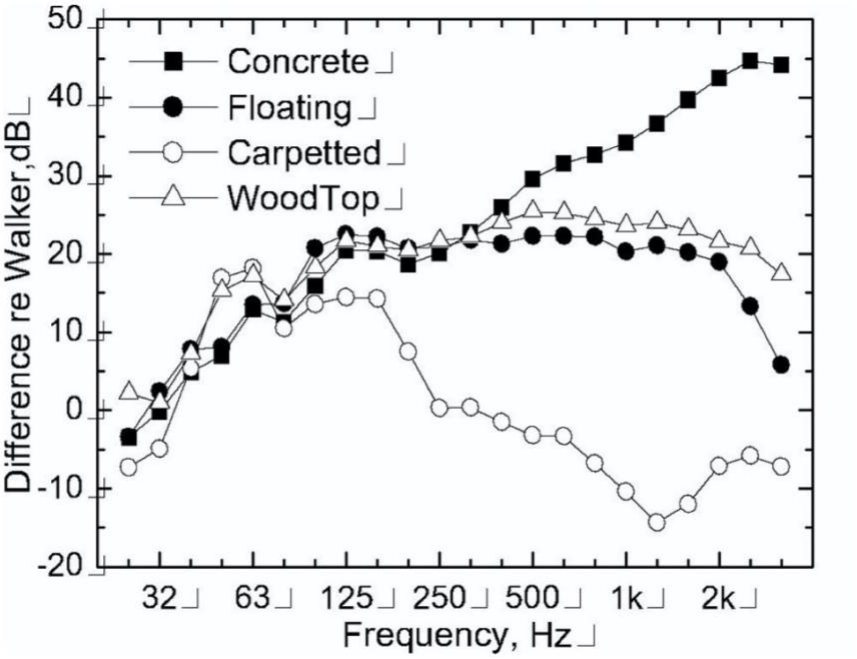

Figure 2.8 Mean difference between tapping machine spectrum and walker spectrum when using different floor toppings [31].

3 Theoretical Background

The following chapter reviews the theory behind the various concepts used in this project to study the source-receiver interaction for impact sources. The sections cover impact sound transmission, power injected and source-receiver coupling, floating floors, standard impact sources, and analytical models

3.1 Impact sound transmission

Impact sound transmission can be described, as shown in Figure **3.1**, by dividing it into two components: direct transmission and flanking transmission. Direct transmission is when the impact sound energy is transmitted directly through the floor, and it is rated by the Impact Insulation Class (IIC). Flanking transmissions are structure-borne transmissions that run across the floors, through the junctions and finally radiate off the walls. Both transmissions are summed to yield the Apparent Impact Insulation Class (AIIC), which represents the apparent transmission. Direct transmission measurements, or the IIC, can only be obtained in the lab where the flanking transmission is controlled and supressed. ASTM E492 [34] is the standard method of testing for the lab measurement of impact sound transmission through a floor-ceiling assembly using the tapping machine as the standard impact source. However, in the field (standard ASTM E1007 [35]), the AIIC is instead acquired through measurements due to the presence of flanking [36].

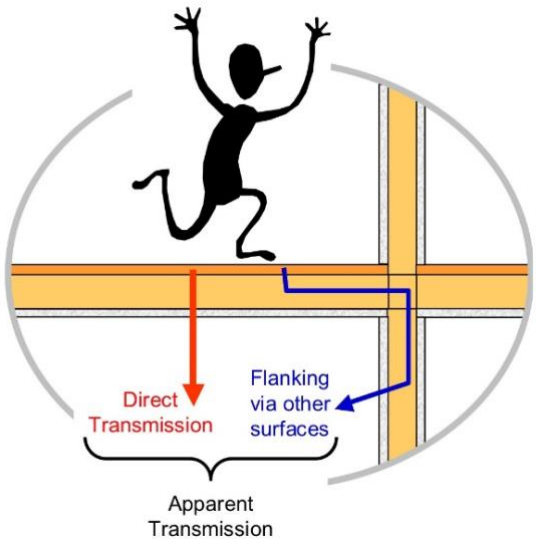

Figure 3.1 Impact sound transmission caused by a walker [36].

Trevor Nightingale developed the 5-factor method, which explains the steps through which flanking transmission occurs [12,13,14]. It separates flanking paths into five components. It is simplified and illustrated in Figure **3.2**. The first factor is the power injected into the structure. How much power is injected by the source into the receiver depends on the source-receiver interaction, which is also called the coupling. The coupling between an impact source and a receiver depends on the mechanical mobility match between the two. The impedance is simply the inverse of the mobility (explained in Section 3.2), where the theory behind the power injected and coupling is also further explained. The second factor is called the attenuation with distance, and it is the distance from the source to the junction. The further the source is to the junction, the more attenuation will occur, and less power is transmitted to the junction, ultimately decreasing flanking transmission. The next factor corresponds to the junction attenuation, which is simply the power attenuated at the junction. Many difficulties have been associated with determining the junction attenuation for lightweight assemblies [37,38]. As for the structural attenuation, it is the fourth factor and corresponds to the attenuation with distance from the junction on the flanking surface in the receiver room. Finally, the fifth and final factor is the radiation of the structure-borne sound into the receiving space, and it is influenced by the radiation impedance between the source and the receiver, also known as the radiation efficiency. The flanking sound power is the result of all five factors [13].

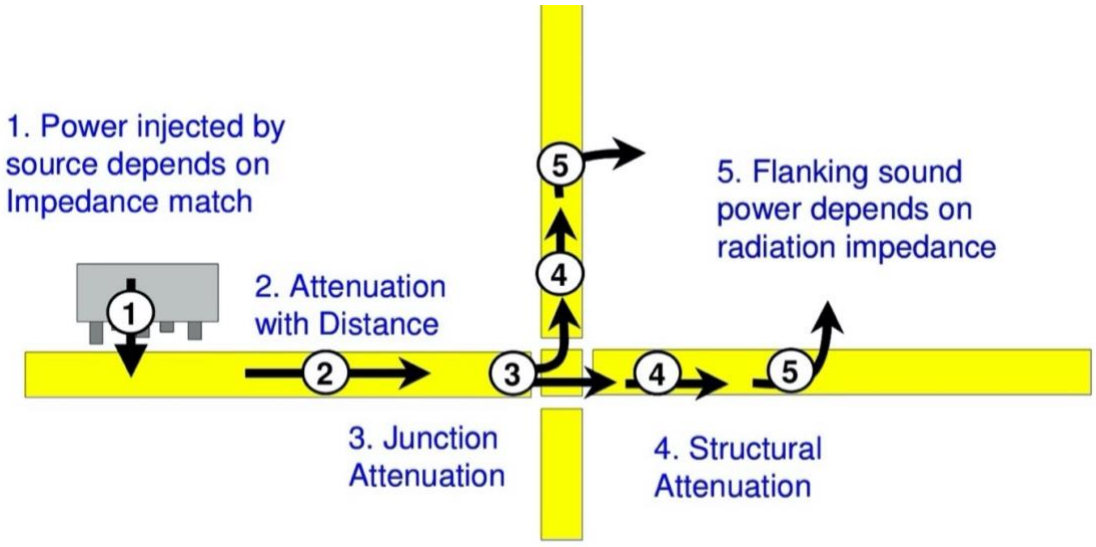

Figure 3.2 Nightingale's 5-factor method for impact sound transmission [12].

In a laboratory environment, the abovementioned flanking influences are minimized. For instance, the specimen being tested will have seals by their edges and corners to prevent transmission through the junctions. On site, flanking transmission paths are not supressed as such. Furthermore, rooms are much smaller and may include objects that would increase attenuation with distance. For these reasons, on site measurements take flanking into consideration by using the metric AIIC while lab measurements will yield IIC.

All impact sound transmission testing standards essentially follow the same procedures. In a source room, which is on top of the receiving room separated by the floor assembly being tested, an impact is made using a standardized impact source, such as the tapping machine or the impact rubber ball. The impact excites the assembly structurally, and the sound pressure level is measured in the receiving room [27].

This thesis investigates the first factor from Nightingale's 5-factor method: the injected power. More specifically, it investigates how the power injected is influenced by the source-receiver interaction. As read from Figure **3.2**, the power injected depends on the impedance match between the source and the receiver. That is equivalent to saying the power injected depends on the mobility match between the two, since mobility and impedance are inverses of each other. The mobility match and its effect on the power injected is represented by the source-receiver coupling function, which is introduced next.

3.2 Power Injected & Source-Receiver Coupling

The power injected into a receiver structure by a source at impact may be expressed as

$$\underline{Q} = \left|\frac{\underline{v_r}}{\underline{Y_r}}\right|^2 \cdot \underline{Y_r} \tag{1}$$

All variables are frequency dependent. The underbar underneath the variables means that they are complex numbers. In Equation 1, $\underline{v_r}$ is the vibrational velocity of the receiver at the point of contact

between the source and receiver at impact, while $\underline{Y_r}$ is the mechanical mobility of the receiver. The variables are expressed in the frequency domain.

The mechanical mobility $\underline{Y}$, shown by Equation 2 below as the velocity divided by the force, represents the willingness of a structure to vibrate when a certain harmonic force is applied to it. The velocity $\underline{v}$ represents the vibration of the structure while the force $\underline{F}$ is the applied harmonic force on the structure. Therefore, between two structures with different mechanical mobilities, the one with a higher mobility requires a smaller applied harmonic force for it to vibrate the same amount. The impedance is the inverse of the mobility: the force divided by the velocity. It is just the opposite way to express the response of a structure to a harmonic force, by describing the resistance of a structure to vibrate rather than its willingness [39].

$$\underline{Y} = \frac{\underline{v}}{\underline{F}} \tag{2}$$

Figure **3.3** shows a linear network analogy representing a source-receiver system. It is used to yield the variables $\overline{v_r}$ and $\overline{F_c}$, which are the velocity of the receiver at contact and the force applied at that contact point; they are shown by Equations 3 and 4 respectively. The free source velocity, $\underline{v_{sf}}$, is a property of the source, and it represents its internal velocity when unconstrained. It describes the source activity by rating its internal vibration. $\underline{Y_s}$ is the source mobility [11, 40, 41].

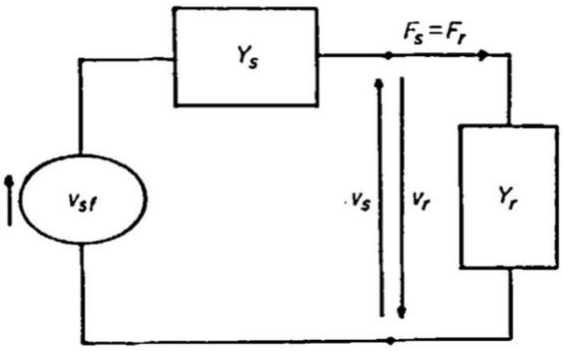

Figure 3.3 Electrical linear network analogy for a source-receiver system [11].

$$\underline{v_r} = \left(\frac{\underline{v_{sf}}}{\underline{Y_s} + \underline{Y_r}}\right) \cdot \underline{Y_r} \tag{3}$$

$$\underline{F_C} = \frac{\underline{v_{sf}}}{\underline{Y_s} + \underline{Y_r}} \tag{4}$$

The power injected may also be represented by Equation 5, as only the product of two variables: the source descriptor and the coupling function [11].

$$\underline{Q} = \underline{S} \cdot \underline{C} \tag{5}$$

Shown in Equation 6, the first parameter $\underline{S}$ is the source descriptor, a complex variable which has the dimension of power. It characterizes the impact source as it depends only on the free source velocity, $\underline{v_{sf}}$ and the complex conjugate of the source's mechanical mobility, $\underline{Y_s}^*$. The source descriptor accounts for the source's internal vibration, through the free source velocity, as well as its dynamic properties at the contact point, through the mobility (of the source). It is unique to every source and therefore can be used to compare different sources. In the context of this thesis, the best source will have the lowest source descriptor value, as it will yield the lowest magnitude of power injected on the same receiver. The asterisk represents the complex conjugate of the complex value [11].

$$\underline{S} = \frac{\left|\underline{v_{sf}}\right|^2}{\underline{Y_s}^*} \tag{6}$$

Alongside the source descriptor, the second variable upon which the power injected depends on is the coupling function, presented in Equation 7. The coupling function $\underline{C}$ is a function of both the mobilities of the source and receiver. It describes the interaction of the dynamic properties of the source and receiver (their mobilities) at the contact point; it represents the source-receiver

interaction for impact sources. It is a representation of how that interaction would facilitate the transfer of power through their interface. It can be perceived as a transfer function between the source descriptor and the power injected. The higher the coupling function value, the more power is allowed to be injected by the source to the receiver [11]. It is expressed as follows:

$$\underline{C} = \frac{\underline{Y_s}^* \cdot \underline{Y_r}}{\left|\underline{Y_s} + \underline{Y_r}\right|^2} \tag{7}$$

α, shown in Equation 8, is the ratio of the magnitude of the receiver and source mobilities. The phase difference between the receiver and source mobilities is given by $\Delta\phi$, shown in Equation 9. They may both be used to rewrite the coupling equation seen in Equation 7 as the one seen in Equation 10. Moreover, the coupling function can be illustrated in a plot as a function of α and $\Delta\phi$, as shown in Figure **3.4**. Figure **3.4** shows the level of the coupling function versus the ratio of receiver to source mobility, α, for various phase differences, $\Delta\phi$. It is a useful plot which depicts how the mobilities (and phases) of a source and receiver interact with one another, and ultimately how that affects the power injected by a source into a receiver for impact sources [11]. It is seen from Figure **3.4** below that the magnitude of coupling is at its maximum when the mobility of the source and the receiver match and when their phase difference is at its largest; that is when source mobility and the receiver mobility are complex conjugates of each other. On the other hand, when the source and receiver mobilities differ widely in magnitude, there is a lot less coupling between them, and ultimately, less power transmitted into the receiver by the source. From top to bottom, the different curves correspond to the phase differences of π, $\frac{5}{6}\pi$, ¾ π, ½ π, $\frac{1}{3}\pi$, and 0 [11, 41].

$$\underline{\alpha} = \frac{\underline{Y_r}}{\underline{Y_s}} \tag{8}$$

$$\Delta\phi = \phi_r - \phi_s \tag{9}$$

$$\underline{C} = \frac{|\underline{\alpha}|}{|1+\underline{\alpha}|^2} \cdot e^{j\phi_r} \tag{10}$$

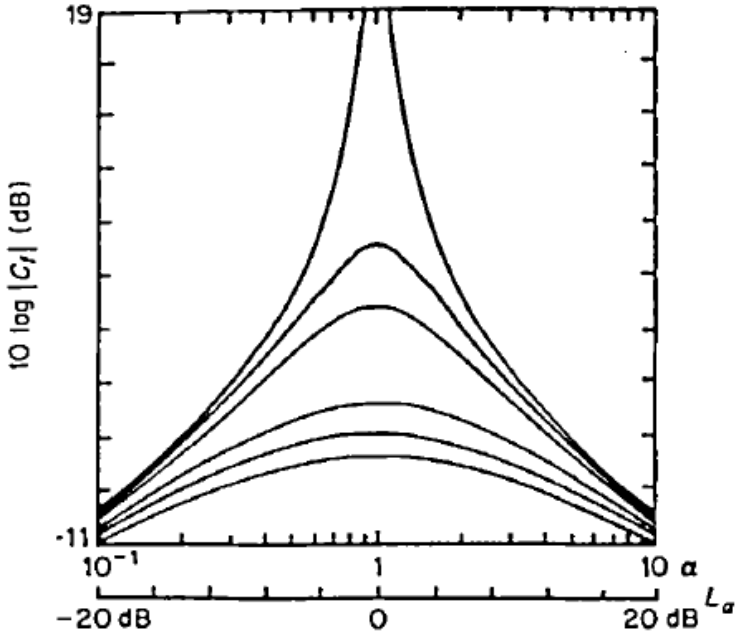

Figure 3.4 Coupling as a function of receiver-to-source mobilities ratio and their phase difference. From top to bottom, the different curves correspond to the phase differences of π, $\frac{5}{6}\pi$, ¾ π, ½ π, $\frac{1}{3}\pi$, and 0 [11].

The case in which the source mobility is much greater than the receiver mobility (α <<< 1), which corresponds to the left side of Figure **3.4**, is called the blocked condition. The opposite case, when the receiver mobility is much greater than the source mobility (α >>> 1), which corresponds to the right side of the figure, is called the free source condition [11, 41]. When either one of these approximations is made, the source-receiver interaction is neglected altogether. This thesis investigates the validity of the blocked condition in particular, as it is an assumption that is often made when it comes to impact sound transmission (it is often assumed that the source mobility is much greater than the receiver mobility).

When the blocked force condition approximation is made, the contact force $\underline{F_c}$, found in Equation 4, is replaced with the blocked force $\underline{F_b}$. The free source velocity, $\underline{v_{sf}}$, is now dependent upon the blocked force instead of the contact force. The blocked force can be defined as the force required to prevent a source from vibrating [42]. Moreover, since it is assumed that the source mobility is much greater than the receiver mobility, we can omit the receiver mobility from Equation 4. Finally, we can rearrange for the free source velocity to yield:

$$\underline{v_{sf}} = \underline{F_b} \cdot \underline{Y_s} \tag{11}$$

Similarly, when making the blocked condition approximation, the receiver mobility may be omitted from the denominator of the coupling function (Equation 7). Afterwards, if we substitute the source descriptor (Equation 6) and the coupling function into the power injected equation (Equation 5), we obtain the following Equation 12 for the power injected when the blocked force condition approximation is made:

$$\underline{Q_b} = \left|\underline{F_b}^2\right| \cdot \underline{Y_r} \tag{12}$$

Equation 12 implies that the power injected into a structure by an impact source when the blocked force condition approximation is made is independent of the source mobility, which also means that the source-receiver interaction will have no effect on it. It is only dependent on the receiver mobility, as well as the blocked force of the source. In order to investigate the validity of the blocked force condition approximation and study the actual effect of the source-receiver mobility on the power injected, E_Q is calculated by Equation 13. E_Q is the relative error in percent between the power injected (Equation 1), versus the power injected when the blocked force condition approximation is made (Equation 12). Note that Equation 13 is only dependent on the source mobility and the receiver mobility and that expressed as a percentage.

$$E_Q = \left[1 - \left(\frac{\left|\underline{Y_s} + \underline{Y_r}\right|}{\left|\underline{Y_s}\right|}\right)^2\right] \cdot 100\% \tag{13}$$

3.3 Floating Toppings

Floating toppings are effective at minimizing vibration transmissions through floor assemblies, ultimately reducing impact sound transmission and improving attenuation. They are also often referred to as floating floors. The improvement of impact sound insulation, ΔL, is the metric used to quantify the acoustical attenuation effectiveness of a floating floor. Floating floors consist of a floating slab which sits on top of a resilient interlayer, which rests on the base floor, as seen from Figure **3.5**. The resilient interlayer is highly elastic and decouples the floating slab from the base floor. It is also assumed that the floating slab is decoupled from the lateral walls as well [43].

Floating floors can be modelled as mass-spring-damper systems, with the floating slab being the mass (represented by *m*), and the resilient interlayer being the spring (with stiffness constant *k*) and the damper (with damping constant *c*), as shown in Figure **3.5** below.

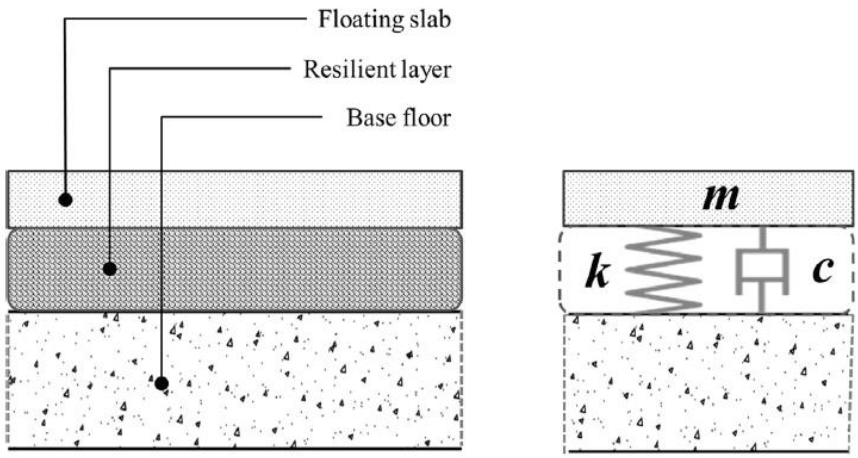

Figure 3.5 Section of a floating floor setup and mechanical model [43].

ASTM E2179 [44] dictates the standard test method followed for the laboratory measurement of the effectiveness of a floating floor in reducing impact sound transmission. The improvement of impact sound insulation of a floating floor, ΔL, shown by Equation 14, is defined as the difference between the sound pressure level in a receiving room due to an impact on the base floor, L_{n0}, and the corresponding sound pressure level caused by the same impact on the floating floor on top of the base floor, L_n [43].

$$\Delta L = L_{n0} - L_n \tag{14}$$

Figure **3.6** shows the results obtained at the National Research Council Canada (NRC) floor-testing facility of the improvement of a laminate floating floor on a 6-inch concrete slab. It is representative of a typical set of results for the improvement of a floating floor; as shown, they are much more effective at higher frequencies.

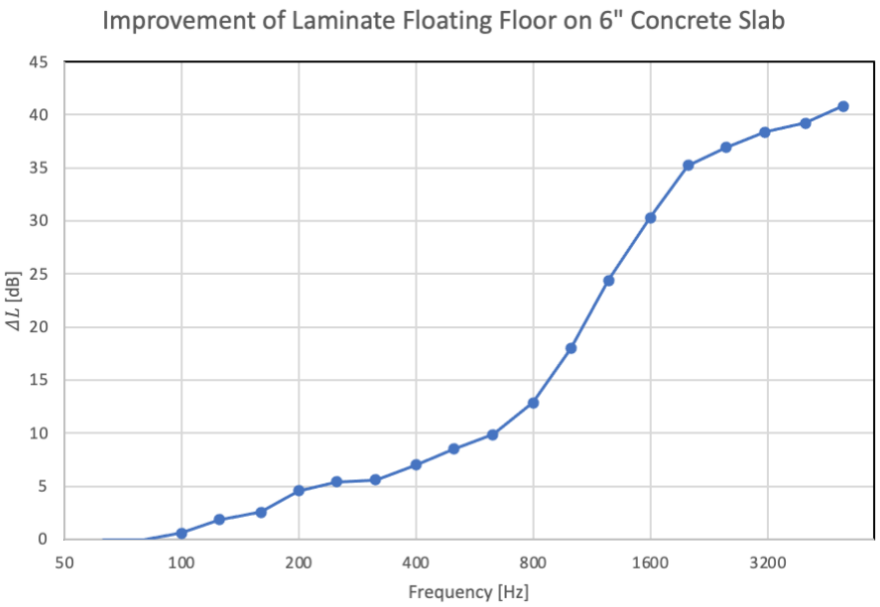

Figure 3.6 Improvement of a laminate floating floor on a 6-inch concrete slab [45,46].

Floating floors are of particular interest when discussing the source-receiver interaction because they generally increase the mobility of the receiver structure. This will affect the source-receiver interaction, and depending on the source, could bring α closer to 1. This could be problematic when assuming the blocked force condition, which assumes the source mobility to be much greater than the receiver mobility. Moreover, floating floors may introduce resonance frequencies at lower frequencies, which would ultimately increase the mobility of the receiver at those frequencies, making the source-receiver interaction more relevant [16].

In a follow-up study where floor assemblies with floating floors were tested [47], it was seen that adding a floating floor to two very different heavyweight and lightweight base floors had almost the same effect on the measurements taken with the tapping machine and the impact rubber ball. This implies that even with applying a floating floor, the source-receiver interaction does not have a significant effect since the source mobility is still much greater than the receiver mobility, and the blocked source condition approximation still holds. However, the study from reference 47 was only based on one analytically modelled floating floor. The current project investigates the effects of floating floors further by taking actual measurements of specimen with floating floors.

3.4 Analytical Models

In this section, a simple analytical model is shown for the mobility of an infinite plate, which is used to model the mobility of the floor receivers, as well as a model for the mobility of a lumped mass, which is used to model the mobility of the steel hammer heads of the tapping machine. The analytical models are used for reference and comparison with the measured data.

3.4.1 Mobility of a homogeneous, infinite plate

While there are more advanced models, such as one for the mobility of a finite plate [41], the model shown in Equation 15, representing the mobility of a homogenous infinite plate, will suffice for the purpose of this study. B is the bending stiffness, ρ is the density of the material and h is the height of the plate.

$$Y_f = \frac{1}{8 \cdot \sqrt{B \cdot \rho \cdot h}} \tag{15}$$

The equation for the bending stiffness B of an infinite plate is given by the Equation 16, which depends on C_L, the speed of sound of longitudinal waves in a homogenous, infinite plate, ρ and h.

$$B = \frac{{C_L}^2 \cdot \rho \cdot h^3}{12} \tag{16}$$

However, for orthotropic materials such as CLT, whose properties depend on the measurement direction, the effective bending stiffness is calculated. The effective bending stiffness of an

orthotropic material $B_{effective}$ is defined in Equation 17, where B_x and B_y are the bending stiffnesses in the x-direction and y-direction, respectively

$$B_{effective} = \sqrt{B_x \cdot B_y} \tag{17}$$

The equation for the speed of sound of longitudinal waves in a homogenous, infinite plate C_L is shown by Equation 18, where E is Young's modulus and v is Poisson's ratio.

$$C_L = \sqrt{\frac{E}{\rho \cdot (1 - v^2)}} \tag{18}$$

3.4.2 Mobility of a lumped mass

The mobility of the tapping machine steel hammer heads is modelled using the Equation 19, which represents the mobility of a lumped mass. The mass of the steel hammer head of the tapping machine is $m_h =$ 0.5kg and $j = \sqrt{-1}$. The mobility of a lumped mass is given by

$$Y_h = \frac{1}{j \cdot \omega \cdot m_h} \tag{19}$$

Although there exists a more sophisticated analytical model for the blocked force of the ISO tapping machine [48], for the purpose of this thesis, the simple model shown below by Equation 20, where h_d is the drop height and f_r is the hammer frequency (10Hz), was sufficiently accurate; that is because all the models differ only in the frequency range and all give the same answer for the entire frequency range which we consider for this project, which is 20-3000Hz.

$$F_b = 2 \cdot f_r \cdot m_h \cdot \sqrt{2 * g * h_d} \tag{20}$$

4 Methods and Materials

The following chapter outlines the methods and materials used for this project. It begins with the methods, followed by the materials and tools used to implement the methods.

4.1 Methods

In order to attain the objectives of this project, which are to investigate the significance of the source-receiver interaction and to find the most appropriate measurement setups for the mobility of the sources and receivers, the following methodology was applied. Firstly, the mobility of the impact sources was measured. The sources include the two most common standard impact sources, namely the tapping machine and the impact rubber ball, as well as the foot of a human walker, with and without shoes. The second step was to measure the mobility of the floor receivers. The receiver specimen included a bare 6-inch concrete floor, the same concrete floor but with a laminate floating topping, a bare 5-ply CLT floor, and the same CLT floor but with a laminate floating topping. Afterwards, the injected power was computed for every source-receiver combination when making the blocked force approximation (neglecting the source-receiver interaction) and considering the source-receiver interaction. Finally, the source-receiver interaction and its influence in each source-receiver combination was analyzed with the help of the relative error percentage between both the powers injected (when making the blocked force approximation and when considering the source-receiver interaction). To find the most appropriate measurement configurations for both the impact sources and floor receivers, multiple measurement settings and setups using various tools were attempted and compared.

4.2 Materials

The materials comprise of the excitation tools including the impact hammer and electrodynamic shaker, the standard impact sources, namely the tapping machine and the impact rubber ball, the floor receiver specimen, the various sensors used, the data acquisition device, and the force plate. Manufacturers, model numbers, and specifications are provided as well.

4.2.1 Excitation Tools

The excitation tools used in this project, namely the impact hammer and the electrodynamic shaker, are instruments that are commonly utilized for the measurements of mechanical mobility

of a specimen. For this project, they were used to measure the mobility of both the impact sources as well as the receiver floor assemblies.

Impact hammer

Manufactured by PCB Piezotronics, the Impact Hammer Model 086B20 (short sledge) was used, which is shown in Figure **4.1**. It is a part of the Impulse Hammer Kit No. 291B20, which also includes a force sensor (Model 205M08) and two accelerometers (Models 302A02 and 308B). Moreover, also included in the kit are four different types of hammer tips that are available for use: super soft (grey), soft (brown), medium (red), and hard (black).

Figure 4.1 The Impact Hammer with the hard tip.

The impact hammer is operated by tapping it lightly next to the desired measurement position, where an accelerometer will be placed. It is connected to a force sensor, which provides a measured force signal at impact. That force signal is then used alongside the corresponding acceleration response obtained via the accelerometers placed on the floor to compute the mobilities. However, since the mobility is the velocity over force, the acceleration signal must first be integrated to obtain the velocity.

The selection of the type of hammer tip depends on the floor being tested. The heavier a structure, the harder of a hammer tip can be used. However, when the hammer tip is too hard for the floor being tested, it overloads the input of the soundcard, which is based on the combination of excitation, sensor sensitivity and input range of the soundcard. This produces an error known as clipping. On the other hand, using a softer hammer tip decreases the effectiveness of the excitation, making it ineffective for higher frequencies. Therefore, the hardest hammer tip which can be used on a floor without causing the measurement to clip should be the one that is selected for a measurement. In this project, the hard tip (black) was used for the bare floor measurements while the medium tip (red) was used for the specimen with floating floors.

The benefits of the impact hammer are its portability and ease of use. However, at higher frequencies, depending on the specimen being tested and the type of hammer head used, its excitation does not work as well and inconsistencies in the force signals could occur.

Electrodynamic shaker

For the electrodynamic shaker, the K2004E01 model by The Modal Shop, shown in Figure **4.2**, was used. It can provide up to 31N peak sinusoidal force and is run through a 12-21 VDC supply. One main benefit of this model is that it does not require a separate power amplifier to function, as it already includes an integrated amplifier [49]. This makes the measurement setup of the electrodynamic shaker, which is laborious as is, one step simpler.

Figure 4.2 The K2004E01 electrodynamic shaker by The Modal Shop [49].

The electrodynamic shaker is mounted to a shaker support structure which keeps it in place during measurements. For floor specimen measurements, it is attached to a horizontal shaker support, as shown in Figure **4.3**. For the measurements of the impact sources, it is attached to a vertical shaker support, as shown in Figure **4.4**. The shaker can slide across the shaker supports and is locked in position when the measurement is ready to be taken. An impedance head, which is a sensor that measure both force and acceleration, is mounted to the shaker's stinger. The stinger is the column sticking out of it (as seen in Figure **4.2**), used to pinpoint the measurement position. Finally, the shaker injects a force through the stinger, which excites the specimen. The impedance head provides both the acceleration and the force at the point of measurement. As with the impact hammer, the acceleration is integrated to yield the velocity, which is used alongside the force to obtain the mobility.

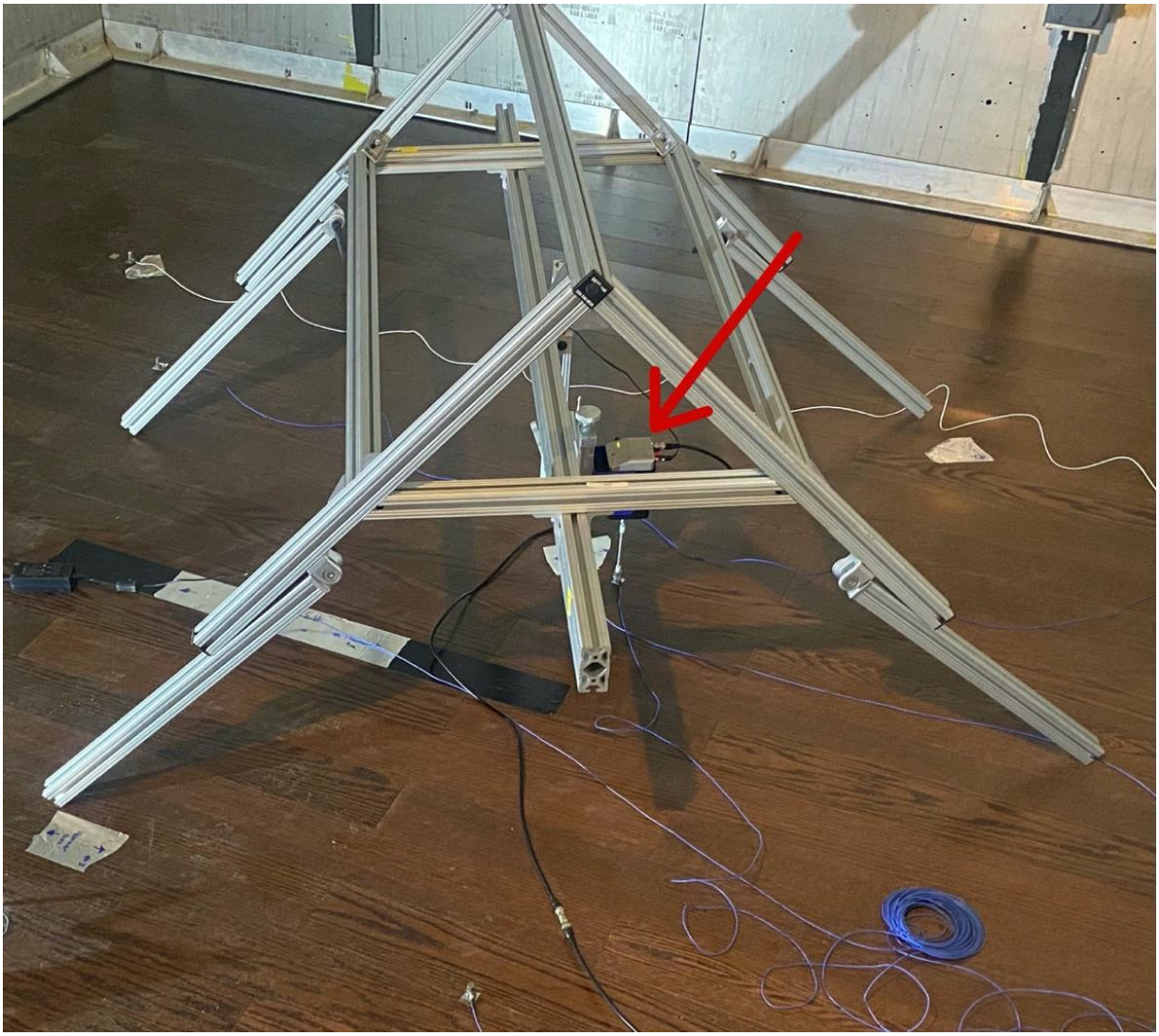

Figure 4.3 Electrodynamic shaker mounted to horizontal shaker support during floor measurement.

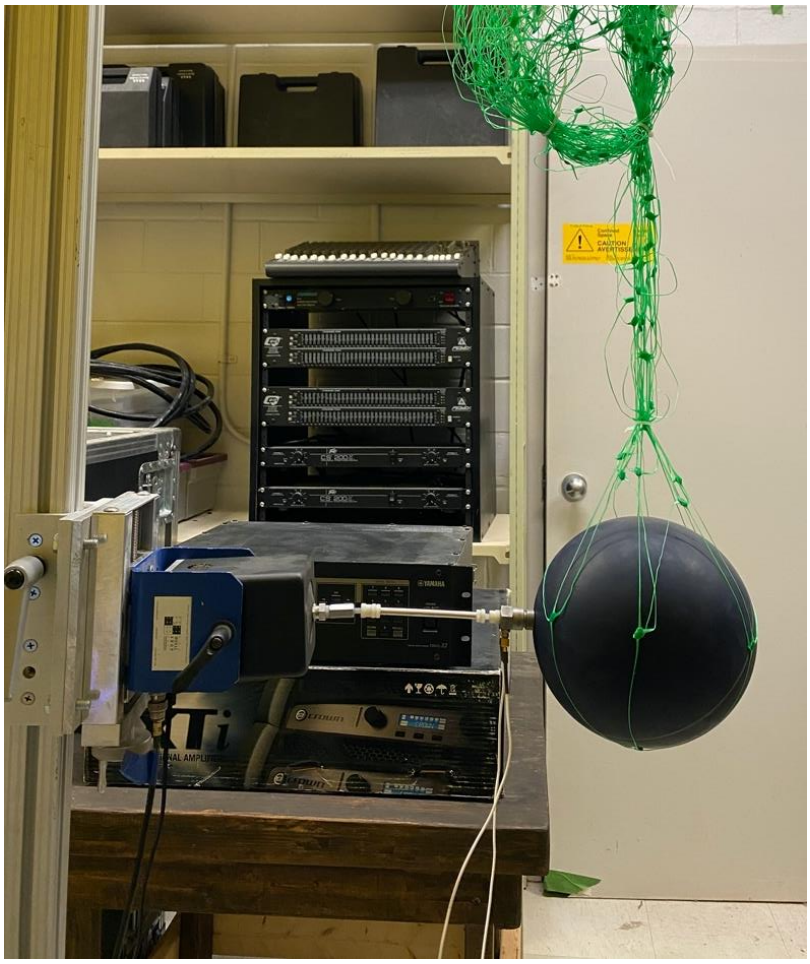

Figure 4.4 Shaker mounted to vertical support during measurement of impact rubber ball.

The issues seen with the impact hammer at higher frequencies do not occur with the shaker. Its disadvantage is its setup; it is a lot more strenuous. A comparison of results obtained by the impact hammer and electrodynamic shaker is elaborated upon in the Results Section (Section 7.1).

4.2.2 Standard Impact Sources

This subsection presents the standard impact sources, whose mobilities were measured for the purpose of this project. They are the two most used standard impact sources in the industry, namely the standard tapping machine and the impact rubber ball, respectively. It also includes some of their specifications as well as pictures of them. More details on these standard impact sources are reviewed in the Literature Review (Chapter 2).

Tapping machine

The tapping machine, shown in Figure **4.5**, is a standard impact source, as described in the Literature Review. It continuously drops, one after the other, five 500g +/- 6g, steel hammers with spherical contact points, spaced apart by 100 +/- 3mm, onto the test floor from a height of 40 +/- 3mm at a frequency of 10 drops per second (or 2 drops per second per hammer), producing steady state noise [50].

Figure 4.5 The standard Tapping Machine.

Impact rubber ball

The impact rubber ball is the second most commonly used standard impact source. It weighs 2.5 +/- 0.1kg and has a diameter of 178mm. It is dropped from a height of 1 meter and produces an impact sound, as opposed to the continuous noise of the tapping machine [28]. It was redesigned in 2001 by Japanese company RION and made with silicone rubber instead of the former Styrene Butadiene Rubber to make it more resistant to the effects of varying temperatures. The one-meter-long stick seen in Figure **4.6** is used to help take the measurement from the correct

height. Although the rubber ball has been shown not to be a linear source, it has been shown that the error related to small variations in drop height is small [27].

Figure 4.6 The Japanese Impact Rubber Ball.

4.2.3 Floor Receiver Specimen

The following subsection lists the measurement specimens for this project, in the order of the tests. It provides their dimensions and mass per unit area.

Bare Concrete Slab

A 6-inch (152.4mm) bare concrete slab was used for this project. It has a mass per unit area of 350 kg/m^2. C_L is 5572.78 m/s and B is 21.07 MPa.

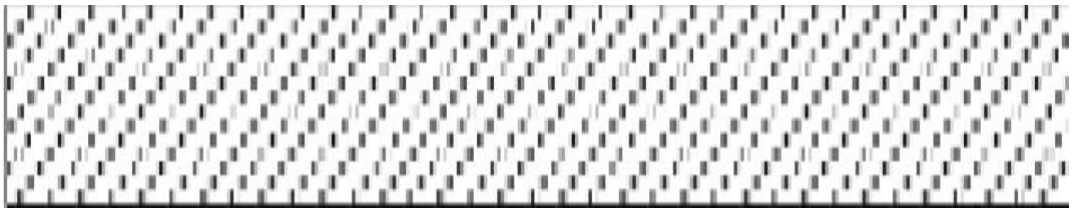

Concrete Slab with Laminate Floating Floor

Next, a laminate floating topping was installed on the same 6-inch concrete slab shown above. The laminate floating topping is made out of a 2mm cork interlayer and 8mm laminate top layer.

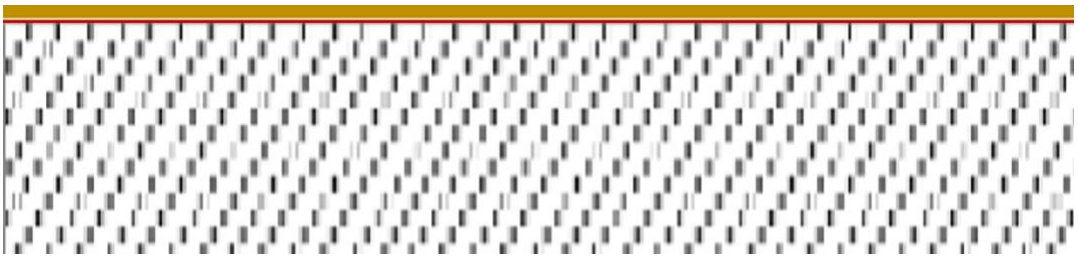

Bare CLT Slab

The following specimen is the CLT slab. It is a 5-ply CLT slab, with a thickness of 175mm. Its mass per area is 91 kg/m^2. C_{L_1} and C_{L_2} are 6264.7 m/s and 1400.83 m/s and B_x and B_y are 9.11 MPa and 0.46 MPa, respectively. The effective bending stiffness $B_{effective}$ is 2.04 MPa.

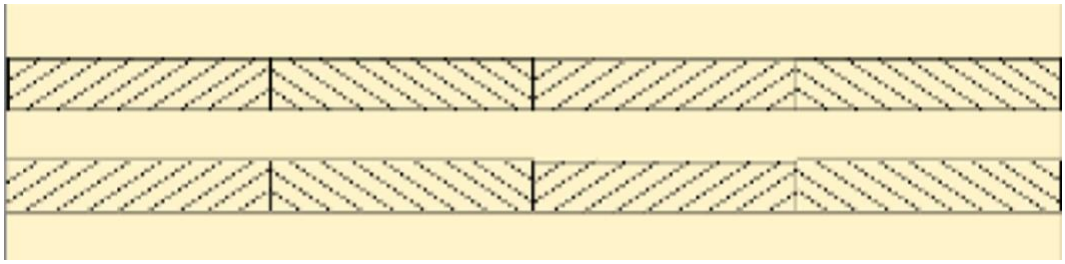

CLT with Laminate Floating Floor

Finally, the CLT with laminate floating floor specimen used the same CLT slab shown previously and the same floating floor as the one used for the 6-inch concrete slab.

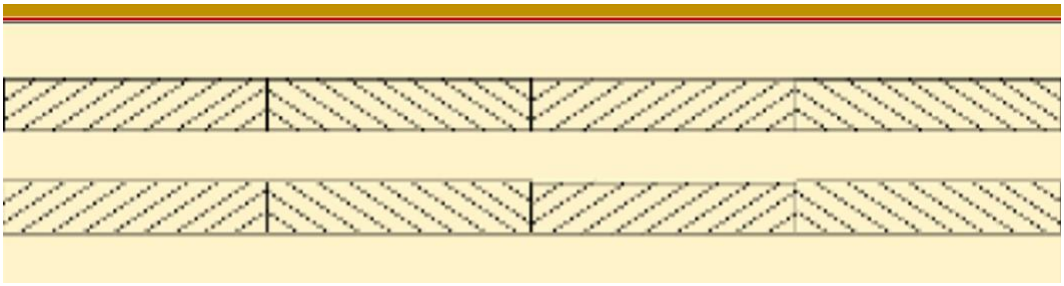

4.2.4 Sensors

Several types of sensors were utilized in this project: accelerometers, a force sensor, and an impedance head. Each type is elaborated upon in the following subsections. All sensors used in this project are manufactured by PCB Piezotronics. Before the commencement of floor specimen measurements, all accelerometers were calibrated to ensure accurate readings.

Accelerometers

Accelerometers of model 352C33 were used in the measurements involving the floor specimen. They measure the acceleration of the specimen at the point where it is mounted. This measurement gives insight on the vibration caused at the point of measurement due to the excitation provided. To mount an accelerometer to a floor specimen, as seen in Figure **4.7**, a small magnetic plate is kept in position using a double-sided adhesive tape, and the accelerometer is then placed on the magnetic plate.

Figure 4.7 Accelerometer mounted to a floor receiver specimen.

Force sensors

Similar in appearance to the accelerometers (*e.g.*, Figure **4.7**), force sensors measure the force provided at the point of measurement. The model 205M08 force sensor was used during this project when floor specimen measurements using the impact hammer were made. The force sensor is connected to the impact hammer directly and measures the force due to the impact caused by the hammer at the point of contact with the floor.

Impedance head

An impedance head is a sensor that measures both the acceleration and the force at the point of measurement. It can be viewed as an accelerometer and force sensor combined into one. In this project, an impedance head (model 288D01) was utilized in measurements involving the electrodynamic shaker, as it is attached to the stinger of the shaker. Impedance head model 288D01 is shown below by Figure **4.8**.

Figure 4.8 Impedance head model 288D01 by PCB Piezotronics.

4.2.5 Data Acquisition Device (DAQ)

A soundcard may be defined as a data acquisition device, which is connected to a computer to acquire and play audio data. In this project, the cDAQ-9178 model by National Instruments was used and is shown in Figure **4.9**. It includes eight slots, and each slot can be connected to four sensors. During a measurement, all sensors in use are connected to the soundcard. The soundcard is in turn connected to a computer where all data is handled and processed through MATLAB. Multiple measurement settings, such as measurement time and output voltage when using the electrodynamic shaker, are also set using a computer.

Figure 4.9 The cDAQ-9178 Soundcard by National Instruments [51].

4.2.6 Force Plate

The PF-10 force plate manufactured by Rion was used in the measurement of the blocked force of the impact rubber ball. To find the blocked force of an impact source, the force plate must be placed on a rigid, heavyweight surface, such as in Figure **4.10**, to ensure that the mobility of the source is much greater than that of the floor, which it rests on. The force plate is connected to the cDAQ-9178 Soundcard. There are three force sensors located underneath the plate. To find the blocked force of a source, it is simply dropped on the plate. It is noted that the PF-10 force plate has its lowest resonance frequency at 1600Hz [27]; the results obtained at a greater frequency will have to be neglected.

Figure 4.10 The PF-10 force plate resting on a concrete floor

5 Measurement Setup

In this chapter, setups used in the measurements of impact sources and floor specimen are shown in detail. The National Research Council Canada (NRC) floor testing facility, which was utilized in the measurements of floor specimen in this project, is introduced. Next, the measurement setups for the mobility of the impact sources, namely the standard tapping machine and impact rubber ball, as well as a human walker with and without shoes, are shown. Afterwards, the measurement setups and measurement positions for both the floor and ceiling of the floor specimen are illustrated. Finally, the measurement setup to attain the blocked force of the impact rubber ball and tapping machine using the force plate is described.

5.1 Facility

The facility for the mobility measurements of the floor specimen is the NRC floor testing facility found in building M59 on the Montreal Road campus in Ottawa, Ontario, Canada. The facility is made of two acoustic chambers, one above the other, separated by the floor specimen under test. The specimen, with an exposed area of 4.7m x 3.8m, is placed onto a concrete movable frame, as shown in Figure **5.1**, which is then slid in between the chambers. Once the frame is in place, neoprene seals between the frame and the chambers are inflated to supress the effects of flanking transmission. The lower acoustic chamber is made from concrete and is mounted on springs for decoupling and to minimize outside influence. The upper chamber is a lightweight assembly, made of gypsum boards and insulation [52].

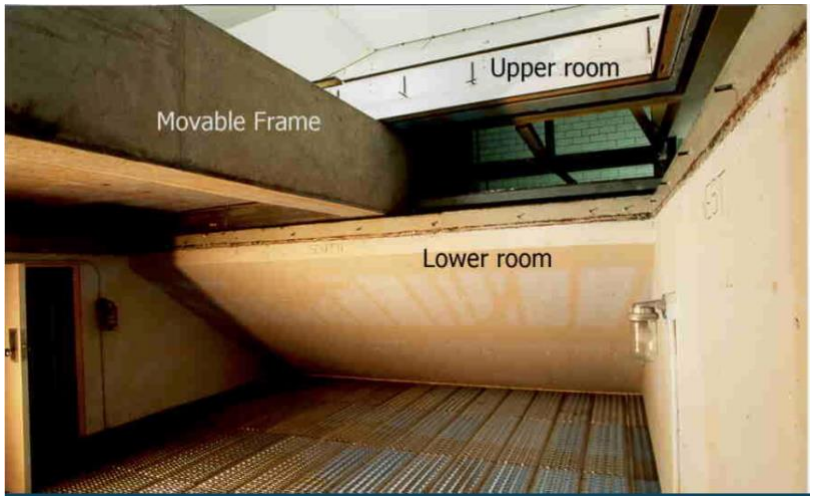

Figure 5.1 Components of the NRC floor testing facility.

The shape of both chambers, seen in Figure **5.2**, along with reflecting panels inside of them contribute to the creation of a diffuse sound field, also reducing modal effects. Finally, the chambers' large volumes help to maintain the diffuse sound field to low frequencies, allowing for better measurements to be taken at lower frequencies [52].

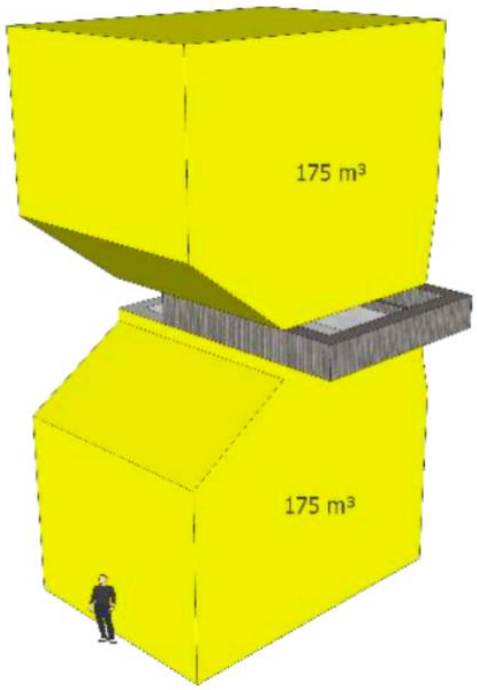

Figure 5.2 Shape and dimensions of the NRC floor testing facility [52].

5.2 Mobility of Impact Sources

In this section, the numerous setups for the measurements of the mobility of the impact sources are outlined. It begins with the standard impact sources, starting with the impact rubber ball and followed by the tapping machine. The measurement setups for the mobility of a human walker, with and without shoes, are also shown.

Also, different measurement settings were iterated when the electrodynamic shaker was used; the variables were the measurement time and the output voltage provided by the shaker. For example, for one of the measurement setups involving the impact rubber ball (seen in Figure **5.3**), the measurement time was varied between 1.5, 5, 10, and 15 seconds, while the output voltage was set

as 1, 2.5, 5, 10, 25, and 50 mV. It was concluded that for this particular measurement setup, the combination that provided the results in most agreement with previous findings and with the least inconsistencies and oscillations was when the measurement time was 5 seconds and the output voltage 25mV. Various combinations of measurement time and output voltage settings were iterated for all measurements involving the electrodynamic shaker, and all combinations were analyzed and compared with previous studies in order to finally pick the most appropriate one.

5.2.1 Impact Rubber Ball

Measuring the mobility of the impact rubber ball includes a number of challenges. A suitable setup for the ball had to be found. Having it resting on a surface could have an effect on the results due to the normal forces acting against it. Therefore, it was attempted to also have it suspended freely. For implementation, it was hung from the ceiling using a net, a rope, and zip ties. However, in that position, it was difficult to keep it steady during the measurements; the force applied on the rubber ball by the electrodynamic shaker would cause it to move. To prevent that, multiple combinations of measurement settings, namely the measurement time and output voltage, were attempted. Another issue arises when trying to keep maximum contact between the ball and the shaker's impedance head, since the ball is spherical, and the impedance head is flat. This caused the ball and impedance head to easily lose contact during a measurement, when a force is injected by the shaker on the ball. Given those difficulties, one of the objectives of this project is to find the most appropriate setup and settings to conduct the mobility measurements of the sources.

In order to address the several abovementioned challenges, multiple measurement setups were attempted, which can be divided into vertical measurements and horizontal measurements. These are further categorized into measurements taken when the impact ball is either suspended or rested. For the vertical-suspended set of measurements the ball was hung freely from the ceiling, as explained in the previous paragraph. The impact rubber ball's mobility was measured vertically from underneath using the electrodynamic shaker, as seen below in Figure **5.3**.

Figure 5.3 Vertical-suspended measurement setup of the rubber ball mobility.

However, the weight of the ball may have influenced the results for this set of measurements. Therefore, vertical-resting measurements, shown in Figure **5.4**, where the ball is resting on a surface, were attempted. The mobility is measured from above, with one set of measurements taken with the ball resting directly on a heavyweight (low mobility) surface (left picture in Figure **5.4**), while another was taken with the impact ball resting on its designated stand (right picture in Figure **5.4**).

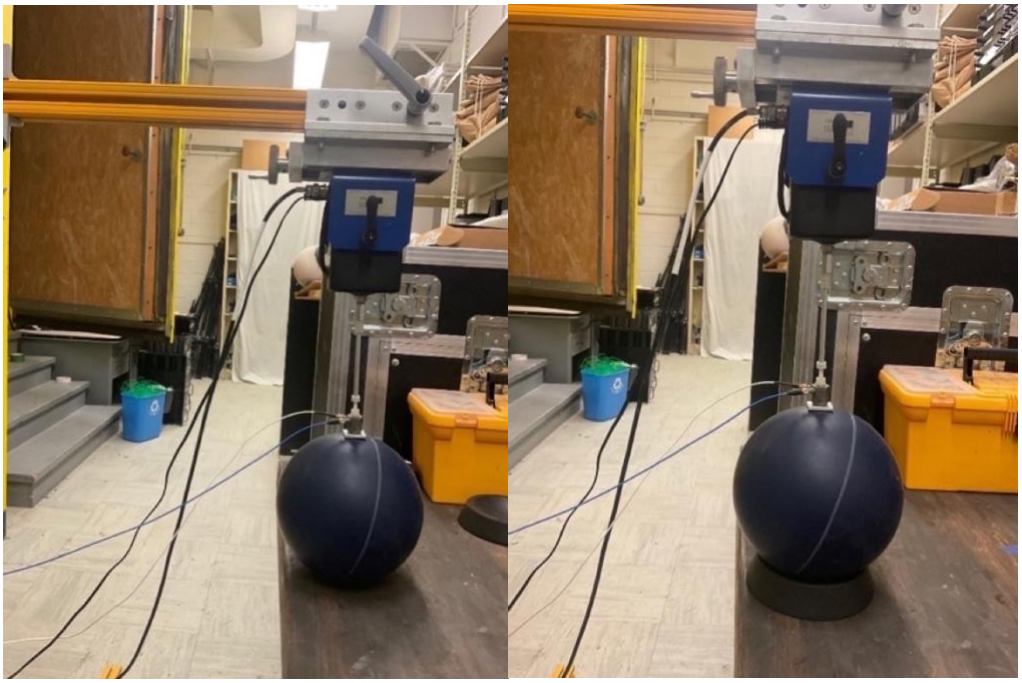

Figure 5.4 Vertical-resting setup for the mobility of the impact rubber ball, on a heavyweight surface (left) and on rubber ball stand (right).

For the setups shown in Figure **5.4**, the normal force acting on the ball by the surface, upon which it is resting on, could have had an effect on the results. Therefore, measurements were taken horizontally, where the impact rubber ball was both suspended and resting were attempted. The left side of Figure **5.5** shows the former, while the right side shows the latter. When resting, as mentioned earlier, the normal forces could have an effect. As for when it was suspended, measurements were run with three different setups: with the ball suspended freely, with the ball lightly supported with fingers on the opposite side of shaker, and with the ball suspended at a slight angle, lightly pushing against the shaker's stinger. The last two were to ensure that the ball does not move during the measurement, while trying to have a minimum effect on the freeness of the suspended impact rubber ball.

Figure 5.5 Horizontal measurement setups for the mobility of the impact rubber ball, suspended (left) and resting (right).

5.2.2 Human Foot

The mobility of the human foot was measured using two different setups on both feet of three individuals, with and without shoes. The first setup is shown in Figure **5.6**, where the individuals are sitting on a chair and have their legs resting while the measurement is being performed horizontally.

The second setup has the individuals sitting on an elevated surface with their legs freely suspended from the end of the surface. The mobility is then measured vertically from underneath, as shown in Figure **5.7**. The results are discussed in Chapter 7.

Figure 5.6 Horizontal measurement setup of foot of human walker with and without shoes

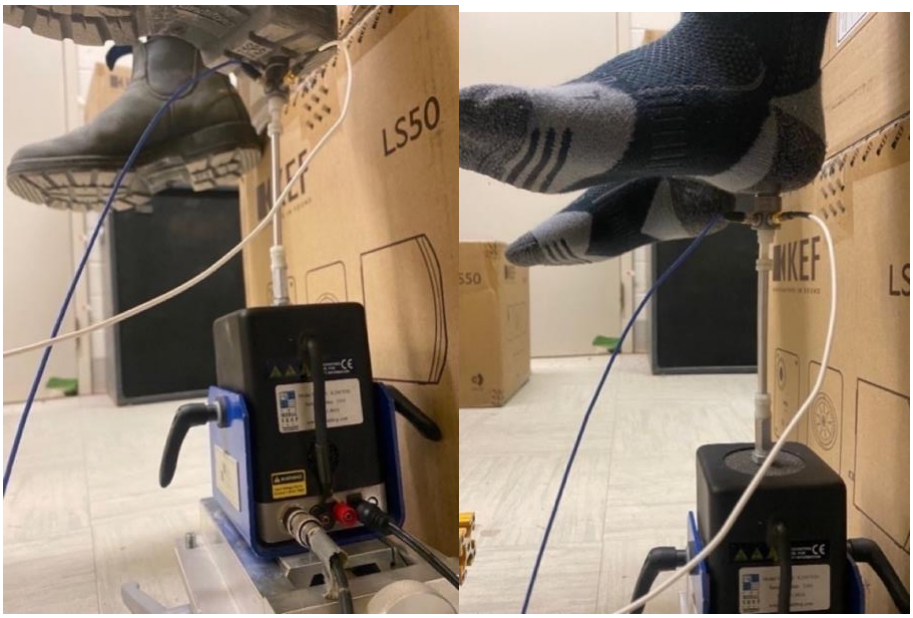

Figure 5.7 Vertical measurement setup of foot of human walker with and without shoes.

5.2.3 Tapping Machine

The mobility of the tapping machine was measured by using the shaker on one of its steel hammers, measuring from underneath as shown in Figure **5.8**. The shaker was set on the floor while the tapping machine was elevated from both ends using bricks, allowing the stinger to make contact vertically with one of the steel hammers.

Figure 5.8 Measurement setup of the tapping machine.

5.3 Blocked Force of Sources

In order to acquire the blocked force of standard impact sources, the PF-10 Rion force plate, described in Subsection 4.2.6, was used. It was placed on a heavyweight, concrete floor, as illustrated in Figure **4.10**, where the impact rubber ball and the standard tapping machine hammer were dropped on it from their standard drop heights of 1m and 40mm, respectively.

Given the large uncertainty with the blocked forces of the walker with and without shoes due to the difficulties associated with their measurements using the force plate, they were replaced with the blocked force of the impact rubber ball since the mobility of the rubber ball is much closer to that of the walker with and without shoes than that of the mobility of the tapping machine. This will be presented later in Figure **7.5**. While this may be a source of error when finding the powers injected, Equation 13 shows that the relative error percentage between both powers injected (with and without considering the source-receiver interaction) does not depend on the blocked force of the source.

5.4 Mobility of Floor Receivers

For the measurement setup for the floor mobility measurements, there are seven positions on the top side of the specimen where the accelerometers were placed. Four of them were also excitation positions where the electrodynamic shaker, impact hammer, standard impact rubber ball, and standard tapping machine were used to excite the specimen and take measurements. When exciting the floor receivers with the impact hammer, four taps are performed with the hammer, and the results from the four taps were averaged for more representative data. More on the processing of the data is explained in Chapter 6. Figure **5.9** shows the coordinates of seven accelerometer positions that were consistently implemented on every specimen, and four of these positions were also excitation positions. Figure **5.10** shows the positioning of the accelerometers (circled in red) on an actual floor-receiver specimen for the measurement of its mobility.

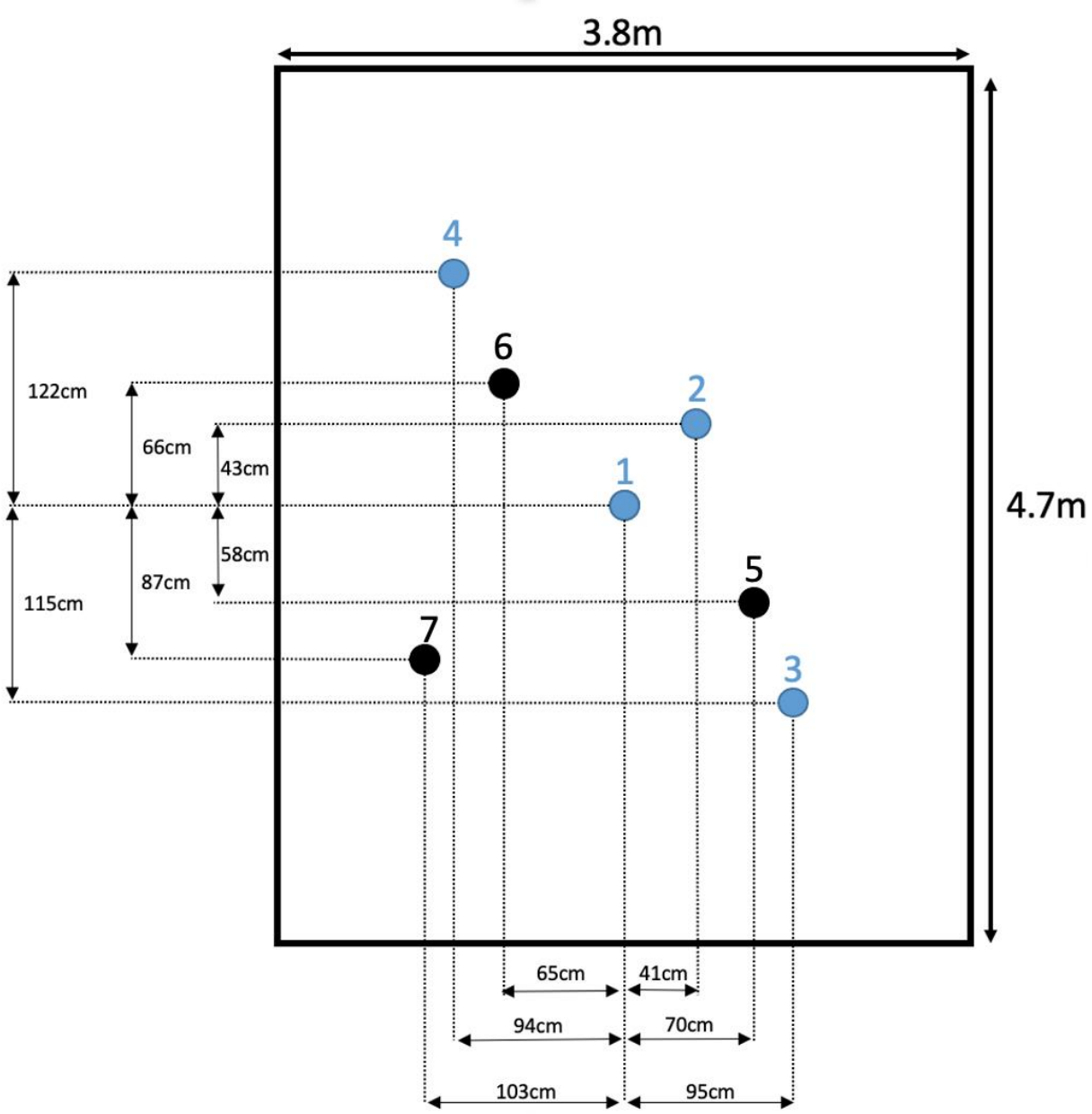

Figure 5.9 Coordinates of the seven accelerometers and four excitation positions (in blue) on the floor (top surface) of the floor specimen.

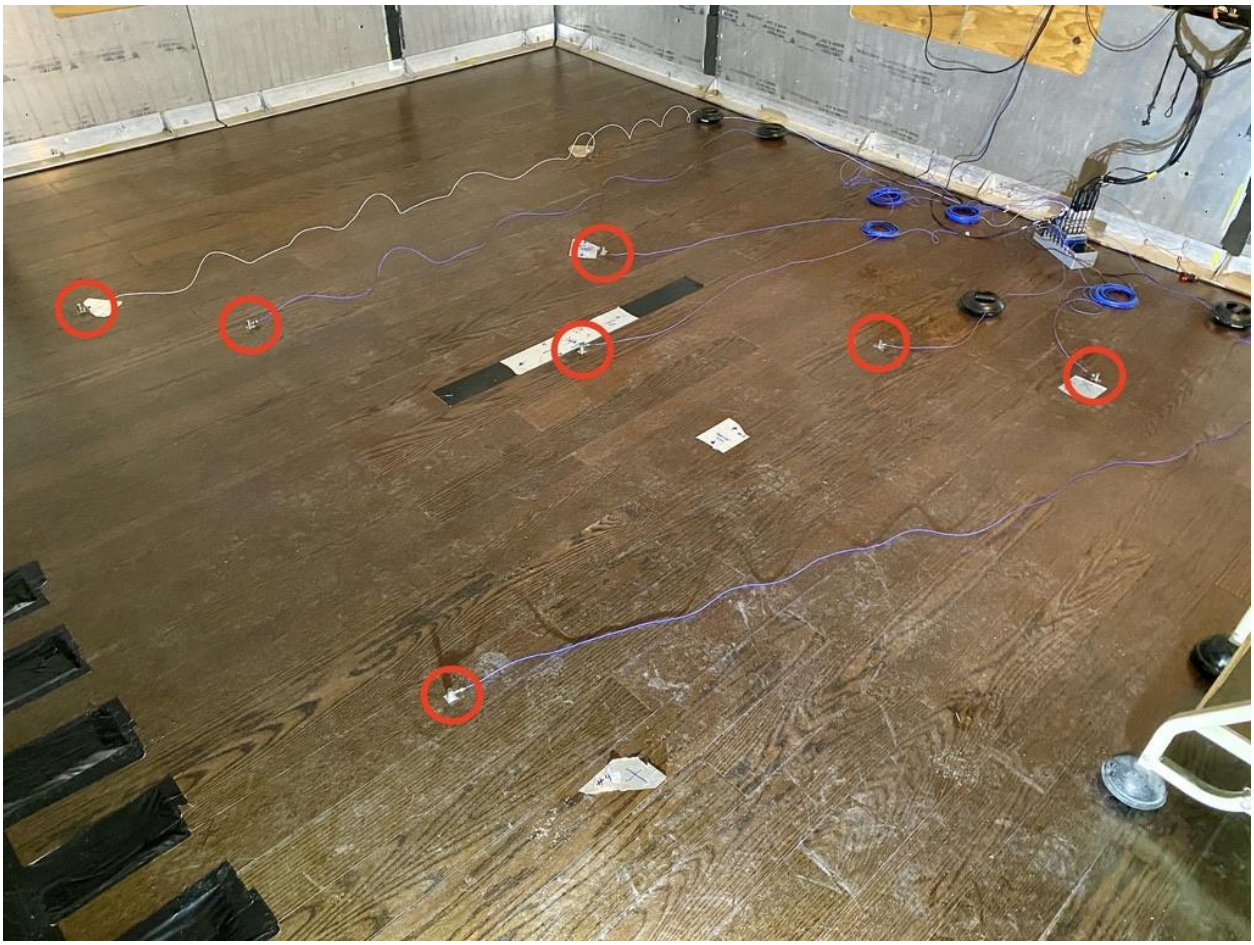

Figure 5.10 Positioning of the accelerometers (circled in red) for the measurement of the mobility of a floor specimen.

While the positioning of the accelerometers and excitation positions was random, it was intended that they cover most areas of the floor. It is important to note that when measuring the mobilities, a measurement taken by the impact hammer or electrodynamic shaker at a certain excitation position will provide the point mobility for that position and the transfer mobility for the six remaining positions. Having multiple measurement and excitation positions allow us to average the results yielded by all these positions, ultimately providing more representative data. For example, in order to get the mobility of a floor, the average of the transfer mobilities over the four measurement positions was used. More details on data processing are given in Chapter 6.

As for the ceilings, there are eight accelerometer positions, with their coordinates laid out in Figure **5.11**. Those accelerometers yield the transfer mobility between the excitation position on the floor to their respective positions on the ceiling (the bottom surface of the floor), through the floor. As with the floor assemblies, positions were picked at random and were maintained for the remainder of the specimen tested. Figure **5.12** shows the ceiling in the lower chamber during the floor specimen measurement.

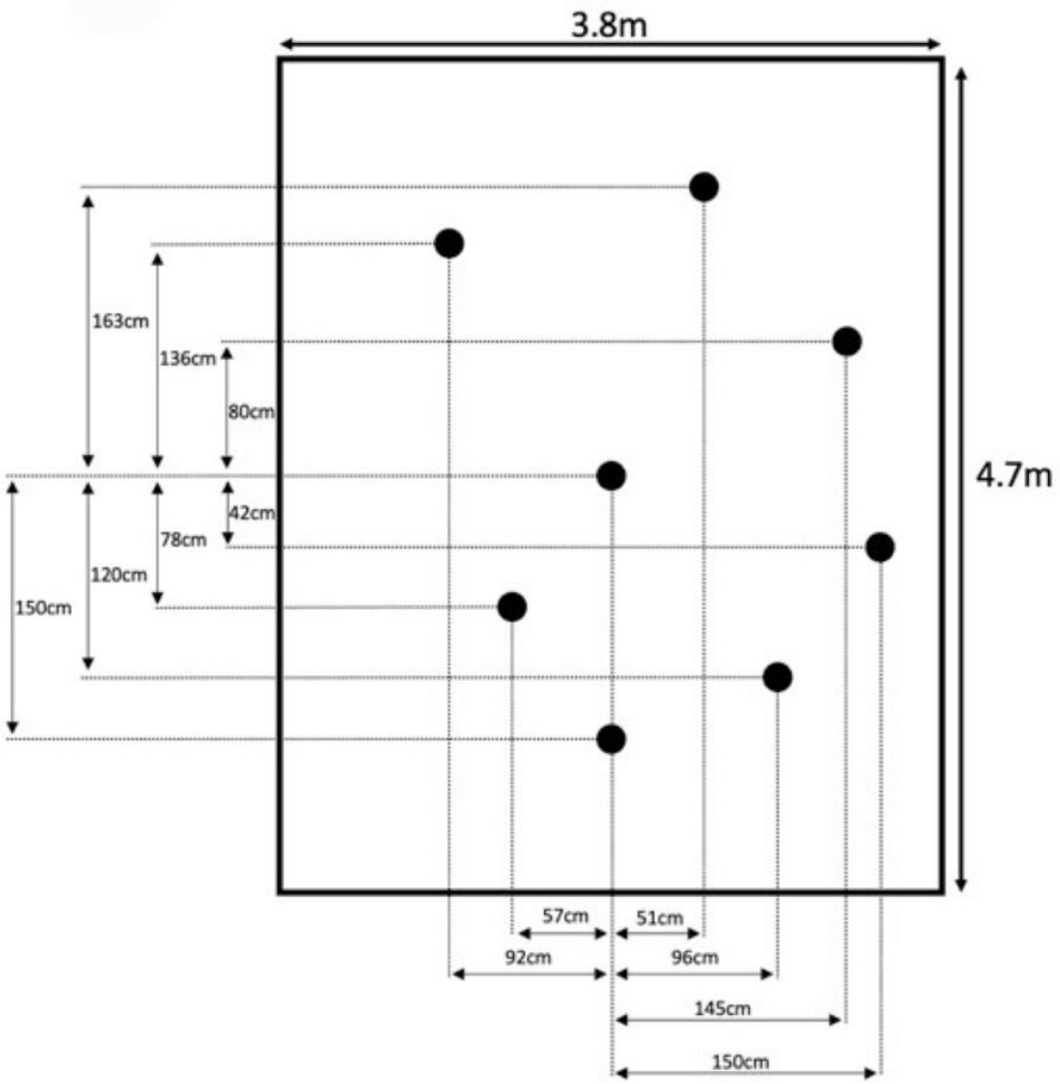

Figure 5.11 Coordinates of the eight accelerometers on the ceiling of the floor specimen.

Figure 5.12 Lower chamber during floor testing.

6 Data Processing

The following chapter describes the post processing of the data acquired through the measurements using the impact hammer and electrodynamic shaker. It begins with a section about the post processing involved with obtaining the mobility of the sources. Then, it proceeds with a section on the post processing of the data used to yield the point and transfer mobilities on the floor receivers. Moreover, the 'Receivers' section includes an explanation of the procedure followed in order to yield the overall mobility of a floor specimen and its corresponding overall ceiling mobility. All data was acquired and processed through MATLAB.

6.1 Sources

During the mobility measurements of the sources, the electrodynamic shaker's impedance head provides both the force at contact as well as the acceleration of the source at that point. Then, the acceleration signal is integrated to yield the velocity. The acceleration, force, and velocity are all shown in Figure **6.1** for a case of mobility measurement of a human walker's foot. As seen from the figure, the electrodynamic shaker provides a sinusoidal sweep signal as the force. When using the shaker, there is no averaging involved such as with the impact hammer, seen in the following subsection. Finally, using the force and velocity, the mobility of the source is obtained using Equation 2. The mobility of the foot of the individual from this example is shown in Figure **6.2**.

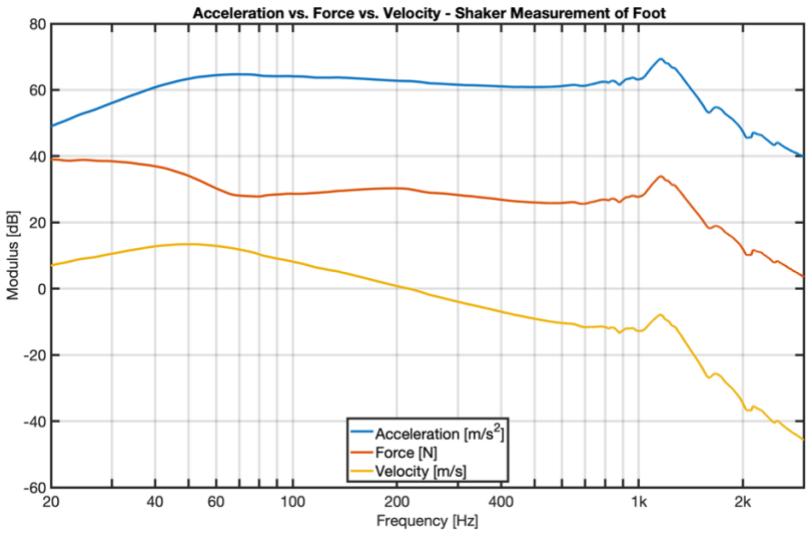

Figure 6.1 Acceleration, force, and velocity yielded by shaker measurement of foot of a human walker.

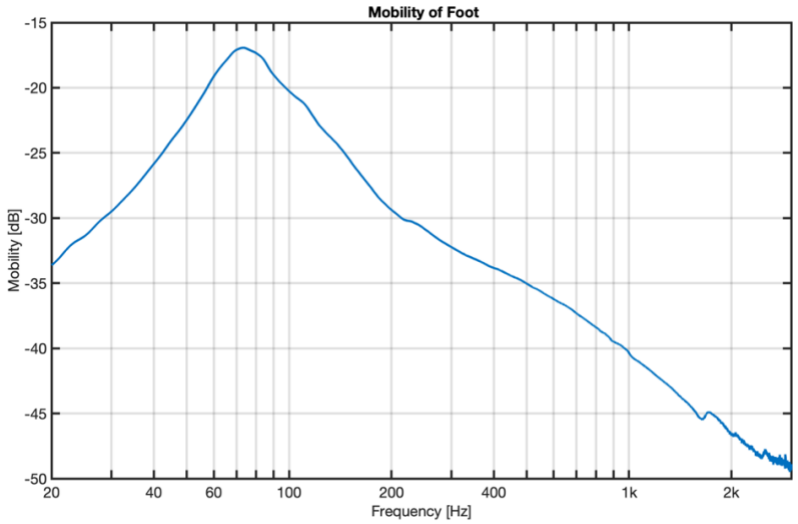

Figure 6.2 Mobility of the foot of a human walker.

6.2 Receivers

The impact hammer was the main excitation tool that was used on all receiver floors. It is operated simply by tapping it at the desired excitation location where there will be an accelerometer mounted. As seen from Figure **5.9**, there are four excitation positions on the floor specimen where measurements are performed using the impact hammer. By tapping right next to the accelerometer, the force sensor within the impact hammer records the force produced by the tap, and the accelerometer mounted to the floor records the vibration of the structure at that location. Therefore, after obtaining the velocity by integrating the acceleration, every measurement position yields a point mobility (corresponding to the position where the measurement is taken) and six transfer mobilities, one between the excitation positions and each of the remaining six accelerometers. As mentioned in Section 5.4, four taps are performed per measurement at a single location. Each set of four taps is averaged for better, more consistent data.

By using the impact hammer, the force impulse signal was obtained through the force sensor built in the hammer. The acceleration signals were also obtained via the accelerometers on the different positions of the floor and ceiling, as seen from Figure **5.9** and Figure **5.11**. Figure **6.3** shows the force signals for the four taps of the impact hammer measurement at Position 2 (as illustrated in Figure **5.9**) of the bare 6-inch concrete floor specimen, while Figure **6.4** shows the corresponding acceleration yielded by the accelerometer at that position.

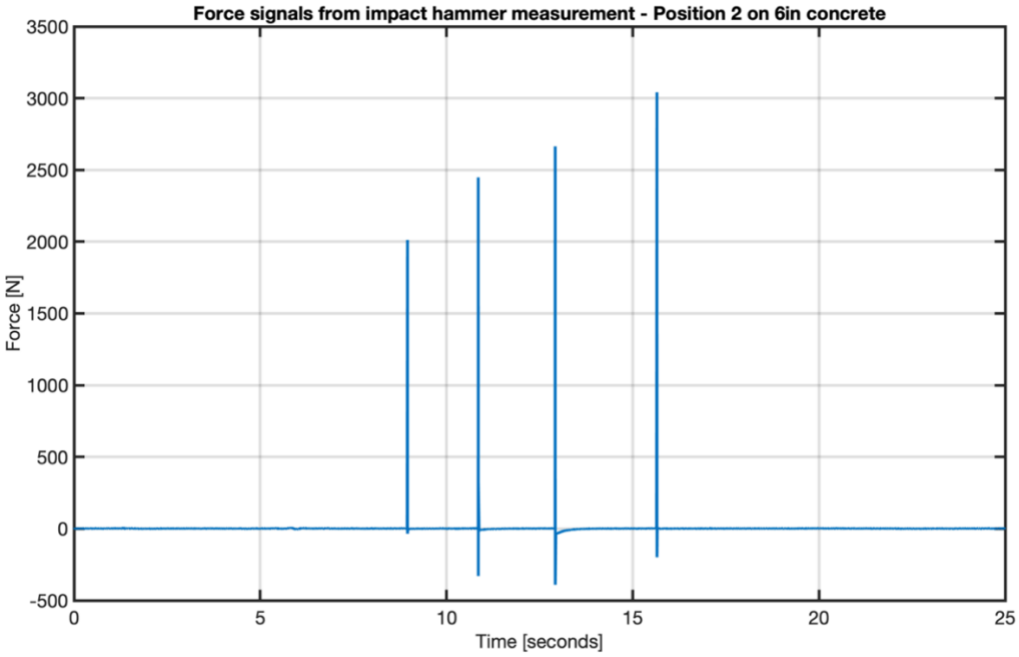

Figure 6.3 Force signals from measurement using the impact hammer (four taps).

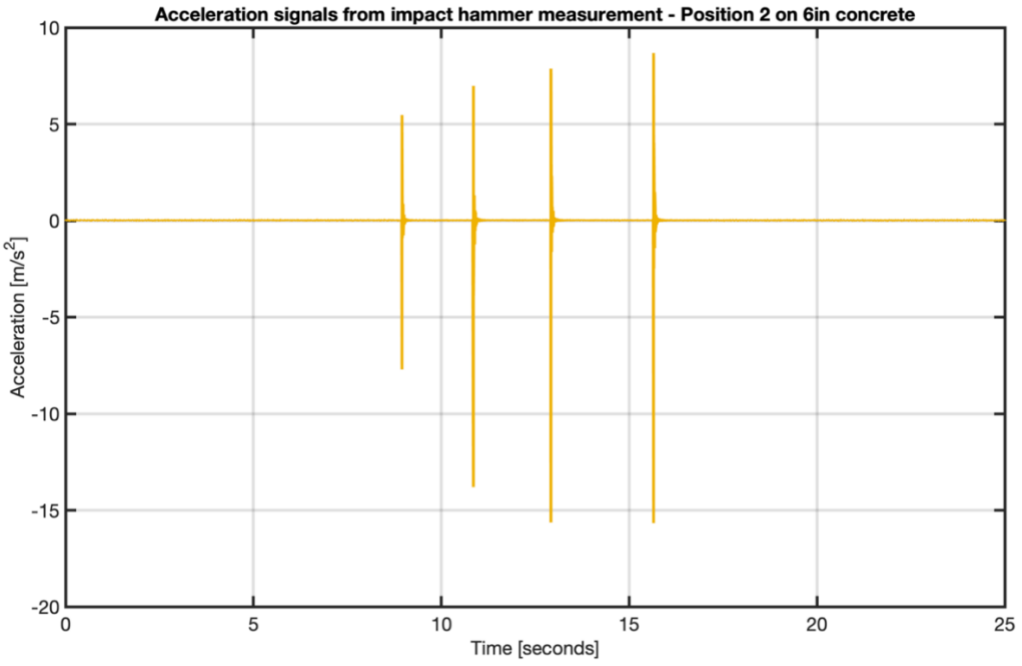

Figure 6.4 Acceleration signals from measurement using the impact hammer (four taps).

Afterwards, every force and acceleration impulse corresponding to each one of the four taps is separated. The force and acceleration signals are then obtained for each individual tap of the impact hammer measurement. Figure **6.5** shows the force impulse measured from the first tap, separated from the rest of the impulses, while Figure **6.6** shows the acceleration yielded by the accelerometer at Position 2. These figures are plotted in the time domain and represent a typical force and acceleration signal using an impact hammer on a floor specimen with accelerometers. The acceleration signals are then integrated to yield their corresponding velocities. Using the force and velocities, we obtain the mobility through Equation 2. Along with the force produced by the impact hammer, the velocity yielded by the acceleration read from the accelerometer at the position of measurement will give the point mobility. The rest of the accelerometers, along with the same force, will yield the transfer mobilities. For example, for a measurement made at Position 2, the point mobility of Position 2 for that floor specimen is obtained, as well as the transfer mobilities between Position 2 and the rest of the accelerometer positions (*i.e.*, excluding the accelerometer at Position 2).

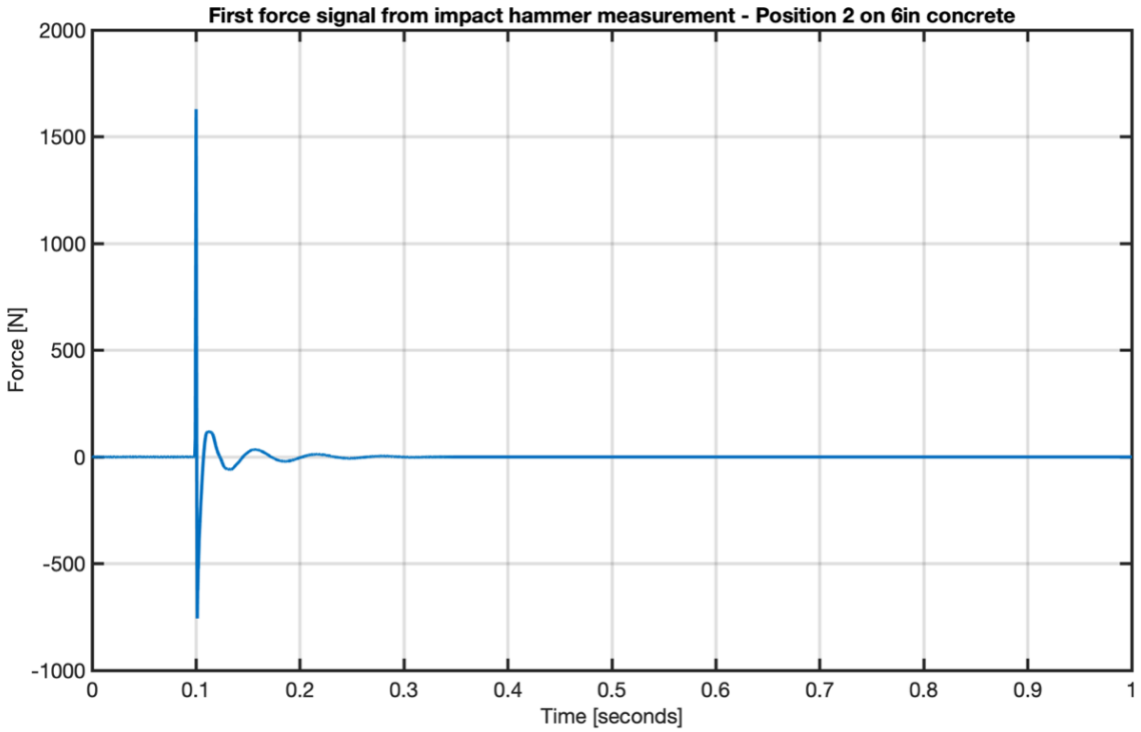

Figure 6.5 First force signal from measurement using the impact hammer.

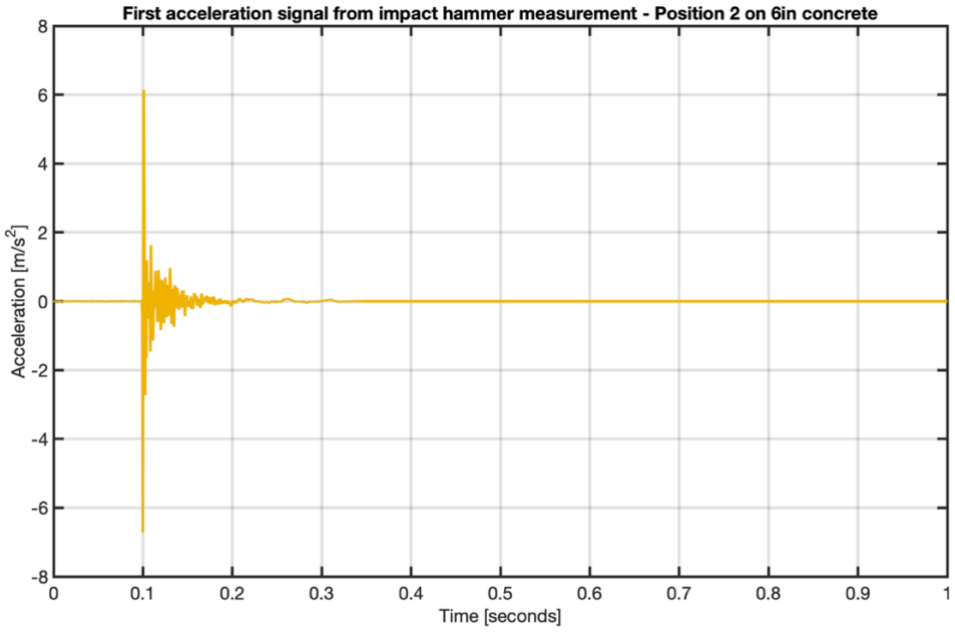

Figure 6.6 First acceleration signal from measurement using impact hammer.

In the frequency domain, Figure **6.7** shows the force, acceleration, and velocity signals of the same tap from Figure **6.5** and Figure **6.6**. The point mobility, also in the frequency domain, obtained from each individual tap performed at Position 2 on the 6-inch concrete slab is shown in Figure **6.8**. The same post processing is applied to all four taps of a given measurement, and for the purpose of having more accurate data and accounting for little irregularities and inconsistencies, the average mobility is obtained.

Figure **6.8** also shows the averaged point mobility obtained from the four taps applied at Position 2 on the 6-inch concrete floor specimen. It is shown that both results are similar up until 1000Hz. Afterwards, results from each tap begin to vary substantially. That is due to the impact hammer's inability to efficiently excite the structure at frequencies above that value. As explained in Subsection 4.2.1., depending on which tip is used for the impact hammer and how heavyweight the structural specimen is, the hammer is effective at exciting the structures only up until a certain frequency. It is the black tip, the hardest one, which was used for the mobility measurements of the 6-inch concrete floor specimen. A softer tip would have provided results only valid for a narrower frequency range.

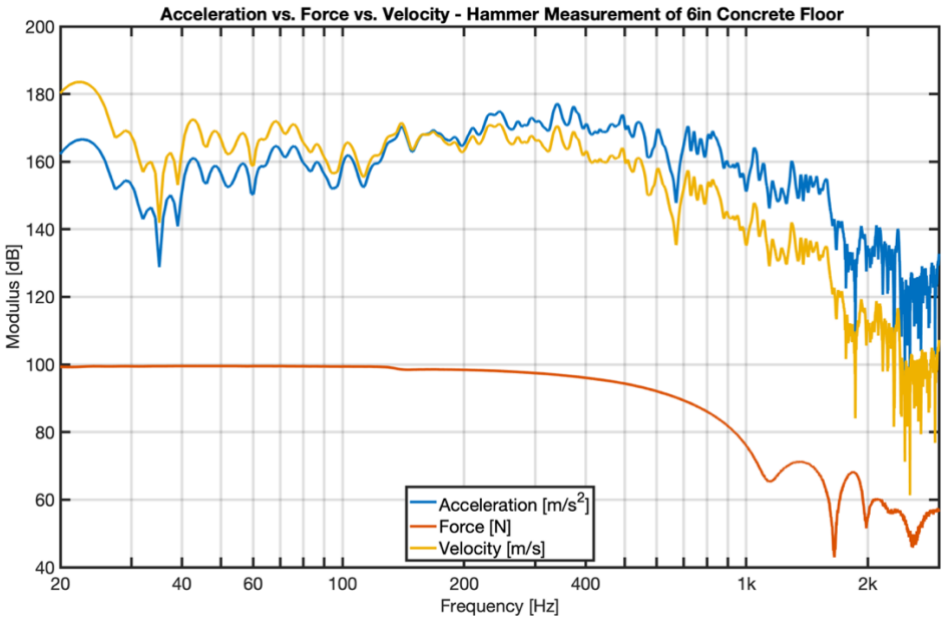

Figure 6.7 The force, acceleration, and velocity signals of the first tap of impact hammer measurement on Position 2 of 6-inch concrete in the frequency domain.

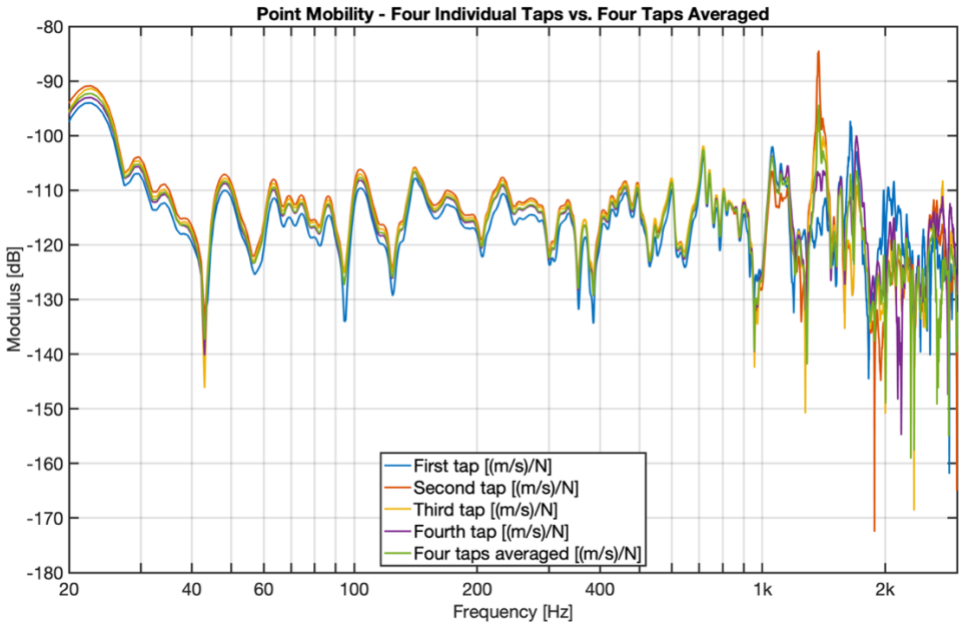

Figure 6.8 Point mobility of Position 2 on 6-inch concrete floor specimen yielded by the impact hammer due to four taps and the four taps averaged.

Figure **6.9** shows the transfer mobilities obtained through the impact hammer measurement on Position 1 of the 6-inch concrete floor. Each line on the graph represents the transfer mobility between Position 1, where the measurement was taken, and the rest of the accelerometer positions.

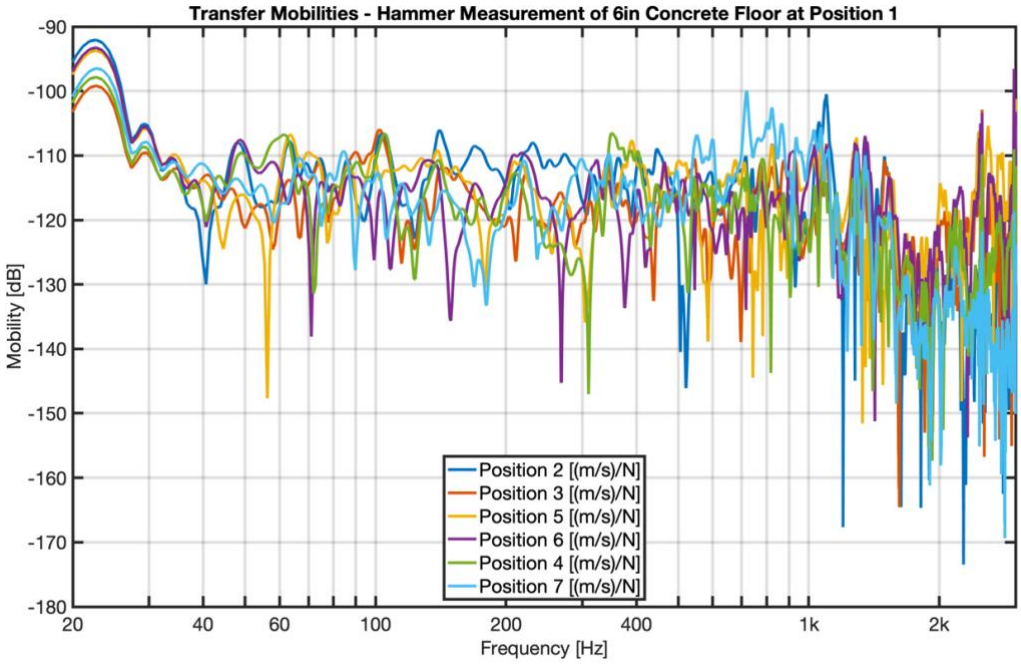

Figure 6.9 Transfer mobilities from impact hammer measurement on Position 1 of the 6-inch concrete floor.

For every measurement, there are two different averages involved: the average transfer mobility and the overall mobility. The average transfer mobility is the average of the six transfer mobilities involved in a single measurement at a specific position, such as the ones seen in Figure **6.9**. Since there are four measurement positions, every floor specimen yields four average transfer mobilities. Figure **6.10** shows the average transfer mobility for each one of the four measurements performed on the 6-inch concrete floor. As for the overall mobility, it is the average of the four average transfer mobilities for a floor. It is essentially the average across measurement positions. To compute this average, the root mean square is taken. Figure **6.11** shows the overall floor mobility of the 6-inch concrete floor, obtained from the average of the four average transfer mobilities seen in Figure **6.10**. The overall floor mobility is used as an estimate for the mobility of the floor as a whole. Finally, mobility results of the floor receivers are shown in the third-octave band, as shown in Figure **6.11**.

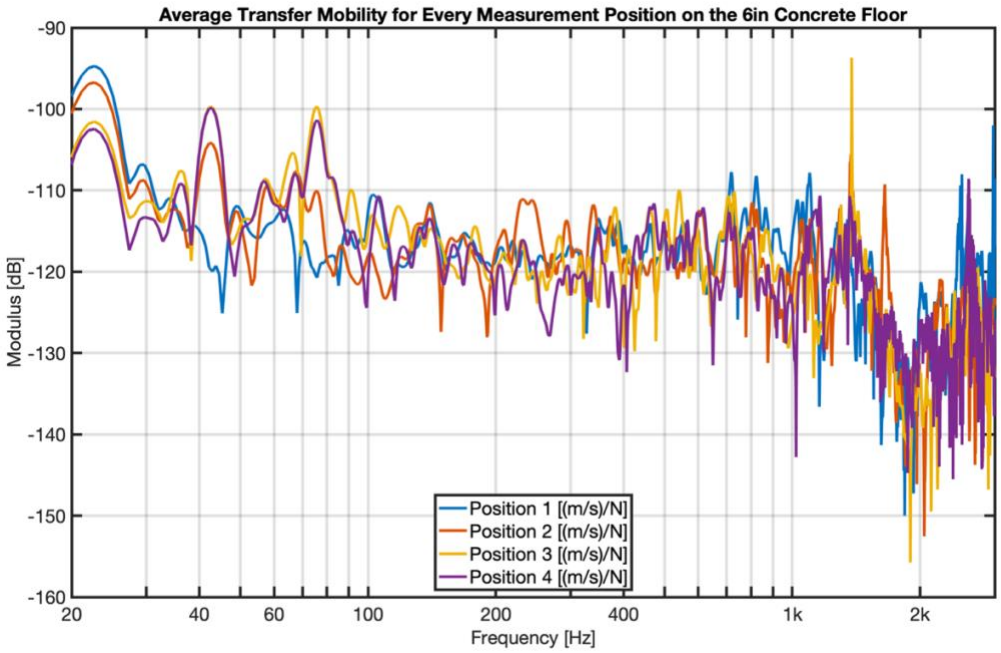

Figure 6.10 Average transfer mobilities for every measurement position on 6-inch concrete floor.

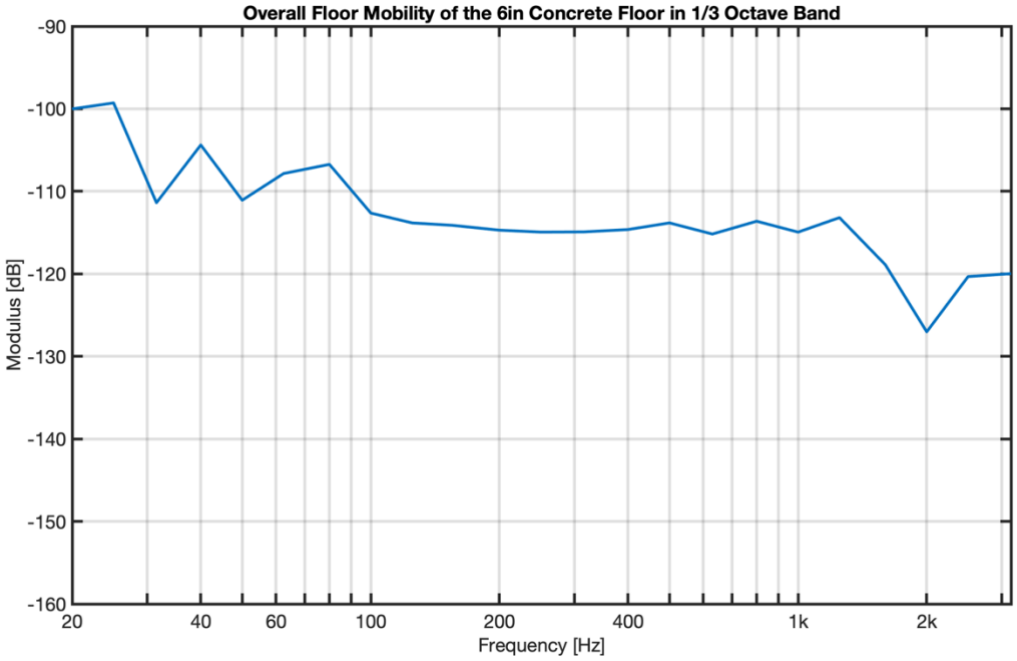

Figure 6.11 Overall mobility of 6-inch concrete floor shown in 1/3 octave bands.

As for the ceilings, the same post processing as the one involving the floors is followed. There are eight accelerometers attached to each ceiling. For each one of the four measurement positions, there are seven transfer mobilities; the accelerometer on the ceiling that is closest to a given measurement position is neglected. Similarly, for each measurement position, the seven transfer mobilities are averaged to get the four average transfer mobilities. Finally, the average transfer mobilities of the ceiling are averaged to yield the overall mobility of the ceiling.

7 Results and Discussion

This chapter presents various results obtained from multiple measurements conducted in this project with the first section, followed by a second and final section, which is a discussion of these results.

7.1 Results

The first subsection presents results yielded for the mobilities of the impact sources while the second one displays the mobilities from measurements on the floor receivers (transfer mobility, overall floor mobility, and overall ceiling mobility). The third and final subsection outlines the power injected when the blocked condition approximation is made and with the consideration of the source-receiver interaction, as well as the relative error percentage between the two. It finally includes a figure, which plots the variability in the coupling function relative to α for each one of the four floor assembly specimen.

7.1.1 Sources

Figure **7.1** shows the mobilities of the rubber ball obtained from the vertical set of measurements seen in Figure **5.3** and Figure **5.4**, while Figure **7.2** shows the impact ball's mobilities from the horizontal set of measurement, as seen in Figure **5.5**. In Figure **7.1**, the yielded mobility of the impact rubber ball for the suspended vertical measurement (blue line) showed the least distortions and fluctuations. As for Figure **7.2**, it shows that most setups provide similar results, with the exception of the suspended freely horizontal measurement setup (blue line).

Figure **7.3** compares the mobility result of highest quality between both sets of measurement. High quality data would show repeatability of results with iterations of measurements. Results were further validated by comparing the first three dips in mobility with the first three free mode shapes found in a previous study at frequencies of 74Hz, 118Hz, and 168Hz [53]. The vertical measurement (from Figure **7.3**) was chosen as the mobility for the impact rubber ball for the rest of the calculations.

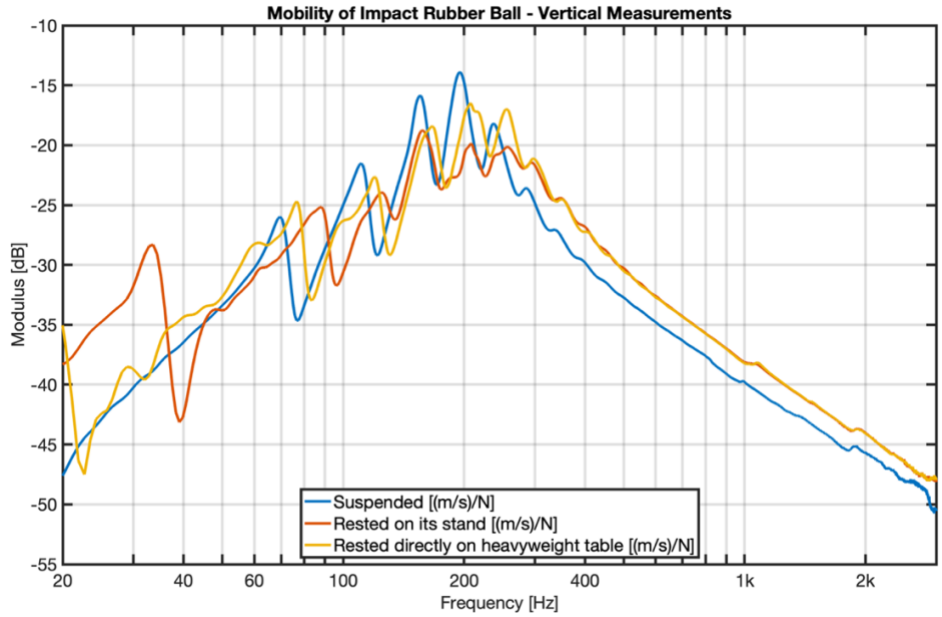

Figure 7.1 Mobility of the impact rubber ball for the set of vertical measurements.

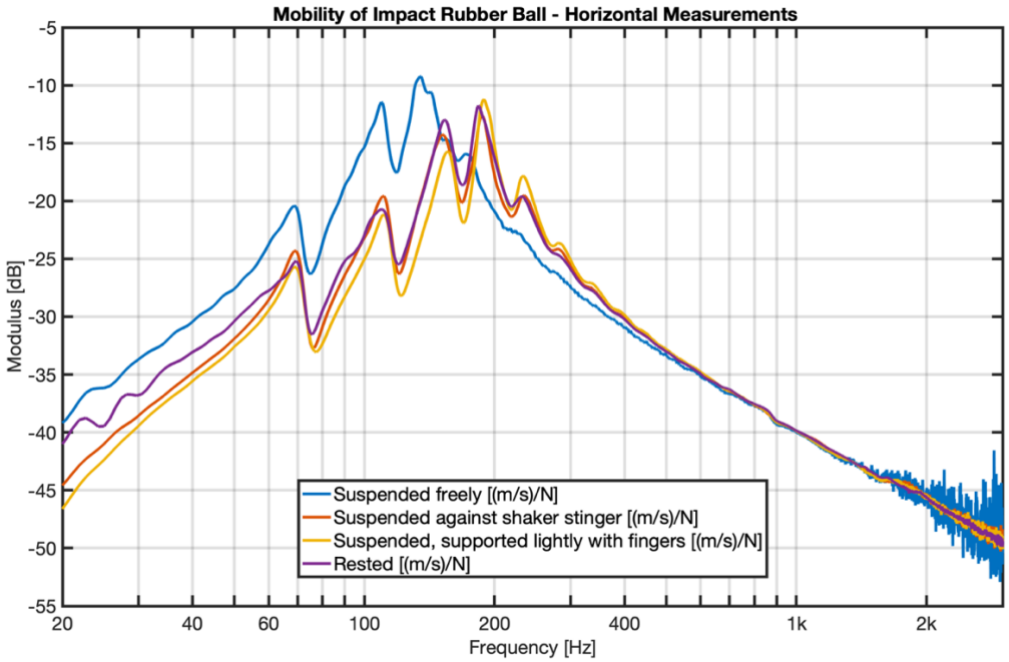

Figure 7.2 Mobility of the impact rubber ball for the set of horizontal measurements.

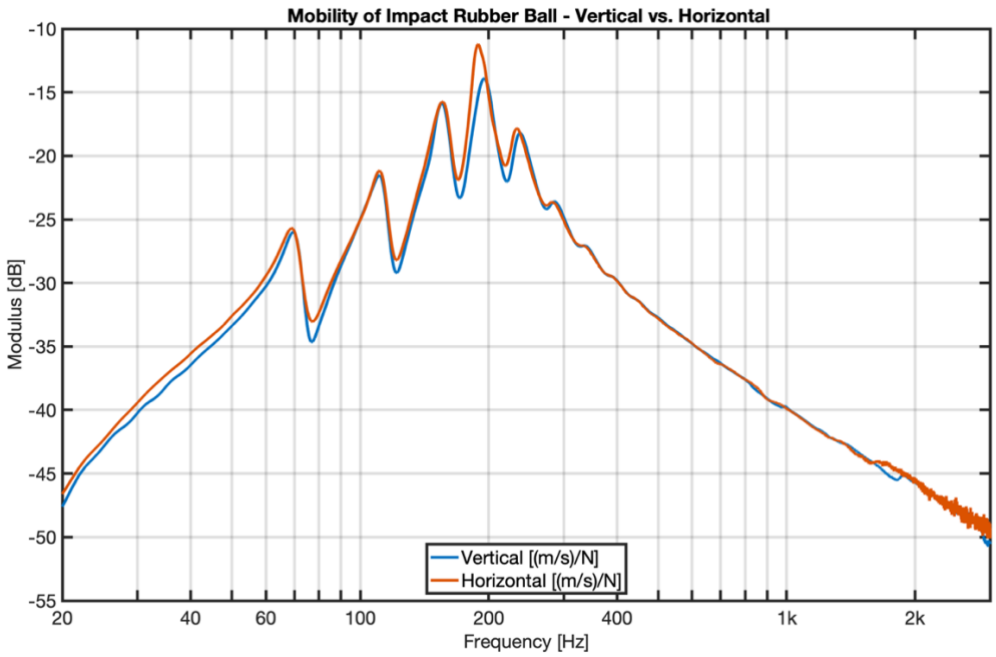

Figure 7.3 Highest quality result for the mobility of the impact rubber ball from the vertical and horizontal sets of measurements.

Figure **7.4** shows the mobility of the foot of a human walker with and without shoes taken horizontally and vertically, as seen in Figure **5.6** and Figure **5.7**. For the case with no shoes, the horizontal measurement was chosen for the remainder of the calculations, and the vertical measurement was picked for the walker with no shoes. That is simply because while results for both measurements setups correlate well with each other for both the walker with and without shoes, the chosen ones show smoother lines which indicate they were higher quality measurements. For the case with no shoes, there is about a 2.5dB difference until 70Hz where they converge almost entirely. As for the case with shoes, they converge at about 400Hz; there is an approximately 7dB difference between 20Hz-60Hz where they converge briefly and then deviate again with a difference of about 5dB between 80Hz-400Hz. In both the case with shoes and without shoes, the deviation between the two curves is likely due to a shift observed in their resonances.

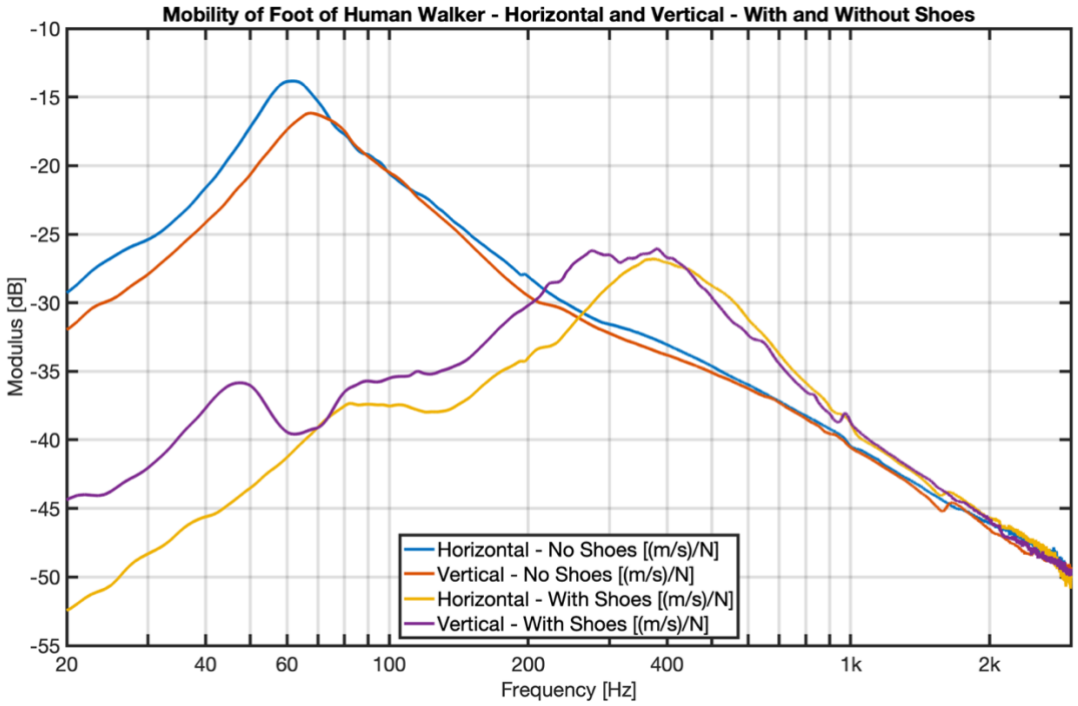

Figure 7.4 Mobility of foot of human walker with and without shoes, taken horizontally and vertically.

The mobility of the tapping machine, both measured and analytically predicted (according to Equation 19), are plotted in Figure **7.5** along with the rest of the previously mentioned sources' chosen mobilities. The measured tapping machine mobility is almost identical to the analytical tapping machine mobility up until approximately 400Hz, after which there is deviation and fluctuations in the graph of the measured tapping machine mobility. This is assumed to be a measurement error, and therefore, the analytical mobility of the tapping machine was considered for the rest of the study. As for the second standard impact source, the impact rubber ball, it increases from about -50dB at 20Hz to -15dB at 200Hz, after which it decreases back to -50dB by 3000Hz. The peak of the mobility of the impact rubber ball, which is -15dB at 200Hz, sits in between the peaks of the mobility of the walker with no shoes, at approximately -15dB at 70Hz, and the mobility of the walker with shoes, at approximately -25dB at 400Hz.

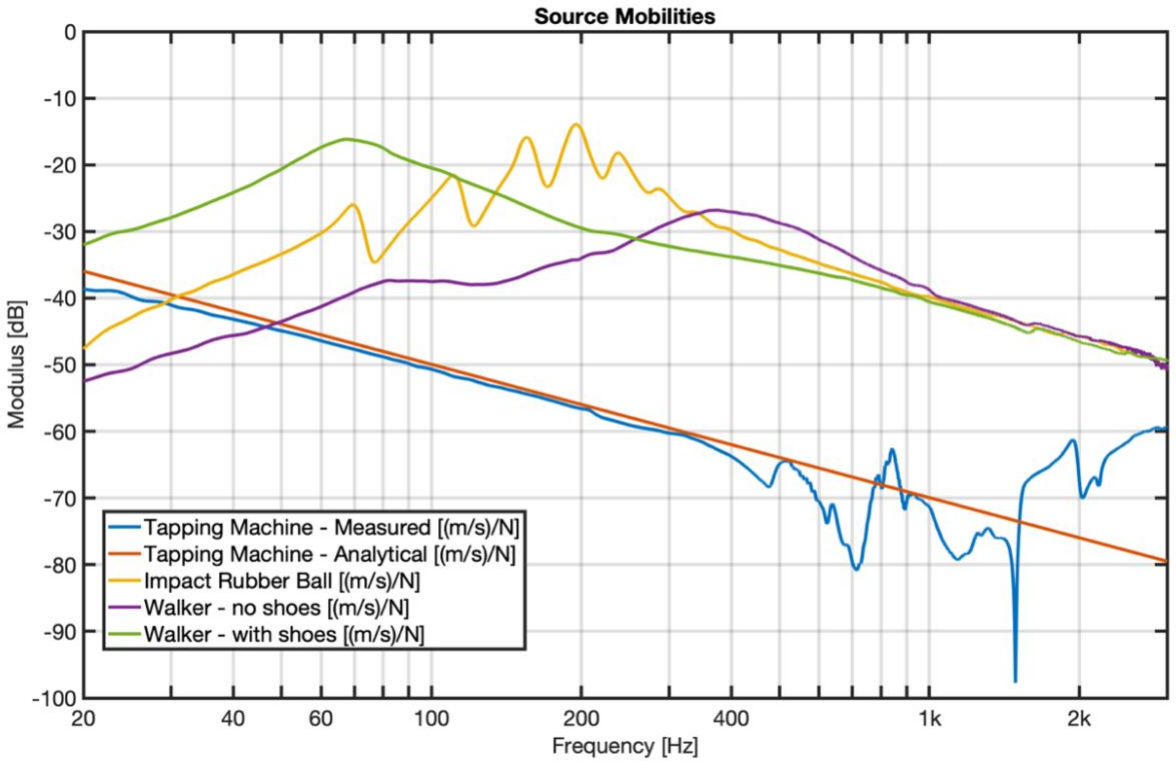

Figure 7.5 Mobilities of the sources.

7.1.2 Receivers

Figure **7.6** and Figure **7.7** compare the overall mobilities of the floor and ceiling using the impact hammer and using the electrodynamic shaker as excitation sources. Figure **7.6** represents the measurements made on the bare concrete floor while Figure **7.7** corresponds to those made on the concrete floor with the laminate floating topping. It is seen from both figures that there are only slight variations between the results yielded from the impact hammer and the electrodynamic shaker. For the bare concrete floor, it is seen from Figure **7.6** that the difference in overall floor and ceiling mobilities between the hammer, and the shaker do not surpass 10dB for the whole range of frequency, except at 2000Hz where there is a large dip for the impact hammer measurements. Between 30Hz-200Hz is where the 10dB difference is found between measurements made with the hammer and the shaker, for both the floor and ceiling, where the shaker provides results with the higher mobility. From 200Hz-500Hz, there is good correlation between both excitation tools with about 1dB difference between the two. Between 500Hz-

1500Hz, there is a 5-8dB difference, after which the dip caused by the hammer occurs and brings the mobilities of both the floor and the ceiling to almost -130dB.

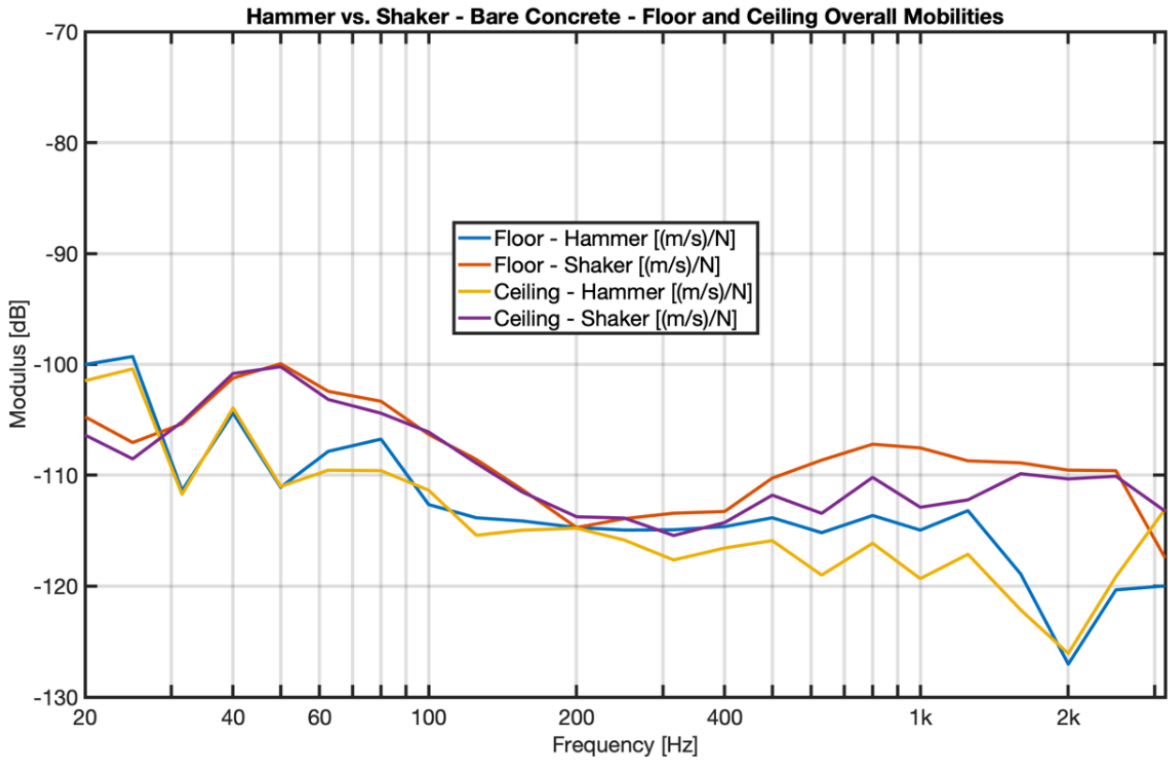

Figure 7.6 Floor and ceiling overall mobilities of the bare concrete floor using both the impact hammer and the electrodynamic shaker.

As for the concrete floor with laminate, Figure **7.7** shows a similar agreeability between the impact hammer and the electrodynamic shaker, with a difference of no more than 2dB between the hammer and shaker for the mobility of the floor (except 500Hz-800Hz where there is a difference of approximately 10dB with the shaker providing the higher mobility). As for the ceiling, there is a difference of about 10dB at 40Hz until they converge at 80Hz and correlate to a maximum difference of 5dB at 400Hz until 1000Hz-3000Hz where there is a difference of about 10dB with the hammer providing the mobility greater in magnitude. Since there is generally good agreeability between floor mobility results between measurements made using the hammer and measurements using the shaker, for the remainder of the floor specimen, only the impact hammer was used to

conduct the measurements, since the electrodynamic shaker is much more laborious and time intensive to use.

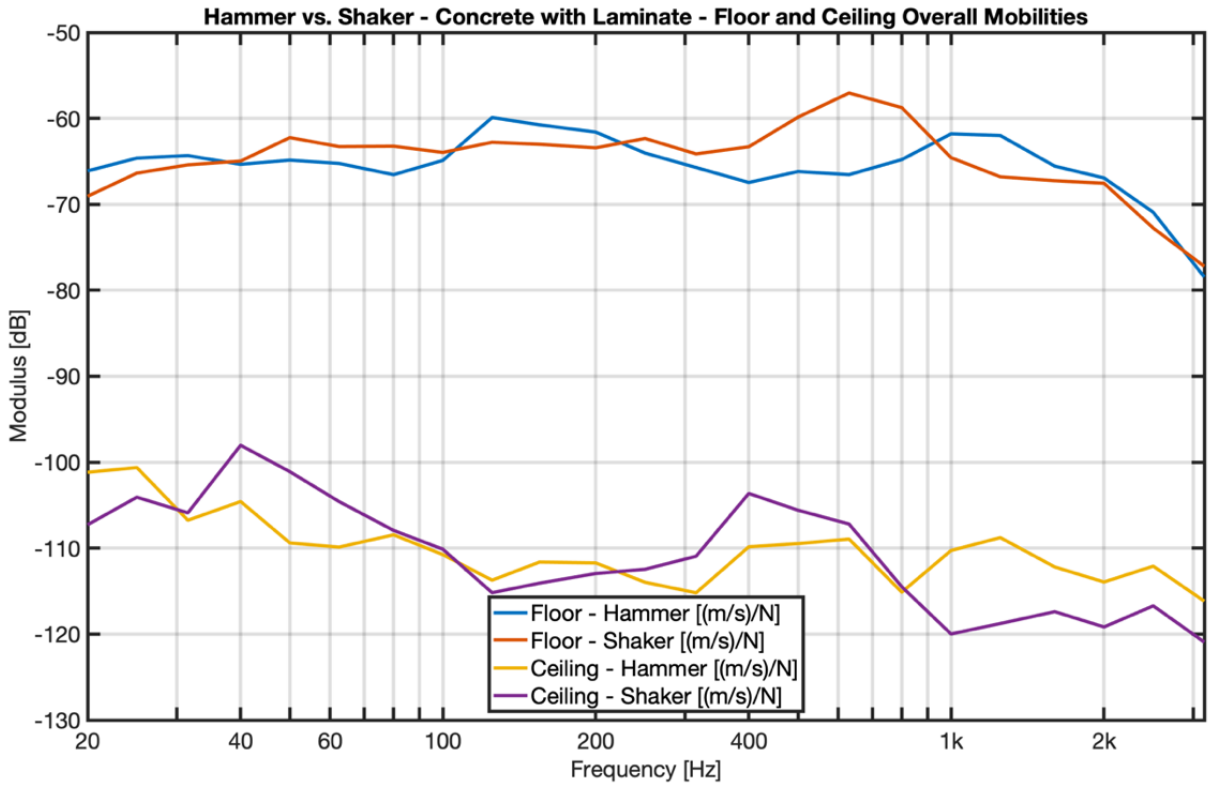

Figure 7.7 Floor and ceiling overall mobilities of the concrete floor with laminate floating topping using both the impact hammer and the electrodynamic shaker.

Transfer mobilities between Measurement Position 1 and all other sensor positions on the bare concrete floor are plotted in Figure **7.8**. For measurements done on Measurement Positions 2, 3, and 4, the transfer mobilities follow a very similar trend; therefore, their figures are not included in this report. It is shown from Figure **7.8** that between 30Hz-1000Hz, the transfer mobilities are mostly between -110 dB and -120 dB for the bare concrete floor.

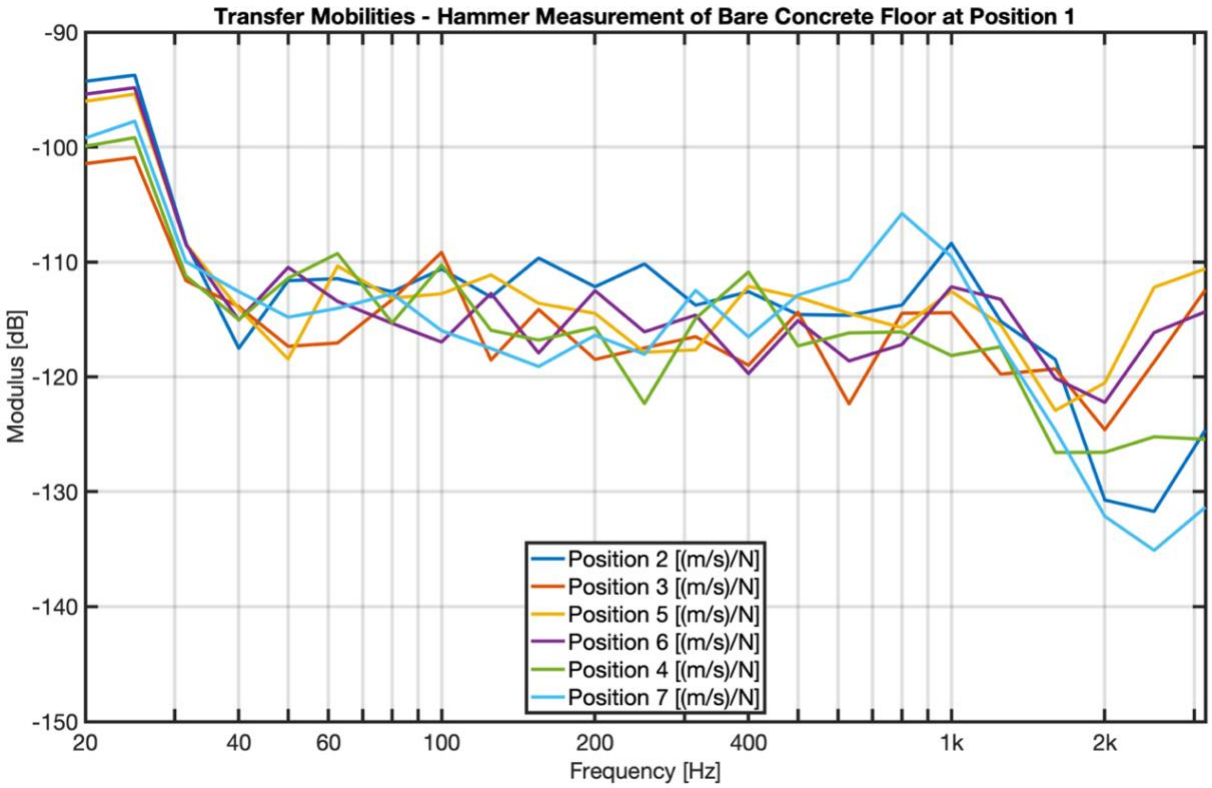

Figure 7.8 Transfer mobilities between measurement position 1 and all other sensor positions on the bare concrete floor.

Figure **7.9** presents the average transfer mobilities yielded from all four measurement positions; for instance, the blue line is representative of the average of all lines from Figure **7.8**. Figure **7.9** shows that correlate very closely (with the exception of a dip at 40Hz by Measurement Position 1 instead of a peak as seen with the rest of the measurement positions), which confirms that the transfer mobilities yielded by all measurement positions follow a similar trend as the one seen in Figure **7.8**.

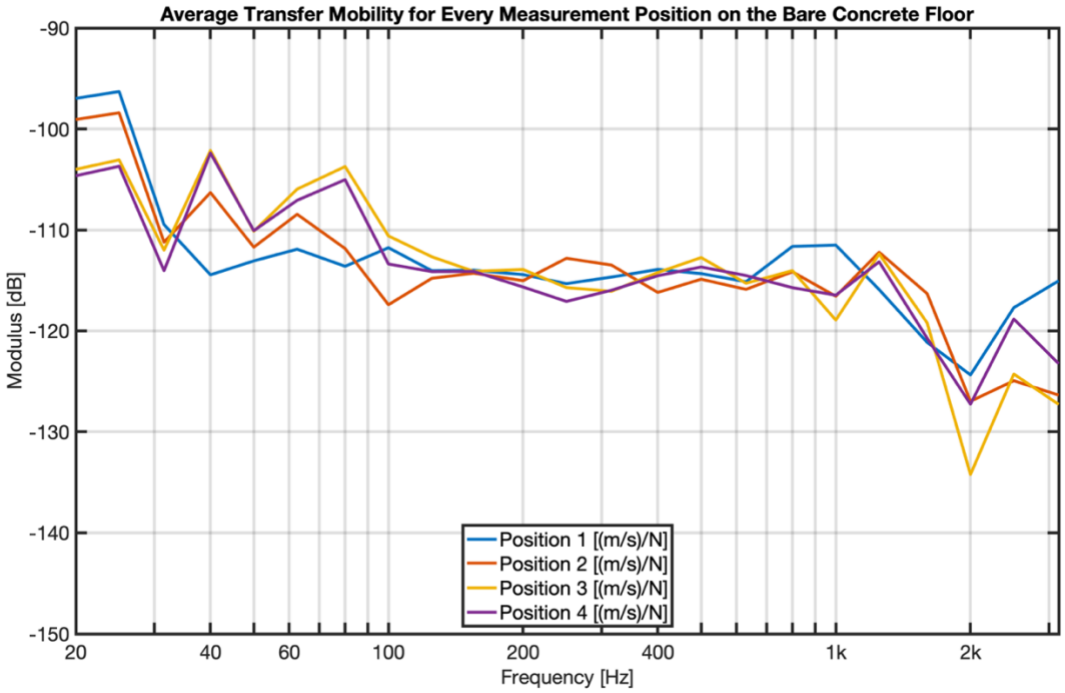

Figure 7.9 Average transfer mobilities for all four measurement positions on the bare concrete floor.

Figure **7.10**, similar to Figure **7.8**, shows the transfer mobilities between measurement Position 1 and all other sensor Positions but for the concrete floor with laminate floating topping. More spread can be seen between the transfer mobilities than in the case of the bare concrete floor. Since the transfer mobilities from the measurement taken at Position 2 yield similar results, the corresponding figure was omitted from this section. While the bare concrete floor's transfer mobilities showed a deviation of generally not more than 10dB from each other, Figure **7.10** shows a greater difference between transfer mobilities when the laminate topping is added, with differences of up to 20dB between Position 3 and Position 6 at lower frequencies (20Hz-200Hz) as well as 15dB between Position 4 and Position 5 at mid frequencies (300Hz-600Hz).

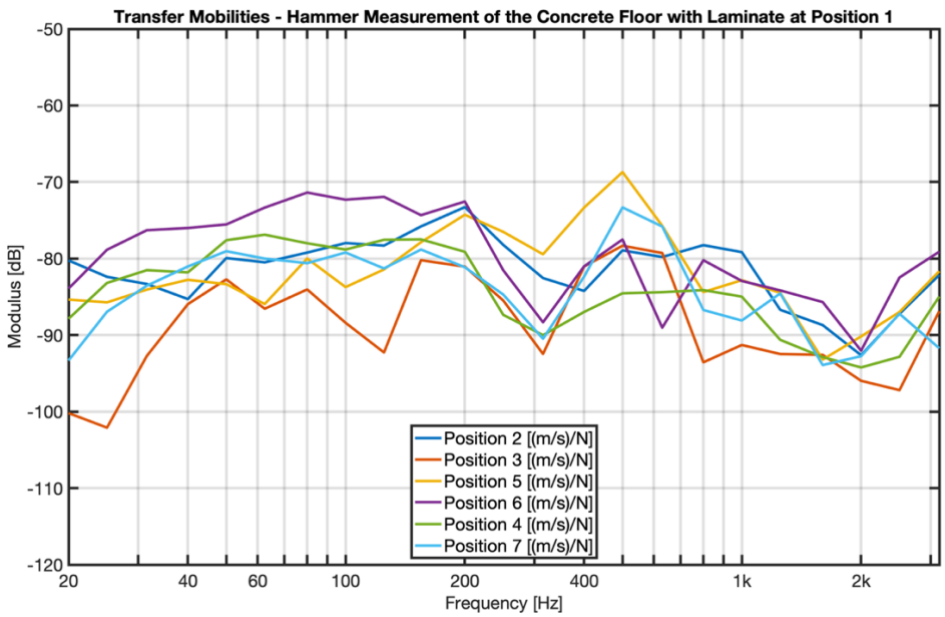

Figure 7.10 Transfer mobilities between measurement position 1 and all other sensor positions on the concrete floor with laminate floating topping.

As for the transfer mobilities at Position 3, it is shown from Figure **7.11** that there is even more of a spread between them. Here, Position 5 reads the highest transfer mobility (-90dB to over -60dB) and Position 2 reads the second highest (-100dB to about -65dB). The measurement at Position 4, similar to Position 3, yields transfer mobilities that are also further spread out from each other in comparison to transfer mobilities results from Measurement Positions 1 and 2, except that it is the transfer mobility between Position 6 and 4 having the highest in magnitude (-85dB to -58dB) and the transfer mobility between Position 3 and 4 having the lowest in magnitude (-95dB to -80dB). Figure **7.12** represents the average transfer mobilities for all four measurement positions on the concrete floor with laminate floating topping. In comparison to Figure **7.9**, which shows the average transfer mobilities for the bare concrete floor, there is a much larger spread between the average transfer mobilities yielded by each measurement position.

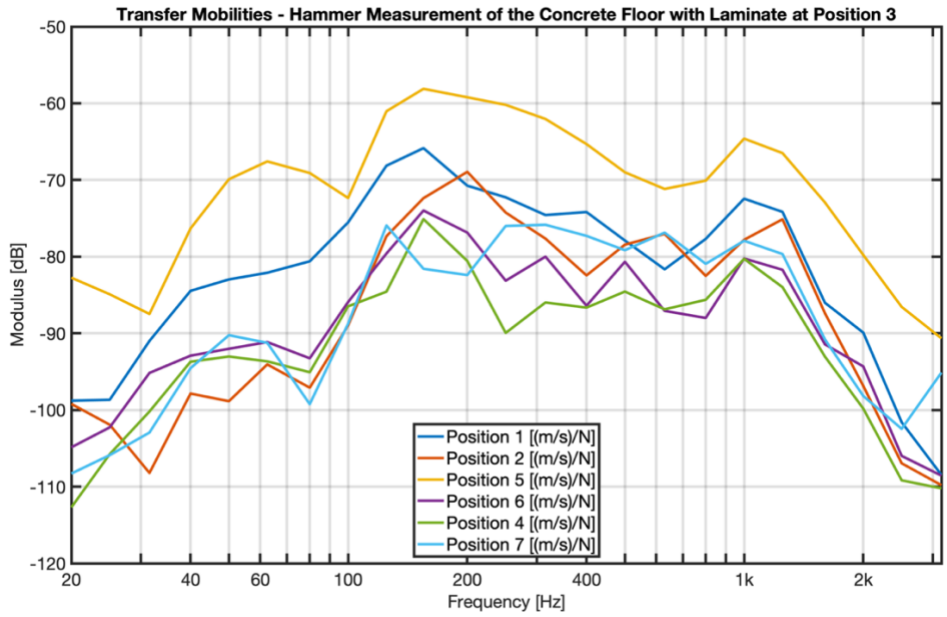

Figure 7.11 Transfer mobilities between measurement position 3 and all other sensor positions on the concrete floor with laminate floating topping.

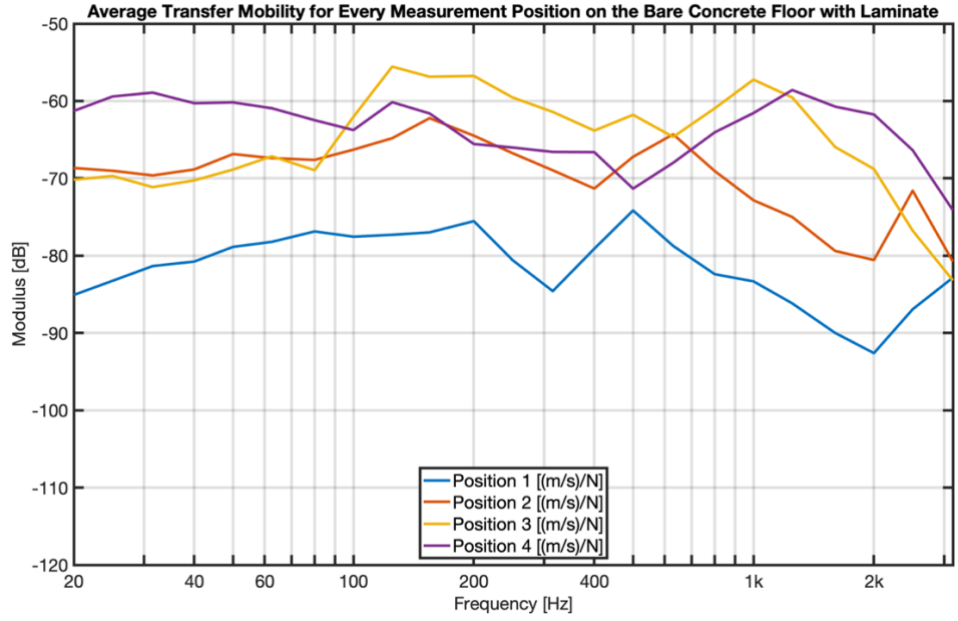

Figure 7.12 Average transfer mobilities for all four measurement positions on the concrete floor with laminate floating topping.

As for the bare CLT floor, its transfer mobilities yielded from the measurement at Position 1 are shown in Figure **7.13**. A separation can be seen between the transfer mobilities; Positions 2, 4, and 6 have higher mobilities (between -70dB and -110dB) than Positions 3, 5, and 7 (between -80dB and -140dB). The separation begins at 30Hz and increases in magnitude as the frequency increases, with the two abovementioned groups of measurement positions further diverging from each other. A similar trend is seen from the measurements taken at Positions 2 and 4 for the bare CLT floor.

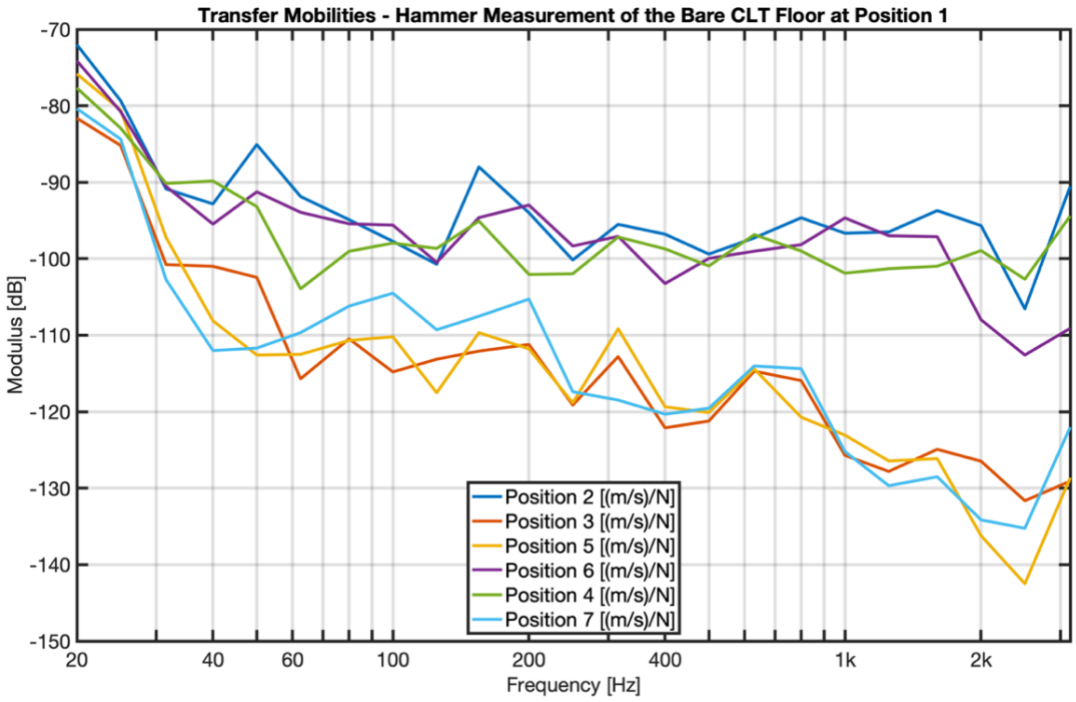

Figure 7.13 Transfer mobilities between measurement Position 1 and all other sensor positions on the bare CLT floor.

However, while measurements at Position 3 also show a separation, it is Position 5 and 7 that have the higher mobilities (between -95dB to -110dB for frequencies between 60Hz-3000Hz) compared to the rest of the positions (between -105dB to -145dB for the same frequency range). Otherwise, the plot is similar in trend to Figure **7.13**. The separation into two groups of values is due to the CLT specimen being comprised of two individual pieces; a separation was present in the middle of CLT floor specimen. Due to the separation, when taking the average transfer mobilities, only the sensors on the same half of the excitation position are considered. In Figure **7.13** and

Figure **7.14**, these would be the transfer mobilities which appear to be grouped higher than the rest (*i.e.*, 2, 4 and 6 for Measurement Position 1 and 5 and 7 for Measurement Position 3).

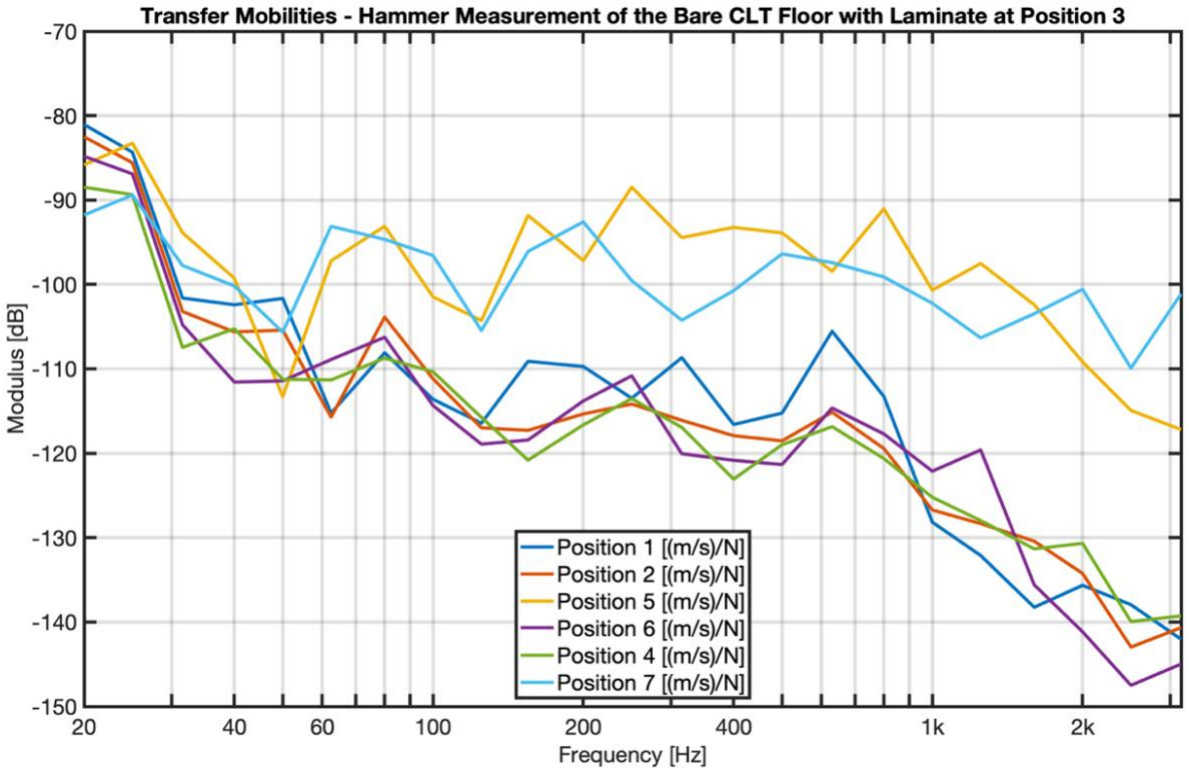

Figure 7.14 Transfer mobilities between measurement Position 3 and all other sensor positions on the bare CLT floor.

Figure **7.15** shows the average transfer mobilities for all four measurement positions on the bare CLT floor. It is seen in Figure **7.15** that all four Measurement Positions for the CLT floor yield average transfer mobilities, which are similar to each other in trend. The difference in magnitude between the four of them does not surpass 10dB for the majority of the frequency range, with the exception of higher frequencies (2000Hz-3000Hz) and a dip by Position 3 at 60Hz while the rest of the measurement positions show a peak.

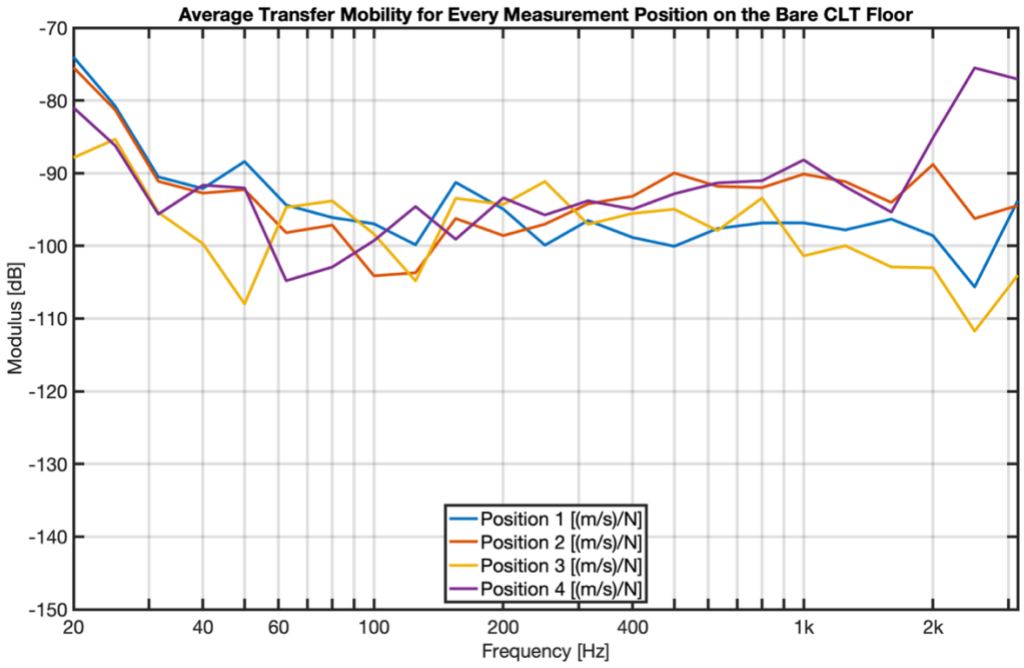

Figure 7.15 Average transfer mobilities for all four measurement positions on the bare CLT floor.

The transfer mobilities between measurement Position 1 and all other sensor positions on the CLT floor with laminate floating topping are presented in Figure **7.16**. It shows a spread between transfer mobilities, such as the spread seen in the case of the concrete floor with laminate floating topping in Figure **7.10** and Figure **7.11**. Generally, Position 6 is seen to have the highest transfer mobility, with Position 2 being the second highest (-90dB to -60dB). Furthermore, although there are some separations, it is much less pronounced than the separation seen from the bare CLT floor. Positions 2, 3, and 4 provide similar results, except measurement Position 3 has a greater transfer mobility at Position 5 for the majority of the frequency range. The average transfer mobilities for all four measurement positions on the CLT floor with laminate floating floor are summarized in Figure **7.17**. There is a spread between average transfer mobilities, similar to the one seen in the case of the concrete floor with laminate, in Figure **7.12**. There is a difference of about 20dB for the majority of the frequency range. A difference of 30dB is observed between Position 3 and Position 4 at 40Hz. Between 1000Hz-1500Hz, the difference between the four positions is mostly less than 5dB.

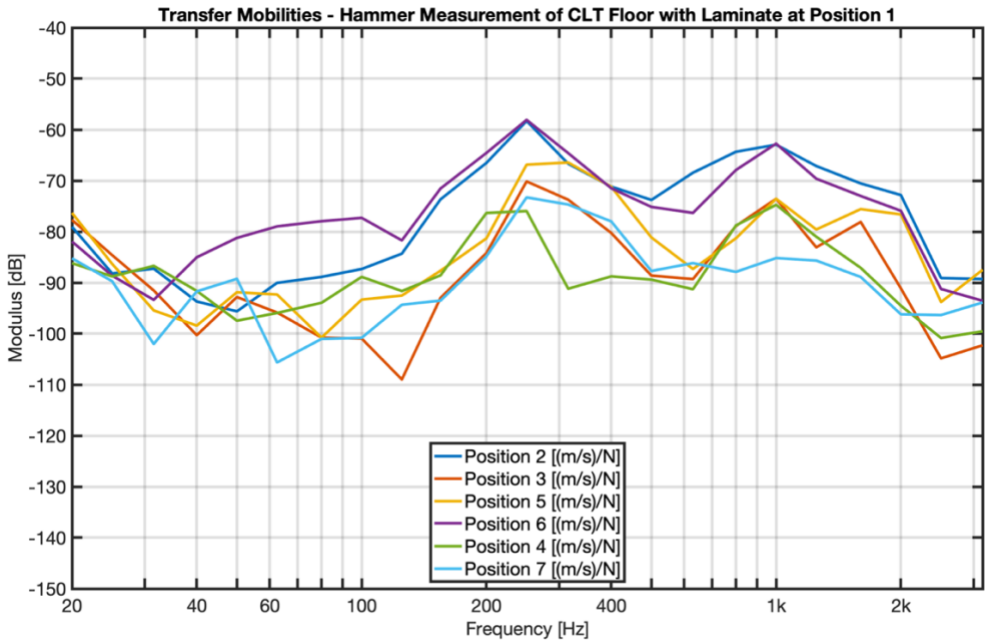

Figure 7.16 Transfer mobilities between measurement Position 1 and all other sensor positions on the CLT floor with laminate floating topping.

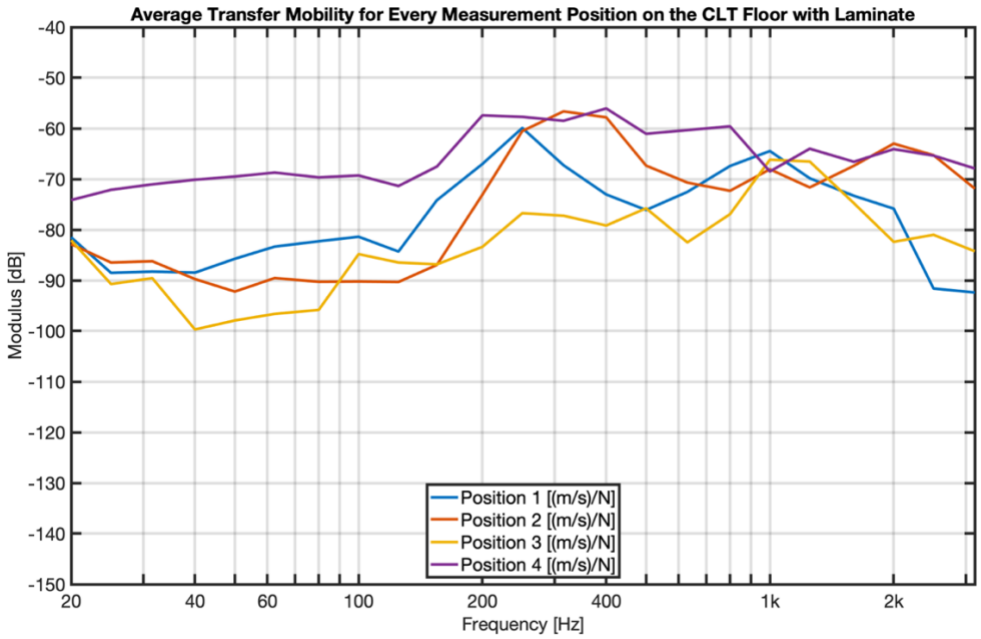

Figure 7.17 Average transfer mobilities for all four measurement positions on the bare CLT floor with laminate floating topping.

The overall floor and ceiling mobilities are shown in Figure **7.18** and Figure **7.19**, for both the concrete and CLT floors, with and without laminate. The analytical mobility of a homogenous, infinite concrete and CLT plates are also plotted in their respective figures for reference and comparison. It is seen from Figure **7.18** below that upon adding the laminate floating floor to the bare concrete floor, the overall mobility of the floor assembly increase by 40-50dB. However, the overall ceiling mobility does not increase as much as the floor over the same frequency range when the laminate floating topping is added; the difference between only reaches 10dB at higher frequencies (1000Hz-3000Hz). Also, it is noted that the mobilities of the floor and ceiling when there is no floating floor do not vary from each other much; the difference between them does not surpass 5dB throughout the entire frequency range. Finally, it is also seen that the overall mobility of the bare floor concrete floor as well as the ceiling with and without laminate generally correlate well with the analytical mobility of concrete, with the highest correlation at frequencies between 100Hz-800Hz.

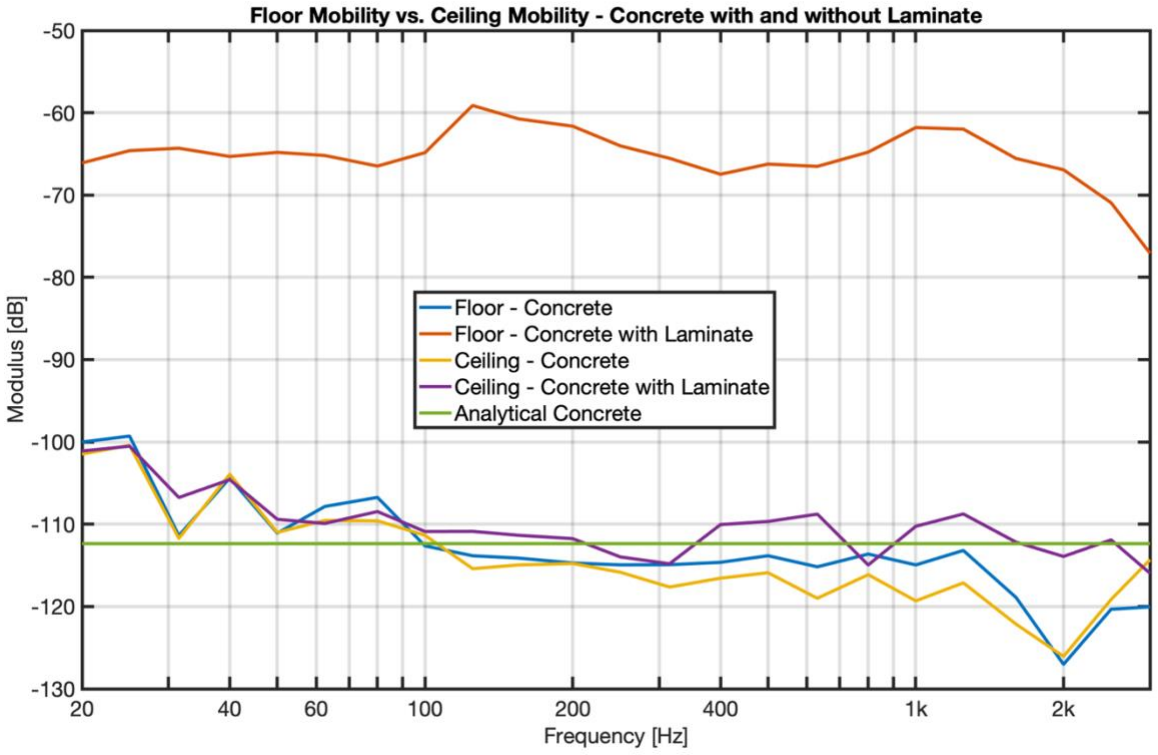

Figure 7.18 Floor mobility vs. ceiling mobility of concrete specimen with and without laminate.

Figure **7.19** shows that for the CLT floor, adding a laminate floating floor causes the mobility to increase as well, as seen with the concrete floor. In the case of the CLT, there is an approximately 20dB increase at lower frequencies (between 20Hz-200Hz), a 35dB increase at mid-frequencies (between 200Hz -400Hz), and about 30dB for the remainder of the frequency range. Like the concrete assembly, the bare CLT floor and the ceiling with and without laminate have similar values until about 400Hz where they start diverging to a difference of almost 20dB at 3000Hz. Across most of the frequency range, the mobility of the bare CLT floor and the ceiling with and without laminate follow analytical mobility of the CLT floor.

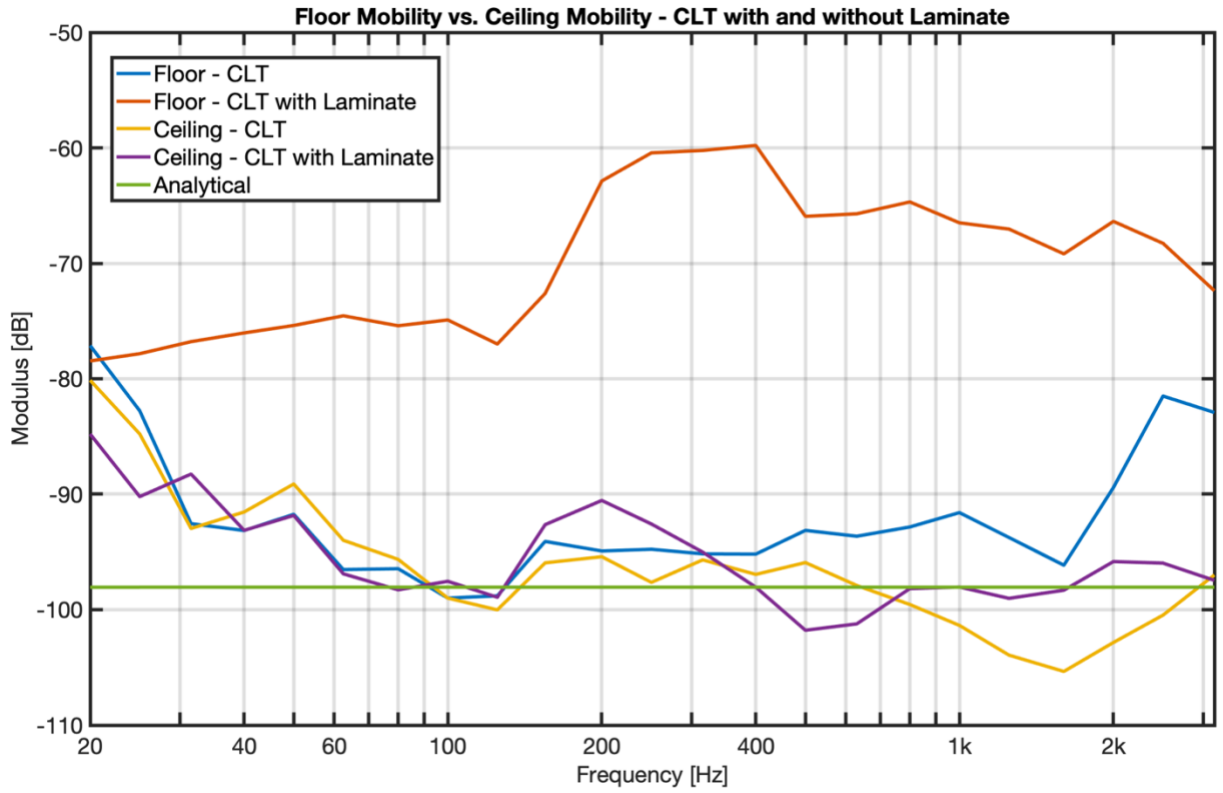

Figure 7.19 Floor mobility vs. ceiling mobility of laminate specimen with and without laminate.

When combining both the impact source and floor receiver mobilities into one plot, as shown in Figure **7.20**, it is seen that the bare concrete and the bare CLT floors have mobilities much lower than the source mobilities, with the exception of the bare CLT floor mobility approaching the tapping machine mobility at higher frequencies. On the other end, the mobilities of the impact

rubber ball as well as the walker with and without shoes are substantially greater than that of the floor receivers. However, when it comes to the mobility of the standard tapping machine, it intersects that of the concrete with laminate at 600Hz and that of the CLT with laminate at 300Hz, 450Hz, and 600Hz. Due to the mobility of the tapping machine matching closely with those of the floors with laminate, we can expect source-receiver interaction to matter most in those two cases.

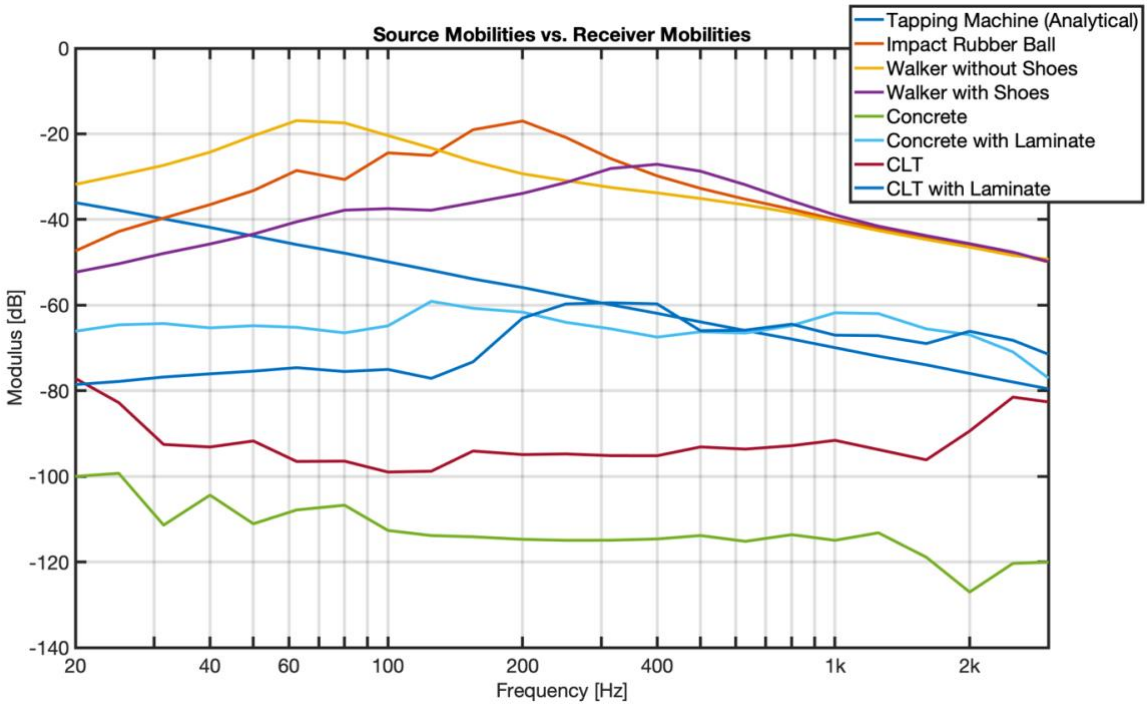

Figure 7.20 Mobilities of the sources vs mobilities of the receivers (floors).

7.1.3 Power Injected Relative Error

As seen from Figure **7.21**, Figure **7.22**, and Figure **7.23**, the power injected relative error percentage between the actual power injected and the power injected with the blocked force approximation is less than 1% throughout the whole frequency range for the cases of the walker, with and without shoes as well as the impact rubber ball on all floor receivers. For the bare floors, namely the concrete and CLT, it remains even lower than 0.1%. Relative to the bare floors, the floor assemblies with laminate floating floors show a higher percentage error; however, it remains below 0.2% for the case of the walker with no shoes, below 0.9% for the walker with shoes, below 0.4% for the case of the impact rubber ball.

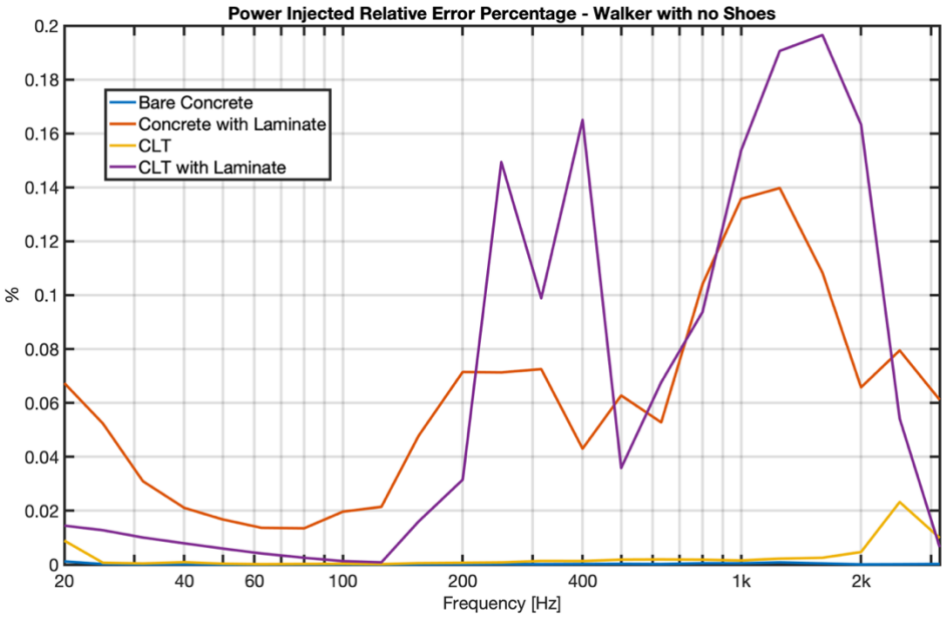

Figure 7.21 Relative error percentage between the actual power injected and the power injected when the blocked force approximation is made for the walker with no shoes.

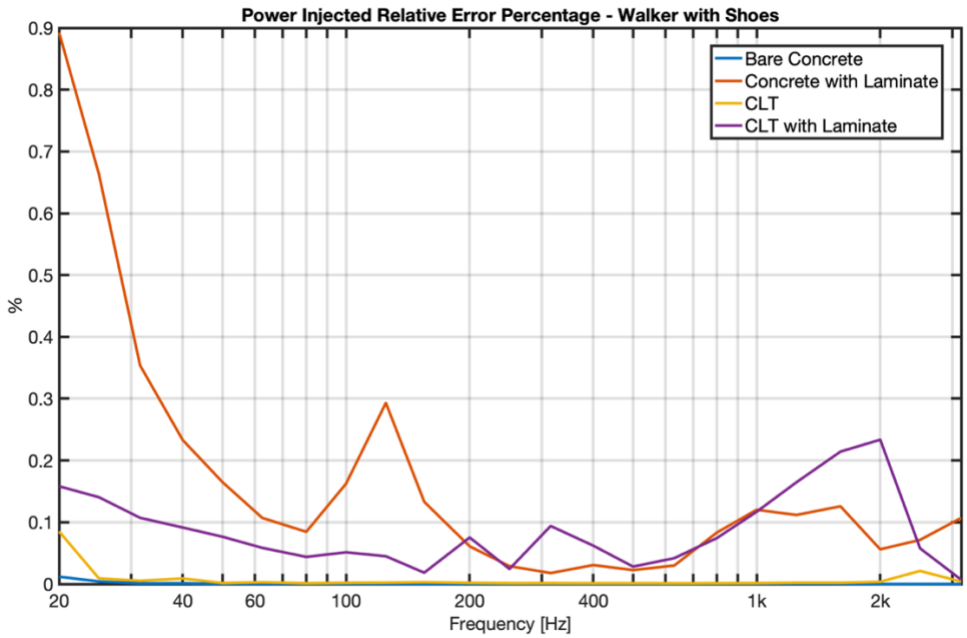

Figure 7.22 Relative error percentage between the actual power injected and the power injected when the blocked force approximation is made for the walker with shoes.

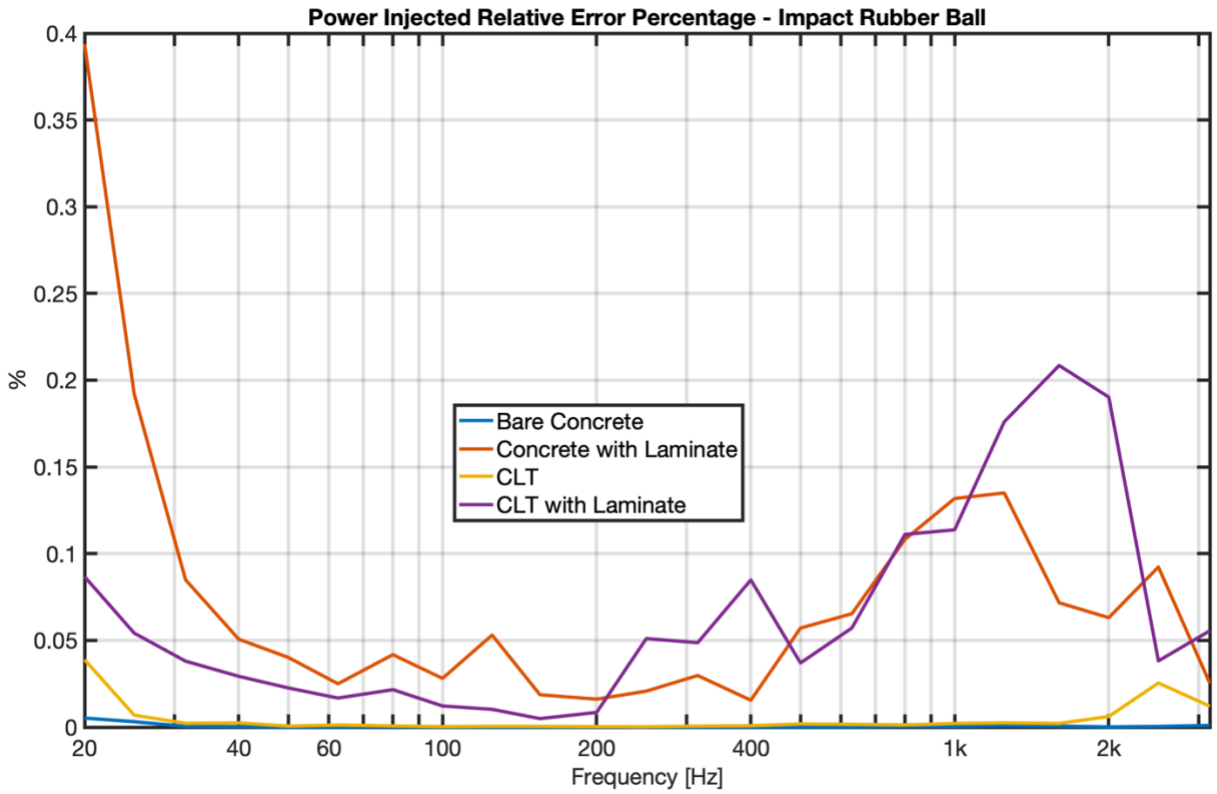

Figure 7.23 Relative error percentage between the actual power injected and the power injected when the blocked force approximation is made for the impact rubber ball.

Figure **7.24** shows the relative error percentage between the actual power injected and the power injected when the blocked approximation is made for the case of the tapping machine. Opposite to the previous cases, the tapping machine does provide considerable relative error percentages, namely when combined with the floor assemblies with laminate floating floor. The power injected relative error percentage for the concrete with laminate reaches almost 15% at 400Hz about, 12.5% at 800Hz, and almost 35% at 2000Hz for the CLT floor with laminate. For the concrete with laminate, the relative error percentage remains below 5% until about 900Hz, after which it increases to between 10%-15% for frequencies between 1000Hz-2000Hz. As for the bare concrete and CLT floors, they both yield error percentages that are lower than 1% throughout the entire frequency range.

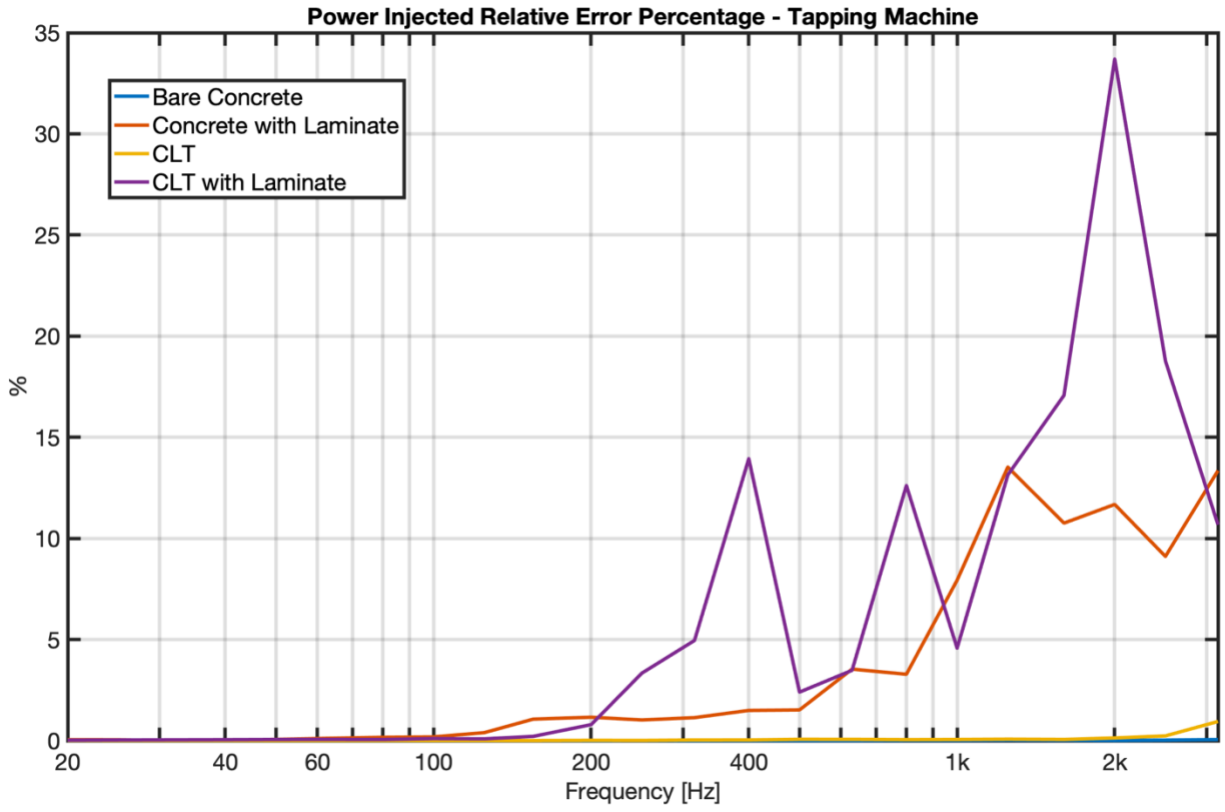

Figure 7.24 Relative error percentage between the actual power injected and the power injected when the blocked approximation is made for the tapping machine.

Plots for the actual power injected and the power injected when the blocked force approximation is assumed for both the concrete with laminate and the CLT with laminate combined with the tapping machine as a source are shown below in Figure **7.25** and Figure **7.26**. When comparing the actual power injected for the cases of the tapping machine in combination with the floors with laminate, good correlation can be seen until about 125Hz for the concrete floor with laminate and 200Hz for the CLT floor with laminate where they start diverging. Figure **7.25** sees a difference of 5dB-10dB between 150Hz to 450Hz while Figure **7.26** sees a difference of 10-15dB between 200Hz-500Hz. A large peak is seen at 475Hz and 1000Hz in Figure **7.25** while two pronounced peaks are seen at 450Hz and 1000Hz in Figure **7.26**. These peaks are attributed to the impact hammer's inefficiency at exciting the floor specimen at these frequencies, which leads to dips in the force spectrum when using the hammer.

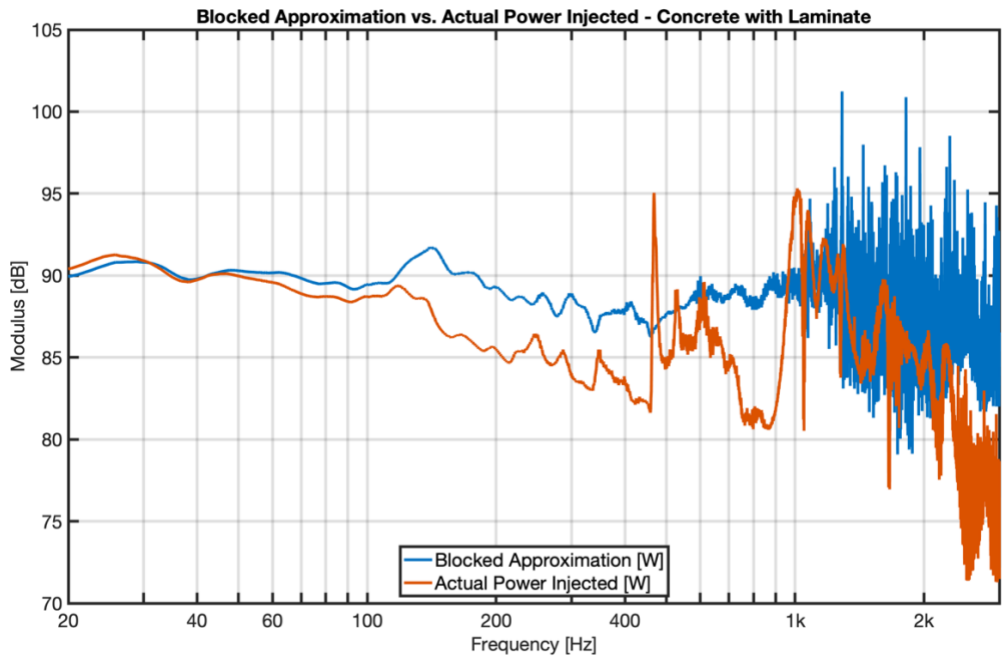

Figure 7.25 The actual power injected vs. the power injected when the blocked approximation is made for concrete with laminate.

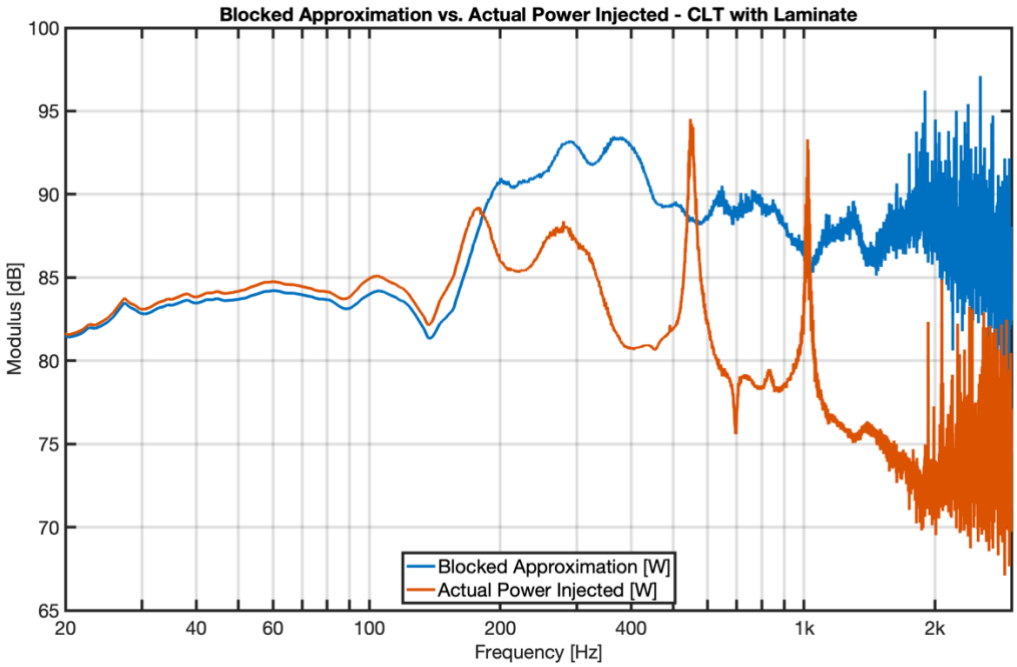

Figure 7.26 The actual power injected vs. the power injected when the blocked approximation is made for CLT with laminate.

Figure **7.27** presents the coupling function plotted against α for all four floor assemblies. It shows that for all floors, as α, or the the ratio of the magnitude of the receiver and source mobilities as seen in Equation 8, increases, then so does the coupling function. The many data points represent the different frequencies. That is until α becomes 0dB, after which point the coupling function decreases again. This is in agreement with Figure **3.4**, which shows that the coupling function is highest when α equals 1 and decreases symmetrically beyond and beneath that point. It also shows that the coupling function is higher for the case of the floors with laminate than the bare floors. Moreover, there is less linearity between α and the coupling function with the floor assemblies with laminate floors than the bare floors, as seen from the red and light blue dots.

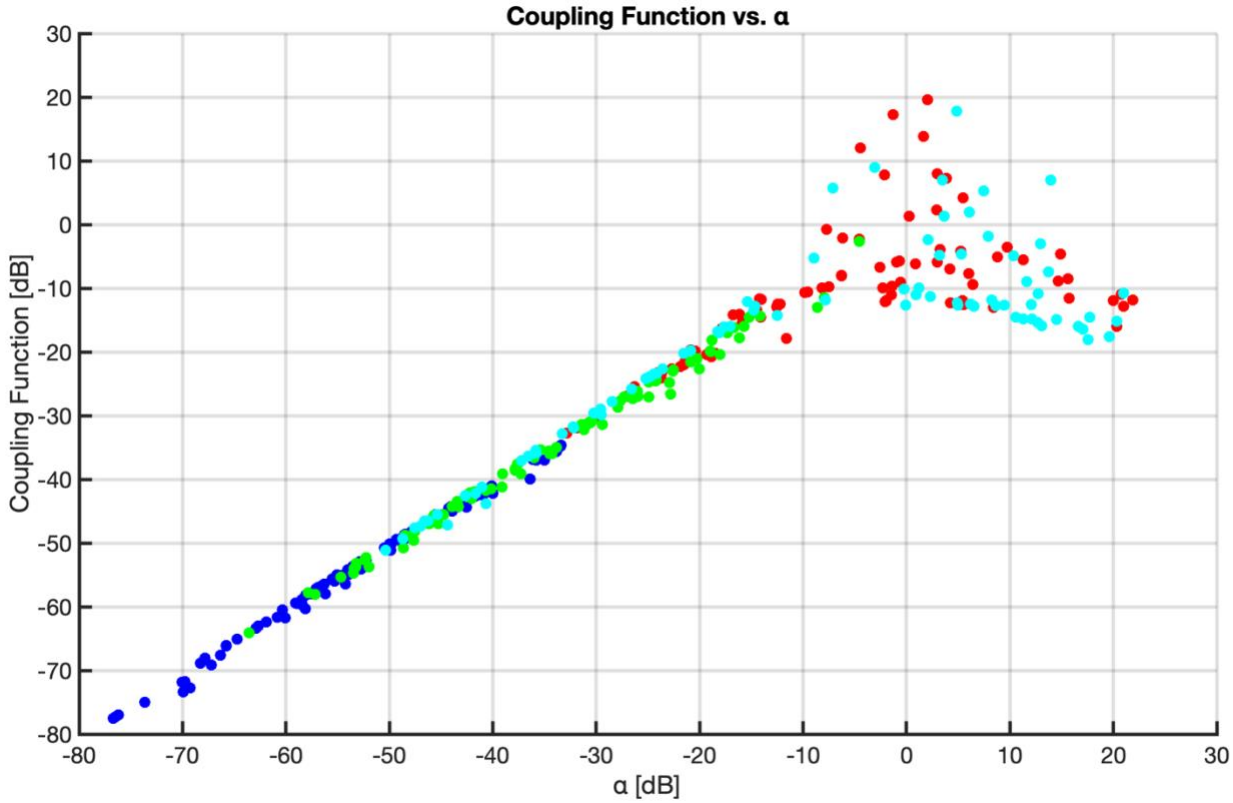

Figure 7.27 The coupling function plotted against alpha for all four floors. Dark blue is concrete, green is CLT, red is concrete with laminate, and light blue is CLT with laminate.

7.2 Discussion

By implementing numerous different measurement setups using a wide array of measurement settings for the measurement of the mobility of each impact source, results were obtained for the mobility of the impact sources. Figure **7.5** shows the mobility of each one of the four impact sources used for this project. The mobility of the walker's foot with and without shoes correlate well with Figure **2.3** in that the mobility of the walker with no shoes is higher than the walker with shoes at lower frequencies until they intersect and diverge, eventually converging at higher frequencies. Moreover, for the walker with no shoes, the peak from Figure **7.5** is very close in magnitude to that of the trough in Figure **2.4**; Figure **2.4** shows the impedance, which is the inverse of mobility. It was not expected for the walker's results to be identical to findings from previous papers as the mobilities of the feet and shoes vary from one individual to another.

The magnitude of the mobility of the impact rubber ball compares closely with that of previous findings throughout most of the frequency range [28,40]. The measured mobility of the standard tapping machine is almost identical (with a difference of less than 1 dB) to that of the analytical one until about 400Hz, after which there are oscillations and inconsistencies with repetition, as mentioned in Subsection 7.1.1. This confirms the validity of the analytical model used for the tapping machine in this project. It can also be seen from Figure **7.5** that the mobility of the impact rubber ball and that of the walker's foot with and without shoes have similar values (between -50dB and -15dB), which all converge at higher frequencies; the tapping machine has a much lower mobility (between -40dB and -80dB).

Regarding the floor receivers, we can see that for the bare concrete floor, there is little variation between transfer mobilities for every measurement position (Figure **7.8**) as well as average transfer mobilities between measurement positions (Figure **7.9**). However, for the concrete floor assembly with the laminate floating topping, Figure **7.10** and Figure **7.11** show more spread between transfer mobilities than the bare concrete floor case. That effect may be attributed to the incorporation of the floating floor, which dampens the transfer mobility between positions. Therefore, as seen more considerably in Figure **7.11**, the transfer mobility is highest between positions that are of closer proximity to each other and lowest between positions which are further in distance from each other.

This spread is translated to the average transfer mobilities at different measurement positions, exhibited in Figure **7.12**.

In the case of the bare CLT floor, similar to the bare concrete floor, there is not much of a spread between transfer mobilities, except for a separation seen where the transfer mobilities at Positions 2, 4, and 6 are higher than the transfer mobilities at 3, 5, and 7 for measurement Positions 1 (Figure **7.13**), 2, and 4 whereas a similar separation is seen at measurement Position 3 (Figure **7.14**) but with transfer mobilities at Positions 5 and 7 being greater in magnitude. This separation is due to the CLT specimen being split in the middle, causing a separation. This is realistic to some real-life CLT floor assemblies. The split causes a drop in transfer mobility between positions on the left side and right side of the partition in the middle. Measurements at Positions 1, 2, and 4 are all made on the upper half of the floor (accelerometer at measurement Position 1 was placed right above the middle position of the floor) while measurements at Position 3 are made on the lower half of the floor, as seen in Figure **5.9**. This explains why transfer mobility results from measurement Position 3 have separation between different positions compared to measurement Positions 1, 2, and 4. However, portrayed in Figure **7.15** are the average transfer mobilities when only considering the transfer mobilities yielded by the accelerometers on the half of the floor where the measurement was made.

As for the CLT floor with laminate floating topping transfer mobilities (Figure **7.16**), much less separation between top positions and lower positions is observed in comparison with the bare CLT floor. That is because the laminate floating topping bridges the split that the bare CLT floor has in the middle. Otherwise, also due to the floating topping, Figure **7.17** shows a spread between the average transfer mobilities, similar to the concrete floor with laminate floating topping.

Upon comparing the overall floor and ceiling mobilities, it is seen from Figure **7.18** and Figure **7.19** that adding a laminate floating topping to the bare floors increases the average mobility of the floor well above those of the bare floor, bare ceiling, and ceiling with laminate, which are not considerably influenced by the addition of the laminate. This makes sense since the floating floor's job is to create a difference between the floor mobility and the ceiling mobility, which translates to there being more vibrations on the floor than the ceiling. Ultimately, this means that

vibrations (or sounds) have been dampened by the floating floor. As seen in the case of the bare floors, there is not much of a difference between the overall floor and ceiling mobilities (less than 5dB at all frequencies except for frequencies above 1000Hz in the case of the CLT), meaning most of the vibrations did transmit through the floor all the way to the ceiling.

It is also seen that adding the laminate floating topping to the concrete floor has a more dramatic effect than adding it to the CLT floor. That may simply be due the mobility of concrete being lower than that of CLT; the laminate floating topping brings the mobility of both floor assemblies to comparable magnitudes, creating a greater difference with the concrete floor.

While the effect of floating topping on the overall mobilities of the floors is a positive one in terms of impact sound transmission control, it will bring the overall mobilities of the floors much closer to that of the impact sources, as seen in Figure **7.20**. This will influence the actual power injected into the floor receivers by the impact sources since it will bring α, as seen in Equation 8, closer to 1 (0dB). From Figure **3.4**, this implies an increase in the coupling function (*i.e.*, an increase in the source-receiver interaction). Moreover, we can see from Figure **7.20** that this will be of most concern when the tapping machine is used as a standard impact source, since it is the closest in mobility to the floors, even intersecting with the floors with floating topping. This makes the blocked force approximation, which neglects the source-receiver interaction's effect on the power injected at impact, less accurate.

Questions regarding the accuracy of the blocked force approximation are further explored by looking at Figure **7.21**, Figure **7.22**, Figure **7.23**, and Figure **7.24**, which represent the power injected relative error percentage for the walker's foot without shoes, with shoes, the impact rubber ball, and the tapping machine, respectively. The error percentage yielded for the walker with and without shoes as well as the impact rubber ball may be deemed as negligible, as they are all below 1%. However, from Figure **7.24**, we see a large increase in error in the case of the tapping machine, namely with the floors with laminate, in comparison with the rest of the impact sources. Additionally, the power injected relative error is greater for the CLT floors than it is for the concrete floors. This is probably because CLT floors are lighter than concrete floors, and therefore, have higher mobilities, which are closer to the mobilities of sources.

Finally, large peaks are observed at higher frequencies in both Figure **7.25** and Figure **7.26**. These are due to the impact hammer's inability to efficiently excite the receiver structures at those frequencies, which causes large amplifications to the power injected. This is a benefit the electrodynamic shaker could have over the impact hammer; it does not produce large dips in force when exciting the floors. However, when considering results in the third-octave band, those peaks and dips are evened out. When comparing hammer and shaker results, they do not make a substantial difference in the overall floor and ceiling mobilities (Figure **7.6** and Figure **7.7**). Furthermore, they are both deficient at exciting floor receivers at higher frequencies (about 1000Hz). As seen in Figure **2.5**, common impact sources do not excite floors at higher frequencies. Therefore, results for frequencies above 1000Hz are influenced by this measurement error.

8 Summary: Conclusions and Future Work

In summary, this thesis investigates the source-receiver interaction's effect for various impact sources used on different floor receivers, both bare and with a floating topping. Floating toppings are of particular concern because while they are commonly used to control impact sound, they are more complicated to model since a floating topping may increase the effect of the source-receiver interaction, which is often neglected when modelling floor assemblies. Better understanding of the source-receiver interaction is a step towards modelling impact sound insulation for the residents of MURBs, who may be detrimentally affected by impact noise.

The abovementioned objective was achieved by first measuring the mobilities of the impact sources as well as the floor receivers (with and without floating toppings) separately, followed by the measurement of the blocked force of the sources. Then, the power injected was computed, when considering and neglecting the source-receiver interaction, for the different source-receiver combinations between impact sources and floor receivers. Finally, the relative error percentage between the two powers injected was plotted and results were analyzed. In order to conduct this experiment, suitable measurement setups for the mobility of both the sources and the receivers had to be determined, using appropriate equipment.

8.1 Conclusions

1) The most appropriate setups for the impact sources, which provide the most reliable and repeatable mobility results are:
    a. Vertical-suspended for the impact rubber ball (Figure **5.3**)
    b. Horizontal for the human walker's foot with no shoes (Figure **5.6**)
    c. Vertical for the human walker's foot with shoes (Figure **5.7**)
2) Conclusions about the impact sources used in this project:
    a. The impact rubber ball is more representative of a human walker, both with and without shoes, than the tapping machine.
    b. The analytical model for the mobility of the tapping machine is accurate.

3) Conclusions about results obtained from the hammer in comparison to those yielded by the electrodynamic shaker:
    a. The difference between overall floor mobilities in one-third-octave band is negligible.
    b. They are both poor at exciting structures at higher frequencies (about 1000Hz).
    c. The hammer causes dips in the force at higher frequencies when exciting the floor receivers which translate to dips in the mobilities which translate to peaks in the power injected.
    d. The electrodynamic shaker is much more difficult and time-demanding to use than the impact hammer.
4) Conclusions about the transfer mobilities and average transfer mobilities:
    a. They are most uniform in the case of the bare concrete floor.
    b. The incorporation of a laminate floating topping causes larger variation between them.
    c. The CLT floor causes a separation between results measured on the upper half of the floor versus the ones measured on the lower half of the floor.
    d. The laminate floating topping on the CLT decreases the abovementioned separation.
    e. The closer transfer mobility positions (between the measurement position and the accelerometer position), the higher the transfer mobility.
    f. Although the abovementioned general trends hold, there will be variation in results between different measurement positions and measurement specimen.
5) Conclusions when comparing the floor and ceiling mobilities with and without laminate:
    a. Adding a laminate floating topping increases the overall floor mobilities.
    b. The addition of the laminate floating topping causes a greater increase on the concrete floor than on the CLT floor.
6) Conclusions about the source-receiver interaction:

a. The source-receiver interaction has the most influence for the case of the tapping machine on the floors with floating toppings.

b. The source-receiver interaction affects the CLT floor more than the concrete one.

c. The source-receiver interaction is negligible for the other impact sources in combination with the floor specimen measured in this project.

8.2 Future work

Future work concerning the source-receiver interaction for structure-borne sound sources on floor assemblies with floating toppings may include the following:

1) A wider variety of floor receiver specimen and floating toppings should be considered.

2) The mobility of more impact sources, such as common items dropping to the floor or a walker with a steel-heeled shoe, may be measured.

3) The electrodynamic shaker could be used in tandem with the impact hammer for all sets of measurements for a more extensive comparison between the two, especially to get rid of the peaks seen on the plots of the actual power injected against the power injected when making the blocked force approximation.

4) For more accurate results, a suitable measurement setup should be found in order to measure the blocked force of the human walker as opposed to substituting it with the blocked force of the impact rubber ball.

5) A relation needs to be found between the actual power injected, the power injected with blocked force approximation, and residents' subjective perceived annoyance to better understand the effect of the relative error between the two powers.

References

[1] Andargie, M. S., Touchie, M., & O'Brien, W. (2021, August). Subjective and objective evaluation of the impact and airborne sound insulation of multi-unit residential buildings. In INTER-NOISE and NOISE-CON Congress and Conference Proceedings (Vol. 263, No. 6, pp. 778-786). Institute of Noise Control Engineering.

[2] Rasmussen, B., & Ekholm, O. (2021, August). Neighbour noise in multi-storey housing-Annoyance and potential health effects. In INTER-NOISE and NOISE-CON Congress and Conference Proceedings (Vol. 263, No. 4, pp. 2783-2792). Institute of Noise Control Engineering.

[3] Maschke, C., & Niemann, H. (2007). Health effects of annoyance induced by neighbour noise. Noise Control Engineering Journal, 55(3), 348-356.

[4] Jensen, H. A., Rasmussen, B., & Ekholm, O. (2018). Neighbour and traffic noise annoyance: a nationwide study of associated mental health and perceived stress. European journal of public health, 28(6), 1050-1055.

[5] Levy-Leboyer, C., & Naturel, V. (1991). Neighbourhood noise annoyance. Journal of Environmental Psychology, 11(1), 75-86.

[6] Lee, P. J., & Jeong, J. H. (2021). Attitudes towards outdoor and neighbour noise during the COVID-19 lockdown: A case study in London. Sustainable Cities and Society, 67, 102768.

[7] Tong, H., Aletta, F., Mitchell, A., Oberman, T., & Kang, J. (2021). Increases in noise complaints during the COVID-19 lockdown in Spring 2020: A case study in Greater London, UK. Science of The Total Environment, 785, 147213.

[8] Şentop Dümen, A., & Şaher, K. (2020). Noise annoyance during COVID-19 lockdown: A research of public opinion before and during the pandemic. The Journal of the Acoustical Society of America, 148(6), 3489-3496.

[9] Flodén, O., & Persson, P. (2021). Robust prediction metrics for structure-borne noise in timber buildings. INTER-NOISE and NOISE-CON Congress

and Conference Proceedings, 263(4), 2348–2359. https://doi.org/10.3397/in-2021-2111

[10] Andargie, M. S., Touchie, M., & O'Brien, W. (2021). Case study: A survey of perceived noise in Canadian multi-unit residential buildings to study long-term implications for widespread teleworking. Building Acoustics, 28(4), 443-460.

[11] Mondot, J. M., & Petersson, B. (1987). Characterization of structure-borne sound sources: the source descriptor and the coupling function. Journal of sound and vibration, 114(3), 507-518.

[12] Quirt, J. D. (2011). Controlling air-borne and structure-borne sound in buildings. *Noise News International*, *19*(2), 37-47.

[13] Zeitler, B., Schoenwald, S., Nightingale, T., & King, F. (2009, August). Simplified method to estimate effectiveness of floor treatments (toppings and coverings). In *INTER-NOISE and NOISE-CON Congress and Conference Proceedings* (Vol. 2009, No. 2, pp. 4514-4522). Institute of Noise Control Engineering.

[14] Nightingale, T. (2008). Controlling Impact Noise in Wood-Frame Multi-Unit Buildings. *ICSV15: 15th International Congress on Sound and Vibration*.

[15] Quirt, J. D., & Nightingale, T. R. T. (2007, August). On a semi-empirical approach to predicting sound insulation in lightweight framed construction. In proceedings of InterNoise.

[16] Zeitler, B., Schoenwald, S., & Gover, B. (2013, June). On the relevance of impact source impedance at low frequencies. In Proceedings of Meetings on Acoustics ICA2013 (Vol. 19, No. 1, p. 015125). Acoustical Society of America.

[17] Standard, A. S. T. M. (2021). E2179. 'Standard Test Method for Laboratory Measurement of the Effectiveness of Floor Coverings in Reducing Impact Sound Transmission Through Concrete Floors'. *ASTM International*.

[18] EN ISO 10140-5. (2021). Laboratory measurement of sound insulation of building elements-Part 5: Requirements for test facilities and equipment.

[19] Shi, W., Johansson, C., & Sundbäck, U. (1997). An investigation of the characteristics of impact sound sources for impact sound insulation measurement. *Applied Acoustics*, *51*(1), 85-108.

[20] Tachibana, H. (1998). Development of new heavy and soft impact souce for the assessment of floor impact sound insulation of buildings. *Proc. Inter-Noise'98*.

[21] Warnock, A. (2002). Prospects for a test procedure for rating floor toppings on joist floors. *The Journal of the Acoustical Society of America*, *112*(5), 2227-2227.

[22] Ljunggren, F., Simmons, C., & Hagberg, K. (2014). Correlation between sound insulation and occupants' perception–Proposal of alternative single number rating of impact sound. *Applied Acoustics*, *85*, 57-68.

[23] Li, Y. J., & Lai, J. C. S. (2000). Prediction of surface mobility of a finite plate with uniform force excitation by structural intensity. *Applied Acoustics*, *60*(3), 371–383. https://doi.org/10.1016/s0003-682x(99)00043-2

[24] Scholl, W., & Maysenhölder, W. (1999). Impact sound insulation of timber floors: Interaction between source, floor coverings and load bearing floor. *Building Acoustics*, *6*(1), 43-61.

[25] Scholl, W. (2001). Impact sound insulation: The standard tapping machine shall learn to walk!. Building Acoustics, 8(4), 245-256.

[26] Inoue, K., Yasuoka, M., & Tachibana, H. (2000, August). New heavy impact source for the measurement of floor impact sound insulation of buildings. In *Proceedings of inter-noise*(pp. 1493-1496).

[27] Schoenwald, S., Zeitler, B., & Nightingale, T. R. (2011). Prediction of the blocked force at impact of Japanese rubber ball source. Acta Acustica united with Acustica, 97(4), 590-598.

[28] Jeon, J. Y., Ryu, J. K., Jeong, J. H., & Tachibana, H. (2006). Review of the impact ball in evaluating floor impact sound. *Acta Acustica united with ACUSTICA*, *92*(5), 777-786.

[29] Lee, P. J., Jeong, J. H., Park, J. H., & Jeon, J. Y. (2006). Comparison of standard floor impact sources with a human impact source. *Transactions of the Korean Society for Noise and Vibration Engineering*, *16*(8), 789-796.

[30] EN ISO 12354-1. (2017). Building acoustics–estimation of acoustic performance of buildings from the performance of elements–Part 1: airborne sound insulation between rooms.

[31] Warnock, A. C. C. (2000, August). Low-frequency impact sound transmission through floor systems. In Proceedings of Inter-noise (Vol. 2000).

[32] Roozen, N. B., Leclere, Q., Urbán, D., Echenagucia, T. M., Block, P., Rychtáriková, M., & Glorieux, C. (2018). Assessment of the airborne sound insulation from mobility vibration measurements; a hybrid experimental numerical approach. Journal of Sound and Vibration, 432, 680-698.

[33] Mayr, A. R., & Gibbs, B. M. (2016). Approximate method for obtaining source quantities for calculation of structure-borne sound transmission into lightweight buildings. Applied Acoustics, 110, 81-90.

[34] Warnock, A. (2002). Prospects for a test procedure for rating floor toppings on joist floors. *The Journal of the Acoustical Society of America*, *112*(5), 2227-2227.

[35] Jeon, J. Y., Ryu, J. K., Jeong, J. H., & Tachibana, H. (2006). Review of the impact ball in evaluating floor impact sound. *Acta Acustica united with ACUSTICA*, *92*(5), 777-786.

[36] Quirt, J. D., King, F., Nightingale, T. R. T., & Craig, B. (2006). *Guide for sound insulation in wood frame construction*. Institute for Research in Construction, National Research Council Canada.

[37] Nightingale, T. R. T., & Bosmans, I. (2000, August). Estimating junction attenuation in lightweight constructions. In *Proceedings of INTERNOISE* (pp. 28-30).

[38] Nightingale, T. R., & Bosman, I. (2000). Power balance methods to estimate junction attenuation in lightweight constructions. *Canadian Acoustics*, *28*(3), 12-13.

[39] Brennan, M. (n.d.). *Mechanical mobility and impedance - UNESP*. Retrieved May 19, 2022, from http://www.dem.feis.unesp.br/gmsint/mobility-and-impedance.pdf

[40] Zeitler, B., & Nightingale, T. (2008). Impedance of standard impact sources and their effect on impact sound pressure level of floors. *Journal of the Acoustical Society of America*, *123*(5), 3358.

[41] Moorhouse, A. T. (2001). On the characteristic power of structure-borne sound sources. *Journal of sound and vibration*, *248*(3), 441-459.

[42] Elliott, A., & Moorhouse, A. T. (2008). Characterisation of structure borne sound sources from measurement in-situ. *Journal of the Acoustical Society of America*, *123*(5), 3176

[43] Schiavi, A. (2018). Improvement of impact sound insulation: A constitutive model for floating floors. *Applied Acoustics*, *129*, 64-71.

[44] Standard, A. S. T. M. (2021). E2179. 'Standard Test Method for Laboratory Measurement of the Effectiveness of Floor Coverings in Reducing Impact Sound Transmission Through Concrete Floors'. *ASTM International*.

[45] Mueller-Trapet, M. (2021, December 22). Test ID: IIF-21-064. Ottawa, Ontario; Building M59, National Research Council, 1200 Montreal Road.

[46] Mueller-Trapet, M. (2022, February 7). Test ID: IIF-22-003. Ottawa, Ontario; Building M59, National Research Council, Montreal Road 1200.

[47] Zeitler, B., Schoenwald, S., & Gover, B. (2013, June). On the relevance of impact source impedance at low frequencies. In *Proceedings of Meetings on Acoustics ICA2013* (Vol. 19, No. 1, p. 015125). Acoustical Society of America.

[48] Brunskog, J., & Hammer, P. (2003). The interaction between the ISO tapping machine and lightweight floors. *Acta Acustica united with Acustica*, *89*(2), 296-308.

[49] *SmartShaker™ with Integrated Power Amplifier*. SmartShaker™ with Integrated Power Amplifier | Excitation | The Modal Shop, Inc. (n.d.).

Retrieved May 26, 2022, from https://www.modalshop.com/excitation/SmartShaker-with-Integrated-Power-Amplifier?ID=272

[50] Girdhar, S., Barnard, A. R., LoVerde, J., & Dong, W. (2021, August). Measuring force and impedance for the tapping machine. In *INTER-NOISE and NOISE-CON Congress and Conference Proceedings* (Vol. 263, No. 6, pp. 767-777). Institute of Noise Control Engineering.

[51] *CDAQ-9178*. NI. (n.d.). Retrieved May 26, 2022, from https://www.ni.com/en-ca/support/model.cdaq-9178.html

[52] Möller, K. (2020). Objective and Subjective Research on Impact Noise (M.Sc. thesis).

[53] Schoenwald, S., & Zeitler, B. (2011, April). Floor excitation with the heavy soft impact source. In *Forum Acusticum* (Vol. 2011, pp. 1-6).